ADA034954

Development of An Al-Mg-Li Alloy

Final Report

T. H. Sanders, Jr.
Physical Metallurgy Division
Alcoa Laboratories
Alcoa Center, Pa. 15069

Naval Air Development Center
Contract No. N62269-74-C-0438
For Naval Air Systems Command

Approved for Public Release
Distribution Unlimited

June 9, 1976

ALCOA

DDC
RECEIVED
JAN 28 1977
C

DEVELOPMENT OF AN Al-Mg-Li ALLOY

FINAL REPORT

T. H. Sanders, Jr.
Physical Metallurgy Division
Alcoa Laboratories
Alcoa Center, Pa. 15069

NAVAL AIR DEVELOPMENT CENTER
CONTRACT NO. N62269-74-C-0438
For Naval Air Systems Command

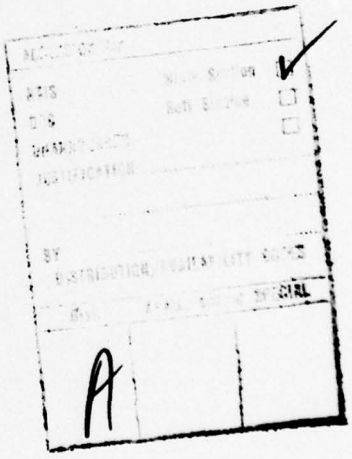

June 9, 1976

APPROVED FOR PUBLIC RELEASE
DISTRIBUTION UNLIMITED

SECURITY CLASSIFICATION OF THIS PAGE *(When Data Entered)*

REPORT DOCUMENTATION PAGE

READ INSTRUCTIONS BEFORE COMPLETING FORM

1. REPORT NUMBER (18) NADC-76397-30 (19)	2. GOVT ACCESSION NO.
3. RECIPIENT'S CATALOG NUMBER	
4. TITLE *(and Subtitle)* (6) Development of an Al-Mg-Li Alloy.	5. TYPE OF REPORT & PERIOD COVERED (9) Final rept.,
6. PERFORMING ORG. REPORT NUMBER (14) 56-76-AH352	
7. AUTHOR(s) (10) T. H. Sanders, Jr.	8. CONTRACT OR GRANT NUMBER(s) (15) N62269-74-C-0438 new
9. PERFORMING ORGANIZATION NAME AND ADDRESS Aluminum Company of America Alcoa Laboratories Alcoa Center, Pa. 15069	10. PROGRAM ELEMENT, PROJECT, TASK AREA & WORK UNIT NUMBERS
11. CONTROLLING OFFICE NAME AND ADDRESS (11) Naval Air Development Center Warminster, PA 18974	12. REPORT DATE 9 June 1976 13. NUMBER OF PAGES 151
14. MONITORING AGENCY NAME & ADDRESS *(if different from Controlling Office)* (12) 149 p.	15. SECURITY CLASS. *(of this report)* 15a. DECLASSIFICATION/DOWNGRADING SCHEDULE

16. DISTRIBUTION STATEMENT *(of this Report)*

Approved for Public Release; Distribution Unlimited

17. DISTRIBUTION STATEMENT *(of the abstract entered in Block 20, if different from Report)*

18. SUPPLEMENTARY NOTES

19. KEY WORDS *(Continue on reverse side if necessary and identify by block number)*

Al-Mg-Li	Precipitation hardening	Al_3Li
Casting	Elastic modulus	Density
Extrusion	Notch Tensile	
Tensile		

20. ABSTRACT *(Continue on reverse side if necessary and identify by block number)*

A program to optimize composition in the Al-Mg-Li system was conducted in two phases. In Phase I, a series of alloys containing Al-3.5 Mg-2.5 Li with Cr, Mn, or Zr was investigated. The alloy containing 0.3% Mn developed the best combination of strength and notch toughness. Under Phase II, effects of Mg and Li content in the Al-Mg-Li-0.3 Mn alloy system were determined. Nine alloy combinations ranging from 1.4 to 3.1 Li and 2.0 to 4.9 Mg were evaluated. Strength and modulus increased and density decreased with increasing Li. Fracture toughness of these alloys were below minimum acceptable levels for commercial product.

DD FORM 1 JAN 73 1473 EDITION OF 1 NOV 65 IS OBSOLETE

406 282

SECURITY CLASSIFICATION OF THIS PAGE *(When Data Entered)*

AB

SUMMARY

The Al-Mg-Li alloy system has demonstrated the potential of providing attractive combinations of density, elastic modulus, and strength, so a program to optimize composition in this system was undertaken. The program was conducted in two phases. In Phase I, a series of alloys consisting of an Al-3.5 Mg-2.5 Li base with recrystallization inhibiting additions of either Cr, Mn, or Zr was investigated. Comparative evaluations of tensile and notch tensile properties were made on six alloys containing two levels of each ancillary element in the extruded, solution heat treated, quenched, and artificially aged condition. The alloy containing 0.3% Mn developed the best combination of strength and notch toughness.

Under Phase II, effects of Mg and Li content in the Al-Mg-Li-0.3 Mn alloy system were determined. Nine alloy combinations ranging from 1.4 to 3.1 Li and 2.0 to 4.9 Mg were evaluated. The primary strengthening agent, Al_3Li (δ'), was confirmed and the beneficial effect of Mg on strength was attributed to a solid solution strengthening mechanism. The presence of the high volume fraction of ordered Al_3Li, a Cu_3Au (Ll_2)-type superlattice, appeared to control the deformation mode. The mechanical behavior of these alloys was thus interpreted in light of the existing models of deformation in ordered alloy systems.

The high rate of work hardening in the Al-Mg-Li alloys was attributed to the ordered, metastable precipitate, the presence of which controls the generation and motion of superlattice dislocations during deformation. The superlattice dislocations are effectively locked during cross-slip. The low notch toughness and fracture along grain boundaries of artificially aged Al-Mg-Li extrusions were attributed to: (a) a build up of high stress concentrations at the boundaries by limited cross-slip and dislocation locking and (b) reduction in grain boundary strength as a consequence of heterogeneous precipitation of Al_2MgLi and/or segregation of trace impurities on grain boundaries.

FOREWORD

This work was performed for the U.S. Naval Systems Command under Contract N62269-74-C-0438. Mr. J. W. Evancho was the project engineer for the initial portion of this contract. Dr. T. H. B. Sanders was project engineer for the final segments. Mr. J. T. Staley supervised their work. The contract monitor for the U. S. Naval Air Systems Command was Mr. E. S. Balmuth.

TABLE OF CONTENTS

LIST OF TABLES

LIST OF FIGURES

Page

BACKGROUND AND OBJECTIVE

The Al-Mg-Li alloy system has a potential of providing high strength in heavy sections, good resistance to stress-corrosion cracking, and high fracture toughness.[1,2] More importantly, this alloy system also has the potential of providing a unique combination of high modulus of elasticity and low density.

Work in the Soviet Union with additions of Zr, Mn, Ti, and Cr resulted in the development of alloy 01420.[3-9] The alloy, which contains 4.0-7.0% Mg and 1.5-2.6% Li, has reportedly been cast in ingots up to 31 inches in diameter and has been fabricated into extrusions, forgings, sheet, and plate.[10] Strengths of the extruded bars and panels exceed strengths predicted from work with ternary alloys by approximately 10 ksi, but strengths of the other products are more in line with expected strengths of ternary alloys. Alloy 01420 also has good fatigue strength in air and corrosive media and it is weldable.[4]

In this country development of an Al-Mg-Li alloy was initiated under Naval Air Development Center Contract No. N62269-73-C-0219 for Naval Air Systems Command. Four high solute alloys were investigated: an alloy containing 5.2% Mg, 2.7% Li, and 0.2% Zr that had been reported by Fulmer Research Institute[2] to develop an attractive combination of tensile properties, toughness, and resistance to stress corrosion; a higher solute alloy containing 6.0% Mg, 3.2% Li, and 0.2% Zr; and similar versions of both of these alloys containing 0.3% Mn instead of 0.2% Zr. Results of the work done on these alloys indicated that high solute Al-Mg-Li alloys are difficult to cast and fabricate, are not as tough as lower solute Al-Mg-Li alloys, and devlop strengths lower than those of leaner Al-Mg-Li alloys. Consequently, development of high solute alloys was terminated.

Sufficient information is not available to determine the composition providing optimum combinations of mechanical properties and corrosion characteristics, fabricability, and castability. During development of alloy 01420, Russian investigators attributed hardening to a transition phase of Al_2MgLi, and the composition of alloy 01420 was selected because it is primarily in the Al_2MgLi phase field. Recent work,[11] however, indicates that the same tranition phase observed by the Russians is responsible for hardening in binary Al-Li alloys, thereby suggesting that compositions in the Al_2MgLi phase field are not necessary for hardening.

Previous work indicated two potential approaches to increase the peak strength and decrease the time necessary to develop peak strength during artificial aging of Al-Mg-Li alloys. Work with the high solute alloys indicated that the yield strength could be increased by more than 20 percent by cold rolling (30 percent reduction) between the solution heat treat temperature and artificial aging.[12]

The effects of deformation on the precipitation reaction can phenomenologically be considered using classical homogeneous nucleation theory.[13] For homogeneous nucleation of a precipitate from a supersaturated solid solution, the Gibbs free energy can be written as:

$$G = \Delta G_{volume} + \Delta G_{surface} + \Delta G_{strain}.$$

Since the matrix is metastable with respect to the precipitate, the ΔG_{volume} term is negative while the $\Delta G_{surface}$ and ΔG_{strain} terms are positive; therefore, the total free energy is then dependent upon the radius of the nucleus of the precipitating phase. The effect of dislocations on the nucleation of a precipitate has been considered theoretically. The underlying assumption is that the presence of the dislocation reverses the sign of the ΔG_{strain} and, therefore, the precipitation reaction is driven in the direction of completion.

In general, most precipitation processes in age-hardenable aluminum alloys can be written according to the following scheme:

supersaturated, solid solution → coherent zone → semicoherent, intermediate precipitate → incoherent precipitate.

By varying the type and number of nucleating sites present, precipitation can occur within the matrix, on dislocations and subgrains, or on grain boundaries. Therefore, depending upon the degree of misfit between the different products in the precipitation reaction, a variety of microstructures can be achieved and explained according to this simple model.

Work done by Hardy[14] suggested that minor alloying additions might provide a similar strength increase in Al-Mg-Li alloys without cold work. Hardy's work indicated that the addition of 0.10% Cd to an Al-Li alloy significantly altered its response to artificial aging. Furthermore, the effect of the Cd addition on the yield strength was comparable to the effect of increasing the solute content and stretching 5 percent before artificial aging. The increased response of the Al-Li-Cd alloy to artificial aging was attributed to facilitated nucleation of the AlLi phase. Most recent reports on the aging kinetics of Al-Mg-Li alloys indicate that maximum strength is associated with precipitation of a transition phase of Al_3Li.[11] Consequently, it was reasoned that Cd additions to ternary Al-Mg-Li alloys could have the same beneficial effect as reported for binary Al-Li alloys with the result that high yield strengths might be produced in Al-Mg-Li alloys without cold working prior to aging.

Additions of Be were also considered.[6,14-18] Minor additions of Cd or Be to Al-Cu alloys facilitate precipitation of θ'.[18-20] Furthermore, additions of both Cd and Be to Al-Cu alloys have an additive effect on precipitation, thereby producing higher strengths than if either Cd or Be were added separately. Because the effect of Cd on precipitation in Al-Li alloys is analogous to the effect of Cd on precipitation in Al-Cu alloys,[18] minor additions of Be or Cd+Be to Al-Li or Al-Mg-Li alloys might also facilitate precipitation, thereby producing high yield strengths.

The objective of this investigation is to determine the Mg and Li contents and the type and amount of ancillary element addition that provide the optimum combinations of strength, toughness, modulus, density, castability, and fabricability and to determine if Cd or Cd+Be affect either response to artificial aging or maximum strength of Al-Mg-Li alloys.

PROGRAM

The work was conducted in two phases. As a result of Phase I (Appendix A), 0.3 percent* Mn was selected as the ancillary element addition.

Under Phase II, effects of Mg and Li content and of Cd and Cd+Be additions were investigated. Solution heat treatment and artificial aging surveys of extruded rod were conducted, and the following properties were determined on extrusions aged to maximum strengths and the results were interpreted in terms of microstructure:

1. Density
2. Elastic Modulus
3. Tensile
4. Notch Tensile

Tensile properties and notch tensile strengths were also determined on extrusions aged beyond maximum strength.

EXPERIMENTAL

Ingot Casting

To determine the effects of Mg and Li content and of Cd and Cd+Be additions on the mechanical properties of an Al-Mg-Li alloy, target compositions in Table 1 were cast as 6-inch diameter D.C. ingots.

*All compositions in this report will be given as weight percent unless otherwise specified.

Because Li readily oxidizes in air, special precautions were followed during melting and casting. All components except Li were melted as 40 Kg charges in a plumbago crucible using a high frequency induction furnace. The melt was fluxed with Cl_2 to remove hydrogen gas and was then covered with a molten KCl-LiCl salt mixture. Elemental Li was added to the meld as 100 g charges. The melt was poured into the pouring trough under a molten KCl-LiCl salt mixture and was then transferred to the mold under an inert gas atmosphere. A single charge produced one 6-inch diameter x 30-inch ingot.

Chemical compositions of the melts were determined and are listed in Table 2.

Fabricating

Two-inch diameter rods were fabricated from the ingots. The ingots were preheated 12 hours at 850°F plus 12 hours at 960°F in an argon atmosphere and were air cooled. The billets were induction reheated to 700°F and direct extruded from a 6-3/8-inch diameter cyclinder to a two-inch rod (extrusion ratio of 10).

Determination of Solution Heat Treatment Practices

Solution heat treatment temperatures were in the range of 800 to 950°F in steps of 25°F. Specimens of the as-extruded products were solution heat treated at the various temperatures for one hour, cold water quenched, and aged 48 hours at 375°F, the aging practice which developed maximum strength in higher solute Al-Mg-Li alloys. Single longitudinal and transverse tension and notched-tension specimens were removed from the center of each sample and were tested,* In addition, specimens were removed from as-extruded samples and from as-extruded samples which had been artificially aged. Standard 0.500-inch diameter tension specimens were used for the longitudinal tests and standard 0.160-inch diameter tension specimens were used for the transverse tests. All notched-tension specimens were of the design illustrated in Figure 1.

Determination of Precipitation Heat Treatment Practices

Samples were removed from the extrusions, solution heat treated one hour at the temperatures given in Table 3, quenched in cold water, and artificially aged for one to 168 hours at 300 to 400°F in increments of 25°F. Rockwell "B" hardness values as a function of time and temperature were determined.

Based on the results of hardness, three aging practices were chosen to evaluate the mechanical properties of the alloys.

*Because the alloy 3 extrusion had a crack running longitudinally near the center, test specimens were removed near mid-radius.

The first practice was designed to produce maximum or near maximum strength for each alloy. The second practice was chosen to produce 90 percent of maximum strength by overaging. A third practice was used on alloys which exhibited two distinct peaks in hardness. In these alloys both strength maxima were explored.

Density

Densities were determined by water displacement technique on machined 1.0-inch x 1.0-inch x 2.0-inch specimens.

Moduli of Elasticity

Elastic moduli were determined for samples aged by practice 1 (peak strength) using duplicate longitudinal specimens of the type shown in Figure 2. Two Micro-Measurement, type CEA-13-062UW-350, strain gauges were applied 180° apart at the midlength of the reduced section of each sample and were wired in series to provide a 700 ohm 1/2 bridge configuration. The strain gauge signal provided the input tc the X axis of an X-Y-Y plotter; and a Revere, 10,000-lb capacity, precision load cell installed in series with the samples provided the input signal for the Y axis of the X-Y-Y plotter.

RESULTS

Ingot Casting

Ingots were cast successfully for all of the alloys except alloy 3 (3.4 percent Li). Three separate attempts were made to cast this alloy; however, all three ingots cracked. One of these ingots was extruded to develop information on the effects of composition on properties. Dye-checked ingot slices showed no porosity. Etched ingot slices are shown in Figures 3 and 4. The etched ingot slice for alloy 4 showed large columnar grains.

Fabricating

The extrusion data are listed in Table 4. The breakout pressure was insensitive to Li content but increased considerably with increasing Mg content (Figure 5).

The extrusions were inspected for rear-end defects by removing one-foot long samples, etching the cross-section, and visually examining the cross-section for defects. The defects were confined to the rear one-foot of all the extrusions. Slices were also removed from locations two feet from the front and one foot from the rear of the extrusions and etched to reveal the macro grain structure. Photographs of the etched slices are shown in Figures 6 through 9. The large columnar grains exhibited in the as-cast structure in alloy 4 (S. No. 427602) carried through the extrusion, resulting in a large grain structure in the product.

Remelt chemical analyses of the extrusions, Table 5, revealed lithium and magnesium contents of up to 0.3% and 0.2%, respectively, lower than the melt analyses.

Determination of Solution Heat Treatment Practices

Solution heat treatment practices for the extrusions were selected on the basis of results of tensile and notch tensile tests of samples which had been removed from extrusions of alloys 1 through 9, solution heat treated at 800 to 950°F, and artificially aged 48 hours at 375°F.

Tensile properties are listed in Tables 6 through 10. Solution heat treatment temperature producing highest tensile properties generally increased with increasing solute content. For alloys within the composition range indicated in Figure 10, as-extruded samples that were artificially aged developed strengths as high as strengths of samples that were solution heat treated prior to artificial aging, thereby indicating that these alloys were not only solutionized during extrusion but that they are also quench-insensitive (extrusions were still-air cooled).

Notch tensile strengths and notch tensile strength/yield strength ratios are listed in Tables 11 through 15. Solution heat treatment temperature did not directly affect toughness; toughness, however, was strongly affected by yield strength and composition (Figures 11 and 12). The bottom of the data band for commercial 2XXX and 7XXX extrusions plotted in Figure 11 shows the effect of yield strength on toughness of commercial alloy extrusions. (Sufficient transverse data for commercial alloy extrusions were not available to plot in Figure 12.) The solid lines in the figures show the effect of yield strength on toughness of Al-Mg-Li extrusions. Two separate strength-toughness relationships are indicated; one for strengths greater than 45 ksi and one for strengths less than 45 ksi. Toughness was much more sensitive to variations in yield strength at strength levels less than 45 ksi than at strength levels greater than 45 ksi. Variation in toughness at a given yield strength is attributed to composition effects. Consequently, the family of lines indicated in the figures represent the strength-toughness relationship for different alloys. The effect of composition on toughness will be discussed in a later section.

Optimum solution heat treatment temperatures for the alloys are listed in Table 3.

Determination of Precipitation Heat Treatment Practices

Rockwell B hardness values of the extrusions after artificial aging are listed in Tables 16 and 17 and Figures 13 through 23.

The response to artificial aging depended significantly on Li and moderately on Mg content:

1. Maximum hardness produced by aging increased considerably with increasing Li content, but increased only slightly with increasing Mg content (Figure 24).

2. Aging temperature producing maximum hardness decreased with increasing Mg content (Figures 13 through 21).

3. Alloys 1, 2, 3, and 5 showed what appeared to be a two-stage aging phenomenon (Figures 13 through 16).

Minor additions of either Cd or Cd+Be slightly affected the aging kinetics of Al-Mg-Li alloys (Figures 25 through 29). As indicated in these figures, Cd or Cd+Be additions primarily affected the initial stage of artificial aging. No significant differences were detected between the alloys containing Cd or Cd+Be.

Tensile Properties

The heat treatment and aging practices listed in Tables 3 and 18 were used to evaluate the different alloys. The longitudinal and transverse tensile properties are given in Table 19. Longitudinal yield strength is plotted versus Mg and Li contents in Figure 30. The yield strength increased considerably with increasing Li content but increased only slightly with increasing Mg content. No significant differences in tensile properties were apparent in samples aged by Practice 3 as compared to those aged by Practice 1.

Specific tensile strength (strength/density) for the highest strength Al-Mg-Li alloy was the same as that of 7050-T76 extrusions.

Densities and Elastic Moduli

Densities from samples aged by Practice 1 (peak strength) are given in Table 20. The effect of composition on density is illustrated in Figure 31. The density was primarily affected by the Li content although both Mg and Li additions decreased density.

Elastic moduli for samples aged according to Practice 1 are listed in Table 21. As indicated in Figure 32, elastic modulus for these alloys ranged from $10.8\text{-}11.8 \times 10^6$ psi, was independent of Mg content, but increased with increasing Li content.

The ratio of elastic modulus:density was up to 30% greater than that of alloy 7050.

Toughness

Notch tensile strengths and notch tensile strength/yield strength ratios are listed in Table 22. All of the alloys developed combinations of toughness and strength below the band for commercial aluminum alloys and transverse toughness was decidedly lower than longitudinal toughness.

Longitudinal toughness was affected by yield strength, composition, and aging practice. Toughness of the peak-aged high solute alloys and of the low solute alloys in the peak aged or overaged condition conformed to the relationship:

$$NTS/YS = a - b\ (Y.S.) + P\ (Composition),$$

as indicated in Figure 33. Toughness generally decreased with increasing Li content (Figure 34). Overaging was detrimental to the toughness of alloys containing 3.5% or more Mg (Figure 35). The magnitude of decrease in toughness with overaging increased with increasing Mg and Li.

Contrary to the effect on longitudinal toughness, composition had no apparent direct effect on transverse toughness although yield strength and aging practice did have an effect. Figure 36 shows the notch tensile strength/yield strength ratios as a function of yield strength for the extrusions aged to maximum strength and for the overaged extrusions. Overaging decreased the combination of strength and toughness of all the alloys. The magnitude of the toughness decrease increased with increasing Mg and Li content (Figure 37).

Neither aging to maximum strength by the alternate practice (Practice 3, Table 18) nor additions of Cd or Cd+Be affected toughness of the extrusions.

Microprobe analyses of fractured longitudinal and transverse notched tensile specimens indicate that Fe, Si, Ti, or minor alloying elements (Cr, Mn, or Zr) do not contribute significantly to the low toughness. Light and scanning electron microscopy indicate that fracture is along high angle boundaries (the extrusions are unrecrystallized), Figures 38 and 39. The fracture surfaces show a high density of depressions, 0.5-1.0 μm diameter.

DISCUSSION OF RESULTS

Precipitation in Al-Li Alloys

The strength of an alloy is related to the resistance to the motion of a dislocation. Plastic deformation in aluminum and

most of its alloys occurs by the motion of unit dislocations moving on close packed planes, {111}, and in close packed directions, <110>.

In precipitation hardening alloys, the increase in flow stress during aging is due to the interaction of dislocations with the pre-precipitates and precipitates. Coherent and partially coherent precipitates may be penetrated by dislocations since the slip systems of the precipitates and the matrix are generally coincident. The strength and microdeformation characteristics of a precipitation hardening alloy will thus depend upon the degree of coherency, size, spacing, uniformity in the distribution of the precipitates, and the crystallographic structure of the precipitate. The crystal structure of the metastable precipitate in Al-Li alloys is different than the structures of the hardening precipitates of commercial aluminum alloys.

In the Al-Li binary alloy, the metastable phase, which forms during aging after solution heat treatment and quenching, is ordered Al_3Li.[11] The structure is the $L1_2$-type (Cu_3Au) and is shown in Figure 40.

There are two unique types of lattice sites in this structure. The A sites are located on the faces of the cube. Since each face is shared by one other unit cell, the six A sites contribute a total of three lattice points per unit cell volume. The B sites are located at the corners of the cube. Each site is shared by eight adjacent unit cells and thus the total number of B lattice sites per unit cell volume is one. This arrangement leads to an A_3B structure. Initially, the four sites are equivalent. However, once a B site is established, the A sites are automatically defined since the structure must be consistent with the composition.

A {100} section through a region of alloy which contains aluminum matrix and Al_3Li precipitate is shown in Figure 41. The open circles represent Al and the solid circles represent Li. The spherical shape of the precipitates has been experimentally verified (Figure 42). Thompson and Nobel[11] have determined the misfit to be approximately -0.2%. The small misfit is consistent with the observation of spherical precipitates.

Using Lifshitz-Wagner formalism, Tamura, Mori, and Nakamura have determined the interfacial energy between the metastable Al_3Li and the Al matrix as 0.18 $\frac{\text{joules}}{m^2}$.[22] In contrast, the interfacial energy of Al_2Cu (θ') has been determined in an Al-4.0 Cu alloy as 1.5 j/m^2.[19] The physical interpretation of the interfacial energy can readily be rationalized on the basis of homogeneous nucleation theory. A low interfacial energy means low activation barrier to homogeneous nucleation. The lower the interfacial energy, the greater the tendency toward homogeneous nucleation.

Although the A_3B, Ll_2-type metastable precipitate is not found in other commercial aluminum base alloys, it is of prime importance in nickel base alloys. The strengthening phase, γ', has an Ni_3X structure, where X = Al, Ti, Si, or Nb. These precipitates are coherent with the matrix and have a low misfit. As the misfit increases in these systems above $|0.3\%|$, the precipitates change from spherical to cubic. Because of the similarity between the Ni-X systems and the Al-Li systems, much of the technology from these alloys can perhaps be utilized and transferred to the Al-Li systems.

Precipitation in Al-Mg-Li and Al-Cu-Li Alloys

As pointed out earlier, the metastable precipitate which forms after quenching an Al-Li binary alloy from above the solvus temperature is the ordered, Ll_2, Al_3Li precipitate. To understand the deformation process and alloy chemistry effects in other Al alloys which contain Li, it is important to know the phases which are precipitating both homogeneously and heterogeneously.

The aging sequence of ternary Al-Mg-Li has been shown by other workers[23] and substantiated in this program as:

$$\text{supersaturated solid solution} \rightarrow \delta'(Al_3Li) \rightarrow Al_2MgLi.$$

The δ' metastable phase is the precipitate which is responsible for strengthening. It is essentially unaltered by the presence of Mg. The beneficial effect of Mg on the mechanical properties of the alloy system is attributed to a component of solid solution strengthening. The Al_2MgLi which transforms from δ' upon prolonged aging is incoherent and as such does not contribute significantly to the strength of the alloy as does the coherent δ'. In addition, Al_2MgLi can precipitate heterogeneously on grain boundaries or subgrain boundaries during either quenching or aging.

Figure 43 is a series of optical micrographs showing the effect of Mg additions on grain boundary precipitation in an Al-2.0% Li alloy.[24] This observation is consistent with the hypothesis that Al_2MgLi is precipitating on the boundaries.

Precipitation in the Al-4.5 Cu-1.5 Li alloy (2020) follows the scheme:

$$\text{supersaturated solid solution} \begin{cases} \rightarrow \text{G.P.I.} \rightarrow \text{G.P.II} \rightarrow \theta'' \\ \rightarrow \delta' \ (Al_3Li) \end{cases}$$

The copper precipitates independently of Li and follows the sequence that occurs in an Al-Cu binary system. Coincidentally, Li precipitates as Al_3Li (δ'). The Al_2Cu-type precipitate can be readily identified by its crystallographic nature with respect to the aluminum matrix (Figure 44). In the early stages of aging, streaking in the selected area diffraction (SAD) patterns are readily identified with Al_2Cu platelets (Figure 44b). The presence of the phase can be demonstrated by the presence of the superlattice reflections in the SAD. A dark-field micrograph of the superlattice reflection shows the very uniform high volume fraction of the phase (Figure 45).

An Al-4.5 Cu-1.5 Li alloy would be an Al-1.88 Cu-5.73 Li alloy based on atomic percent. Because of the facts that Li is so light and the δ' structure has a ratio of 3:1, Al:Li produces a high volume fraction of Al_3Li. The development of the high strength in 2020 alloy is attributed to the co-precipitation of the metastable Al_3Li and Al_2Cu precipitates.

Small additions of Cd have been added to 2020 alloys and improvement in strength resulted. The observation of increased strength in 2020 by the addition of Cd is principally related to the effect of Cd on the Al_2Cu precipitation reaction. The Cd reduces the interfacial free energy between the Al_2Cu and the aluminum matrix from 1.5 to 0.25 J/m^2. The reduction in interfacial energy reduces the barrier to homogeneous nucleation resulting in a finer distribution of the metastable Al_2Cu precipitates. Consequently, a high strength alloy will result when Cd is added to an Al-Cu alloy in which Al_2Cu precipitates form.

Mechanical Properties of Alloys Containing Al_3Li

Based on the preceeding discussion, alloys which contain a sufficient amount of Li to produce a large volume fraction of Al_3Li can be readily classified together. The similarities in these alloys can be rationalized on the effect of the metastable Al_3Li precipitate structure on the mechanical properties of the alloy system.

The motion of a unit dislocation in a superlattice will not recreate the structure in its wake, so disorder, in the form of an antiphase boundary, will result (Figure 46). To eliminate the extra energy necessary to create the antiphase boundary, motion of an identical pair of unit dislocations is required (Figure 47). The dislocations are connected by a strip of antiphase boundary. The separation of the two dislocations is a balance between the repulsive force of the two dislocations of the same sign with the force imposed by the structure to maintain its order. When dislocations move in such a manner, there will be no net change in order behind the dislocation pair. These unit dislocations are referred to as superlattice dislocations.

Coherent, ordered, metastable precipitates in a matrix will also affect the generation and motion of dislocations. The existence of superdislocations in Al-Li binary alloys has been shown by other investigators[20] and has been substantiated in this program (see Appendix C). The slip morphology in alloys which contain ordered precipitates depends upon the precipitate size and volume fraction. For commercially significant Al-Li structures, the volume fraction is high and the precipitates are approximately .07 μm in diameter. The deformation mechanisms can thus be rationalized on the basis of deformation in a structure with ordered precipitates.

The work hardening and fracture characteristics of an alloy can be correlated with its slip character. There are two aspects of slip that must be considered. One is based on continuum plasticity concepts[27] and the other involves the ability of screw dislocations to cross-slip out of the primary glide plane.[25]

For a randomly oriented polycrystal to exhibit constant volume deformation, it must deform on at least five independent slip systems. This condition is easily satisfied in a FCC lattice.

Cross-slip has the important microscopic effect of influencing the rate of work hardening. In a structure which contains a high volume fraction of ordered precipitates, the requirement for motion of paired, identical unit dislocations restricts the ease of cross-slip. The first dislocation of the pair will cross-slip on a particular plane, but the trailing dislocation is forced to cross-slip onto a parallel, but different, plane. Movement on two different glide planes would lead to the creation of an unlimited antiphase boundary, so the unit dislocations become sessile. Other dislocations from the same source will not be able to move large distances before being held up at this barrier. For further slip to take place, sources on neighboring planes will have to become operative. The successive pinning of the dislocations leads to the high work hardening rate in alloys containing a high volume fraction of δ'. Because of the high work hardening rate, the tensile strength of alloys containing only δ' as the hardening precipites is appreciably higher than the yield strength.

The development of large stress concentrations at high angle boundaries would result during deformation because of limited cross-slip. If this stress exceeds the strength of the grain boundary before additional dislocation sources can operate, the boundaries begin to separate.

To produce high strength Al-Li alloys, the rationale in the past has been to add other elements which would either co-precipitate or add a component of solid solution strengthening. The major disadvantage of the approach has been in the stimulation of

heterogeneous precipitation on grain boundaries and on subgrain boundaries. By precipitation on these boundaries, the strength of the boundaries decreases, thus leading to limited elongation prior to fracture along high angle boundaries. Furthermore, analogy to nickel base alloys suggests that trace amounts of certain impurity elements segregated at subgrain boundaries would be more harmful than in conventional aluminum alloys. Fracture mode in nickel base alloys which harden by an Ll_2 metastable phase ($Ni-Ni_3Al$, for example) was intergranular and ductility was unacceptable until impurity levels were reduced by repeated vacuum melting.

CONCLUSIONS

1. Al-Mg-Li alloys containing up to 3.0 Li and 4.8 Mg can be cast and extruded.

2. Extrusion pressure was independent of Li content but progressively increased with increasing Mg.

3. The specific tensile strength (strength/density) of the high strength Al-Mg-Li alloy was the same as that of 7050-T76 extrusions, and the ratio of elastic modulus:density was up to 30% greater than that of alloy 7050.

4. Strength and elastic modulus increased with increasing Li, while density decreased.

5. Mg contributed a component of solid solution strengthening to the alloys and decreased density.

6. An addition of 0.3 Mn suppresses recrystallization in Al-Mg-Li extrusions.

7. Be and Cd additions did not noticeably affect mechanical properties.

8. The high work hardening rate of alloys which contain a high volume fraction of Al_3Li (δ') as the primary strengthening precipitate is attributed to the ordered precipitate structure which effectively locks dislocations.

9. The low notch toughness and fracture along subgrain boundaries of artificially aged Al-Mg-Li extrusions is attributed to: (a) a build-up of high stress concentrations at the boundaries by a combination of limited cross-slip and dislocation locking and (b) reduction in grain boundary strength as a consequence of heterogeneous precipitation of Al_2MgLi or segregation of trace elements on grain boundaries.

RECOMMENDATIONS FOR FUTURE WORK

The next contract period will emphasize matrix deformation and grain boundary and subgrain boundary structure and their relationships to fracture toughness and fracture mode. In light of the model that premature grain boundary failure can be related to heterogeneous precipitation, a series of alloys will be fabricated which will contain lithium as the only strengthening solute. Alloys in the composition range 3.0-5.0 Li will be emphasized since it is this range which will provide the acceptable strength levels necessary for a commercial alloy.

To maintain the desired fine subgrain structure, unrecrystallized extrusions will be evaluated. Also, using material fabricated from powder, high solute (approximately 5% Li), fine grained structure will be possible.

The nucleation of Al_3Li (δ') will be studied utilizing the complementary techniques of differential scanning calorimetry (DSC) and transmission electron microscopy (TEM). The effect of aging temperature, heatup rate, and resultant structure on fracture mode will be carefully investigated. Once an optimum heat treatment practice is established, the extruded alloys will be solution heat treated, quenched, and artificially aged to evaluate their tensile and notch tensile properties.

The postulated effect of impurity segregation will be determined by scanning Auger spectroscopy. If confirmed, efforts will be made to produce a high purity Al-Li alloy for evaluation.

ACKNOWLEDGMENT

I would like to express my thanks to Mr. Paul Maynard of the Columbus Division of Rockwell, International, for providing the 2020 plate used in this program.

TABLE 1

TARGET COMPOSITIONS OF ALLOYS FOR DETERMINATION OF OPTIMUM SOLUTE CONTENT*

Alloy	Mg	Li	Ti	Be	Cd
1	2.0	2.5	0.02	0.005	--
2	2.0	3.0	0.02	0.005	--
3	2.0	3.5	0.02	0.005	--
4	3.5	2.0	0.02	0.005	--
5	3.5	2.5	0.02	0.005	--
6	3.5	3.0	0.02	0.005	--
7	5.0	1.5	0.02	0.005	--
8	5.0	2.0	0.02	0.005	--
9	5.0	2.5	0.02	0.005	--
10	3.5	2.5	0.02	0.005	0.1
11	3.5	2.5	0.02	0.01	0.1

*Alloys will also contain 0.3 Mn.

TABLE 2

MELT ANALYSES - PHASE II INGOTS

Alloy	S. Number	Si	Fe	Cu	Mn	Mg	Cr	Ni	Zn	Ti	Be	Cd	Li
1	427473A	0.04	0.04	0.00	0.28	2.03	0.00	0.00	0.00	0.02	0.004	--	2.52
2	427474B	0.04	0.04	0.00	0.27	2.10	0.00	0.00	0.00	0.02	0.004	--	2.99
3	427475C	0.04	0.04	0.00	0.27	2.02	0.00	0.00	0.00	0.02	0.004	--	3.54
4	427476A	0.04	0.04	0.00	0.28	3.60	0.00	0.00	0.00	0.02	0.004	--	2.00
5	427477A	0.04	0.04	0.00	0.28	3.54	0.00	0.00	0.00	0.02	0.004	--	2.52
6	427478A	0.04	0.04	0.00	0.27	3.51	0.00	0.00	0.00	0.02	0.004	--	2.93
7	427479A	0.04	0.04	0.00	0.28	4.98	0.00	0.00	0.00	0.02	0.004	--	1.50
8	427480A	0.05	0.04	0.00	0.27	5.08	0.00	0.00	0.00	0.02	0.004	--	1.97
9	427481A	0.05	0.04	0.00	0.27	5.12	0.00	0.00	0.00	0.02	0.005	--	2.51
10	427482A	0.04	0.05	0.00	0.27	3.63	0.00	0.00	0.00	0.02	0.005	0.10	2.53
11	427483A	0.04	0.04	0.00	0.27	3.59	0.00	0.00	0.00	0.02	0.008	0.10	2.52

TABLE 3

OPTIMUM SOLUTION HEAT TREATMENT TEMPERATURES
PHASE II EXTRUSIONS

Alloy	Solution Heat Treatment Temperature, °F
1	850
2	900
3	950
4	850
5	950
6	950
7	850
8	850
9	950
10	950
11	950

TABLE 4

EXTRUSION DATA FOR PHASE II SIX-INCH DIAMETER DC INGOTS

Alloy	Ingot S. Number	Reheat Temp., °F	Extr. Temp., °F	Extr. Speed, in./min	Breakout Pressure, ksi	Butt Length, inch	Extrusion S. Number
1	427473A	700	720	4	148	4	427599
2	427474B	700	716	3-1/2-4	99	1-1/2	427600
2	427474B	700	709	3-1/2-4	98	1-1/2	427600
3	427475C	700	704	3-1/2-4	83	1-1/2	427601
3	427475C	700	710	3-1/2-4	79	1-1/2	427601
4	427476A	700	702	3-1/2-4	116	1-1/2	427602
4	427476A	700	710	3-1/2-4	112	1-1/2	427602
5	427477A	700	708	3-1/2-4	111	1-1/2	427603
5	427477A	700	703	3-1/2-4	112	1-1/2	427603
6	427478A	700	701	3-1/2-4	116	1-1/2	427604
6	427478A	700	698	3-1/2-4	112	1-1/2	427604
7	427479A	700	700	3-1/2-4	131	1-1/2	427605
7	427479A	700	711	3-1/2-4	126	1-1/2	427605
8	427480A	700	706	3-1/2-4	128	1-1/2	427606
8	427480A	700	711	3-1/2-4	126	1-1/2	427606
9	427481A	700	698	3-1/2-4	126	1-1/2	427607
9	427481A	700	698	3-1/2-4	126	1-1/2	427607
10	427482A	700	701	3-1/2-4	116	1-1/2	427608
10	427482A	700	710	3-1/2-4	112	1-1/2	427608
11	427483A	700	700	3-1/2-4	114	1-1/2	427609
11	427483A	700	702	3-1/2-4	112	1-1/2	427609

Note: Ingots for alloys 2-11 were cut in half prior to extruding. Data for both halves are indicated.

TABLE 5

REMELT ANALYSES - PHASE II EXTRUSIONS

Alloy	S. Number	Si	Fe	Cu	Mn	Mg	Cr	Ni	Zn	Ti	Be	Cd	Li
1	427599	0.04	0.04	0.00	0.28	2.03	0.00	0.00	0.00	0.02	0.004	--	2.30
2	427600	0.04	0.03	0.00	0.28	1.99	0.00	0.00	0.00	0.02	0.004	--	2.76
3	427601	0.04	0.03	0.00	0.28	1.94	0.00	0.02	0.00	0.02	0.004	--	3.14
4	427602	0.04	0.04	0.00	0.28	3.51	0.00	0.00	0.00	0.02	0.004	--	1.80
5	427603	0.04	0.03	0.00	0.28	3.50	0.00	0.00	0.00	0.02	0.004	--	2.28
6	427604	0.04	0.03	0.00	0.27	3.55	0.00	0.00	0.00	0.02	0.004	--	2.71
7	427605	0.04	0.04	0.00	0.28	4.89	0.00	0.00	0.00	0.02	0.004	--	1.37
8	427606	0.04	0.04	0.00	0.27	4.89	0.00	0.00	0.00	0.02	0.004	--	1.81
9	427607	0.04	0.04	0.00	0.27	4.84	0.00	0.00	0.00	0.02	0.004	--	2.33
10	427608	0.04	0.04	0.00	0.28	3.44	0.00	0.00	0.00	0.02	0.004	0.10	2.26
11	427609	0.04	0.04	0.00	0.27	3.34	0.00	0.00	0.00	0.02	0.007	0.09	2.19

TABLE 6

THE EFFECTS OF SOLUTION HEAT TREATMENT TEMPERATURE ON TENSILE PROPERTIES OF ALLOYS 1 AND 2

Solution Heat Treatment Temperature, °F	Sample Number	Longitudinal T.S., ksi	Longitudinal Y.S., ksi	Longitudinal % El. in 2.0"	Longitudinal R of A, %	Transverse T.S., ksi	Transverse Y.S., ksi	Transverse % El. in 0.64"	Transverse R of A, %
Alloy 1 - S. No. 427599									
800	1	64.5	63.5	1.6[1]	--	55.9	37.8	3.1[1]	3
825	2	62.5	([2])	([1,2])	--	52.6	39.5	3.1	7
850	3	63.2	61.0	1.6[1]	--	53.9	37.6	3.1	6
875	4	63.0	58.3	1.6[1]	--	53.2	39.1	3.1	5
900	5	61.0	55.4	3.1	6	56.0	37.6	3.1	6
925	6	60.0	53.7	6.2	8	52.2	36.8	3.1	4
950	7	58.6	50.5	4.7	7	52.5	37.8	3.1	7
As Extruded/Artificially Aged	8	64.5	61.3	1.6[1]	--	54.1	38.3	3.1	4
As Extruded	9	47.5	33.3	12.5	24	44.6	31.7	10.9	15
Alloy 2 - S. No. 427600									
800	1	65.2	63.5	1.6[1]	--	52.9	41.0	3.1	5
825	2	65.2	([2])	([1,2])	--	56.1	41.9	3.1	2
850	3	67.6	65.0	1.6[1]	--	54.9	43.1	1.6[1]	1
875	4	67.9	67.2	--[1]	--	56.9	46.3	3.1	2
900	5	65.4	([2])	([1,2])	--	59.8	44.1	1.6	4
925	6	67.1	64.6	1.6	1	54.4	43.6	1.6	1
950	7	65.2	59.8	1.6	5	53.4	42.7	1.6[1]	1
As Extruded/Artificially Aged	8	59.9	52.7	1.6[1]	--	53.2	36.4	4.7	4
As Extruded	9	52.2	34.4	9.4	9	44.3	24.3	7.8	9

Samples 1 through 7 solution heat treated 1 hour at temperatures indicated, quenched in cold water, and artificially aged 48 hours at 375°F.

NOTES: 1. Failed outside of gauge length.
2. Failed before 0.2% offset was obtained.

TABLE 7

THE EFFECTS OF SOLUTION HEAT TREATMENT TEMPERATURE ON TENSILE PROPERTIES OF ALLOYS 3 AND 4

Solution Heat Treatment Temperature, °F	Sample Number	Longitudinal T.S., ksi	Longitudinal Y.S., ksi	Longitudinal % El. in 2.0"	Longitudinal R of A, %	Transverse T.S., ksi	Transverse Y.S., ksi	Transverse % El. in 0.64"	Transverse R of A, %
Alloy 3 - S. No. 427601									
800	1	64.1	62.9	--[1]	--	52.5	40.7	3.1	4
850	3	71.8	65.1	2.0	--	56.4	44.3	3.1[1]	1
900	5	74.1	67.1	2.0	--	57.3	45.1	3.1	1
950	7	71.9	66.9	2.0	--	60.2	45.9	3.1	1
Alloy 4 - S. No. 427602									
800	1	57.4	43.4	10.9	21	50.0	32.6	7.8	8
825	2	56.3	41.5	12.5	20	51.2	33.7	6.2	7
850	3	58.2	45.3	10.9	24	46.3	31.1	6.2	11
875	4	59.7	45.5	6.2[1]	7	50.0	32.4	6.2	1
900	5	58.1	43.6	9.4	19	48.3	32.4	6.2	8
925	6	58.9	46.0	9.4	19	52.9	33.4	6.2	8
950	7	57.1	44.6	9.4	19	50.5	32.1	7.8	15
As Extruded/Artificially Aged	8	59.7	45.8	6.2[1]	5	49.0	32.9	6.2	5
As Extruded	9	44.8	24.8	17.2	37	36.3	16.9	15.6	18

Samples 1 through 7 solution heat treated 1 hour at temperatures indicated, quenched in cold water, and artificially aged 48 hours at 375°F.

NOTE: 1. Failed outside of gauge length.

TABLE 8

THE EFFECTS OF SOLUTION HEAT TREATMENT TEMPERATURE ON TENSILE PROPERTIES OF ALLOYS 5 AND 6

Solution Heat Treatment Temperature, °F	Sample Number	Longitudinal T.S., ksi	Longitudinal Y.S., ksi	Longitudinal % El. in 2.0"	Longitudinal R of A, %	Transverse T.S., ksi	Transverse Y.S., ksi	Transverse % El. in 0.64"	Transverse R of A, %
Alloy 5 - S. No. 427603									
800	1	68.4	62.7	1.6[1]	--	60.6	41.8	6.2	3
825	2	68.1	63.0	1.6[1]	--	60.3	41.4	3.1[1]	4
850	3	67.9	60.5	1.6[1]	1	60.1	41.3	3.1[1]	2
875	4	68.2	60.7	1.6[1]	0	60.6	41.6	3.1	5
900	5	67.6	61.2	1.6[1]	2	61.0	40.7	3.1	5
925	6	67.6	59.6	1.6[1]	1	60.4	41.6	3.1	4
950	7	66.9	62.3	1.6[1]	--	59.7	42.1	3.1[1]	1
As Extruded/Artificially Aged	8	68.8	61.6	1.6[1]	1	59.7	41.1	3.1	5
As Extruded	9	61.8	54.4	4.7	8	57.9	33.7	7.8	9
Alloy 6 - S. No. 427604									
800	1	68.6	63.4	1.6[1]	--	54.6	43.6	1.6	1
825	2	70.3	65.3	1.6[1]	1	55.9	44.4	1.6	1
850	3	70.3	65.6	1.6[1]	--	58.7	45.8	1.6	2
875	4	70.8	66.1	1.6[1]	1	60.0	44.9	1.6	2
900	5	70.5	67.1	1.6[1]	--	56.9	45.6	1.6	--
925	6	69.3	64.6	1.6[1]	--	58.4	45.3	3.1	2
950	7	70.3	64.6	1.6[1]	1	64.1	46.0	1.6[1]	1
As Extruded/Artificially Aged	8	66.1	57.7	1.6[1]	1	57.1	38.7	3.1	4
As Extruded	9	62.9	55.9	1.6[1]	1	53.7	30.3	6.2	7

Samples 1 through 7 solution heat treated 1 hour at temperatures indicated, quenched in cold water, and artificially aged 48 hours at 375°F.

NOTE: 1. Failed outside of gauge length.

TABLE 9

THE EFFECTS OF SOLUTION HEAT TREATMENT TEMPERATURE ON TENSILE PROPERTIES OF ALLOYS 7 AND 8

Solution Heat Treatment Temperature, °F	Sample Number	Longitudinal T.S., ksi	Longitudinal Y.S., ksi	Longitudinal % El. in 2.0"	Longitudinal R of A, %	Transverse T.S., ksi	Transverse Y.S., ksi	Transverse % El. in 0.64"	Transverse R of A. %
Alloy 7 - S. No. 427605									
800	1	50.5	27.0	17.2	30	48.0	26.6	15.6	17
825	2	50.5	26.2	20.3	28	48.3	26.7	15.6	18
850	3	47.8	26.9	10.9[1]	7	48.0	24.8	17.2	23
875	4	50.5	27.0	17.2	27	46.0	24.5	17.2	25
900	5	51.0	28.2	17.2	25	47.5	27.0	17.2	21
925	6	50.0	28.0	18.8	28	47.8	27.2	17.2	21
950	7	50.2	28.5	17.2	25	48.0	27.1	14.1[1]	16
As Extruded/Artificially Aged	8	50.5	26.0	20.3	27	45.8	25.2	18.8	24
As Extruded	9	46.5	24.5	23.4	40	42.8	20.5	20.3	26
Alloy 8 - S. No. 427606									
800	1	64.7	46.6	9.4	14	59.9	38.9	7.8	5
825	2	66.3	47.5	7.8	9	58.9	38.0	6.2	6
850	3	65.6	46.3	4.7[1]	4	56.9	38.1	3.1	3
875	4	65.2	45.6	6.2[1]	5	58.7	37.6	4.7[1]	4
900	5	64.1	45.5	6.2	9	57.2	38.8	4.7	4
925	6	64.9	46.8	6.2[1]	5	61.4	38.9	7.8	9
950	7	65.3	45.5	6.2[1]	5	56.9	37.6	4.7	3
As Extruded/Artificially Aged	8	65.3	48.0	9.4	10	53.7	37.4	4.7	4
As Extruded	9	50.5	27.7	23.4	27	49.0	22.8	18.8	26

Samples 1 through 7 solution heat treated 1 hour at temperatures indicated, quenched in cold water, and artificially aged 48 hours at 375°F.

NOTE: 1. Failed outside of gauge length.

TABLE 10

THE EFFECTS OF SOLUTION HEAT TREATMENT TEMPERATURE ON TENSILE PROPERTIES OF ALLOY 9

Solution Heat Treatment Temperature, °F	Sample Number	Longitudinal T.S., ksi	Longitudinal Y.S., ksi	Longitudinal % El. in 2.0"	Longitudinal R of A, %	Transverse T.S., ksi	Transverse Y.S., ksi	Transverse % El. in 0.64"	Transverse R of A, %
Alloy 9 - S. No. 427607									
800	1	69.6	55.4	3.1[1]	--	68.9	43.1	4.7	5
825	2	69.6	57.4	1.6[1]	2	64.6	45.9	4.7	4
850	3	70.0	57.2	1.6[1]	1	62.7	44.9	1.6[1]	1
875	4	69.9	56.4	1.6[1]	1	59.0	43.9	3.1	3
900	5	70.1	57.8	1.6[1]	1	57.6	44.6	1.6	1
925	6	68.6	58.2	1.6[1]	1	53.2	44.6	1.6[1]	1
950	7	68.6	55.7	1.6[1]	2	53.4	44.9	1.6[1]	2
As Extruded/Artificially Aged	8	68.4	51.7	3.1[1]	4	59.5	40.7	3.1	2
As Extruded	9	67.8	51.2	6.2[1]	5	60.3	35.3	6.2	6

Samples 1 through 7 solution heat treated 1 hour at temperatures indicated, quenched in cold water, and artificially aged 48 hours at 375°F.

NOTE: 1. Failed outside of gauge length.

TABLE 11

THE EFFECTS OF SOLUTION HEAT TREATMENT TEMPERATURE ON NOTCH TOUGHNESS OF ALLOYS 1 AND 2

Solution Heat Treatment Temperature, °F	Sample Number	Longitudinal Y.S., ksi	Longitudinal N.T.S., ksi	Longitudinal NTS/YS	Transverse Y.S., ksi	Transverse N.T.S., ksi	Transverse NTS/YS
Alloy 1 - S. No. 427599							
800	1	63.5	78.7	1.24	37.8	52.6	1.39
825	2	(1)	77.6	--	39.5	49.0	1.24
850	3	61.0	78.1	1.28	37.6	54.1	1.44
875	4	58.3	77.1	1.32	39.1	53.9	1.38
900	5	55.4	77.6	1.40	37.6	53.1	1.41
925	6	53.7	76.6	1.43	36.8	54.1	1.47
950	7	50.5	75.8	1.50	37.8	56.2	1.49
As Extruded/Artificially Aged	8	61.3	76.6	1.25	38.3	51.1	1.33
As Extruded	9	33.3	58.7	1.76	31.7	42.1	1.33
Alloy 2 - S. No. 42760							
800	1	63.5	73.0	1.15	41.0	47.0	1.15
825	2	(1)	72.5	--	41.9	46.5	1.11
850	3	65.0	74.1	1.14	43.1	46.0	1.07
875	4	67.2	70.5	1.05	46.3	39.3	0.85
900	5	(1)	72.0	--	44.1	47.2	1.07
925	6	64.6	72.0	1.11	43.6	46.0	1.06
950	7	59.8	70.0	1.17	42.7	44.9	1.05
As Extruded/Artificially Aged	8	52.7	66.4	1.26	36.4	39.3	1.08
As Extruded	9	34.4	56.2	1.63	24.3	40.9	1.68

Samples 1 through 7 solution heat treated 1 hour at temperatures indicated, quenched in cold water, and artificially aged 48 hours at 375°F.

NOTE: 1. Failed before 0.2% offset was obtained.

TABLE 12

THE EFFECTS OF SOLUTION HEAT TREATMENT TEMPERATURE ON NOTCH TOUGHNESS OF ALLOYS 3 AND 4

Solution Heat Treatment Temperature, °F	Sample Number	Longitudinal Y.S., ksi	Longitudinal N.T.S., ksi	Longitudinal NTS/YS	Transverse Y.S., ksi	Transverse N.T.S., ksi	Transverse NTS/YS
		Alloy 3 - S. No. 427601					
800	1	62.9	65.1	1.03	40.7	(1)	--
850	3	65.1	59.2	0.91	44.3	(1)	--
900	5	67.1	62.8	0.94	45.1	(1)	--
950	7	66.9	59.2	0.88	45.9	(1)	--
		Alloy 4 - S. No. 427602					
800	1	43.4	70.5	1.62	32.6	53.9	1.64
825	2	41.5	73.0	1.76	33.7	56.2	1.67
850	3	45.3	70.5	1.56	31.1	57.7	1.86
875	4	45.5	69.5	1.53	32.4	56.7	1.75
900	5	43.6	69.5	1.59	32.4	58.0	1.79
925	6	46.0	71.0	1.54	33.4	58.7	1.76
950	7	44.6	70.5	1.58	32.1	55.7	1.74
As Extruded/Artificially Aged	8	45.8	66.4	1.45	32.9	53.6	1.63
As Extruded	9	24.8	49.0	1.98	16.9	38.3	2.27

Samples 1 through 7 solution heat treated 1 hour at temperatures indicated, quenched in cold water, and artificially aged 48 hours at 375°F.

NOTE: 1. Not determined.

TABLE 13

THE EFFECTS OF SOLUTION HEAT TREATMENT TEMPERATURE ON NOTCH TOUGHNESS OF ALLOYS 5 AND 6

Solution Heat Treatment Temperature, °F	Sample Number	Longitudinal Y.S., ksi	Longitudinal N.T.S., ksi	Longitudinal NTS/YS	Transverse Y.S., ksi	Transverse N.T.S., ksi	Transverse NTS/YS
		Alloy 5 - S. No. 427603					
800	1	62.7	77.1	1.23	41.8	44.4	1.06
825	2	63.0	76.6	1.22	41.4	46.5	1.12
850	3	60.5	73.5	1.21	41.3	46.0	1.11
875	4	60.7	73.8	1.22	41.6	43.9	1.06
900	5	61.2	75.1	1.23	40.7	44.7	1.10
925	6	59.6	74.1	1.24	41.6	43.7	1.05
950	7	62.3	78.7	1.26	42.1	47.0	1.12
As Extruded/Artificially Aged	8	61.6	74.6	1.21	41.1	51.6	1.26
As Extruded	9	54.4	72.0	1.32	33.7	57.7	1.71
		Alloy 6 - S. No. 427604					
800	1	63.4	63.8	1.01	43.6	36.8	0.84
825	2	65.3	65.1	1.00	44.4	38.3	0.86
850	3	65.6	63.3	0.96	45.8	37.3	0.81
875	4	66.1	61.8	0.93	44.9	37.3	0.83
900	5	67.1	58.2	0.87	45.6	39.3	0.86
925	6	64.6	62.3	0.96	45.3	36.3	0.80
950	7	64.6	59.8	0.93	46.0	35.8	0.78
As Extruded/Artificially Aged	8	57.7	55.7	0.97	38.7	36.3	0.94
As Extruded	9	55.9	65.4	1.17	30.3	45.5	1.50

Samples 1 through 7 solution heat treated 1 hour at temperatures indicated, quenched in cold water, and artificially aged 48 hours at 375°F.

TABLE 14

THE EFFECTS OF SOLUTION HEAT TREATMENT TEMPERATURE ON NOTCH TOUGHNESS OF ALLOYS 7 AND 8

Solution Heat Treatment Temperature, °F	Sample Number	Longitudinal Y.S., ksi	Longitudinal N.T.S., ksi	Longitudinal NTS/YS	Transverse Y.S., ksi	Transverse N.T.S., ksi	Transverse NTS/YS
		Alloy 7 - S. No. 427605					
800	1	27.0	52.6	1.95	26.6	43.4	1.63
825	2	26.2	52.6	2.01	26.7	43.9	1.64
850	3	26.9	50.1	1.86	24.8	43.2	1.74
875	4	27.0	51.1	1.89	24.5	43.9	1.79
900	5	28.2	52.1	1.85	27.0	43.4	1.61
925	6	28.0	51.1	1.83	27.2	43.9	1.61
950	7	28.5	50.1	1.76	27.1	41.4	1.53
As Extruded/Artificially Aged	8	26.0	51.1	1.97	25.2	43.9	1.74
As Extruded	9	24.5	43.4	1.77	20.5	44.4	2.17
		Alloy 8 - S. No. 427606					
800	1	46.6	61.3	1.32	38.9	35.5	0.91
825	2	47.5	61.3	1.29	38.0	33.7	0.89
850	3	46.3	59.8	1.29	38.1	35.2	0.92
875	4	45.6	58.0	1.27	37.6	36.8	0.98
900	5	45.5	59.8	1.31	38.8	33.7	0.87
925	6	46.8	57.2	1.22	38.9	33.5	0.86
950	7	45.5	56.2	1.24	37.6	31.2	0.83
As Extruded/Artificially Aged	8	48.0	59.8	1.25	37.4	32.2	0.86
As Extruded	9	27.7	56.2	2.03	22.8	48.0	2.11

Samples 1 through 7 solution heat treated 1 hour at temperatures indicated, quenched in cold water, and artificially aged 48 hours at 375°F.

TABLE 15

THE EFFECTS OF SOLUTION HEAT TREATMENT TEMPERATURE ON NOTCH TOUGHNESS OF ALLOY 9

Solution Heat Treatment Temperature, °F	Sample Number	Longitudinal Y.S., ksi	Longitudinal N.T.S., ksi	Longitudinal NTS/YS	Transverse Y.S., ksi	Transverse N.T.S., ksi	Transverse NTS/YS
		Alloy 9 - S. No. 427607					
800	1	55.4	55.7	1.01	43.1	35.8	0.83
825	2	57.4	59.8	1.04	45.9	32.2	0.70
850	3	57.2	50.1	0.88	44.9	32.7	0.73
875	4	56.4	51.3	0.91	43.9	32.2	0.73
900	5	57.8	54.6	0.94	44.6	28.6	0.64
925	6	58.2	56.2	0.97	44.6	30.1	0.67
950	7	55.7	57.2	1.03	44.9	30.1	0.67
As Extruded/Artificially Aged	8	51.7	52.6	1.02	40.7	36.0	0.88
As Extruded	9	51.2	65.9	1.29	35.3	48.8	1.38

Samples 1 through 7 solution heat treated 1 hour at temperatures indicated, quenched in cold water, and artificially aged 48 hours at 375°F.

TABLE 16

ROCKWELL B HARDNESSES OF ARTIFICIALLY AGED EXTRUSIONS OF ALLOYS 1 THROUGH 6[1]

Time, hrs	Aging Temperature, °F 300	325	350	375	400	Aging Temperature, °F 300	325	350	375	400
	Alloy 1 - S. No. 427599					Alloy 2 - S. No. 427600				
1	47.3	58.2	60.8	62.5	67.2	57.8	62.2	67.8	65.7	69.5
4	56.2	60.3	63.5	66.3	67.7	60.5	66.5	69.3	72.7	73.7
18	64.5	66.5	72.2	72.3	71.5	70.5	73.5	77.5	75.8	76.3
36	63.2	68.8	70.5	71.0	68.7	69.8	74.7	76.2	75.8	76.8
72	65.8	70.7	70.7	71.0	61.5	72.8	74.5	76.0	77.5	68.0
168	70.2	72.2	73.8	68.5	50.0	74.3	77.3	78.2	74.7	55.2
	Alloy 3 - S. No. 427601					Alloy 4 - S. No. 427602				
1	58.5	67.5	64.3	71.8	72.0	50.7	54.7	54.8	60.3	56.8
4	64.0	68.0	72.0	75.8	79.0	55.7	60.2	60.7	60.7	58.3
18	69.5	73.0	79.7	80.3	79.5	61.2	62.7	64.8	61.2	54.8
36	75.7	78.8	78.3	81.3	78.5	61.0	64.2	65.8	62.0	55.3
72	75.2	76.0	78.7	81.7	73.2	65.5	65.7	65.2	61.8	50.7
168	77.0	79.7	83.3	78.2	61.7	67.7	66.3	65.5	58.5	43.2
	Alloy 5 - S. No. 427603					Alloy 6 - S. No. 427604				
1	58.5	66.5	67.5	68.0	72.5	65.0	69.7	72.8	74.2	76.5
4	65.7	69.2	71.0	73.3	73.2	71.0	73.5	76.5	77.3	79.5
18	69.9	72.0	74.8	76.2	74.7	73.5	77.7	79.0	81.2	80.7
36	72.8	75.2	73.7	76.8	73.0	76.2	80.0	81.2	82.3	79.3
72	75.8	77.5	74.8	75.8	66.3	76.5	79.7	82.3	81.3	70.5
168	75.3	78.2	79.3	71.2	56.8	81.2	83.0	81.8	76.0	61.8

NOTE: 1. Indicated hardness values are average of three readings.

TABLE 17

ROCKWELL B HARDNESSES OF ARTIFICIALLY AGED EXTRUSIONS OF ALLOYS 7 THROUGH 11[1]

Time, hrs	Aging Temperature, °F					Aging Temperature, °F				
	300	325	350	375	400	300	325	350	375	400
	Alloy 7 - S. No. 427605					Alloy 8 - S. No. 427606				
1	36.7	34.8	37.7	36.8	35.5	63.2	66.5	68.2	68.2	68.0
4	39.0	38.5	35.2	36.7	36.5	68.3	68.7	71.2	70.7	69.3
18	54.5	43.0	44.7	40.3	39.2	71.2	73.3	73.5	73.2	68.7
36	61.0	46.5	43.8	40.8	43.2	72.8	75.0	74.6	73.7	67.3
72	65.7	56.7	53.2	44.8	45.3	74.7	74.8	74.2	71.2	61.2
168	64.3	57.3	53.2	48.5	46.5	76.0	75.7	73.8	65.2	54.5
	Alloy 9 - S. No. 427607					Alloy 10 - S. No. 427608				
1	66.2	70.2	73.7	73.7	76.8	66.2	65.8	70.5	72.8	73.2
4	70.7	74.7	76.0	78.2	77.8	67.8	68.7	73.7	73.8	76.7
18	74.5	75.8	77.3	78.8	78.5	72.3	72.7	76.8	77.3	75.0
36	78.3	78.3	79.5	80.8	77.3	75.5	77.2	78.0	78.5	70.0
72	79.0	81.2	81.7	79.5	69.8	75.3	79.2	79.8	75.3	61.8
168	81.2	82.5	82.0	73.8	62.8	77.5	79.2	78.7	65.3	61.8
	Alloy 11 - S. No. 427609									
1	62.0	67.2	68.7	71.5	73.5					
4	67.2	68.7	70.7	74.5	77.5					
18	70.2	73.3	76.7	76.5	75.7					
36	75.0	77.5	77.5	79.3	70.7					
72	76.2	78.3	79.8	76.7	63.7					
168	79.5	81.3	78.7	66.3	61.8					

NOTE: 1. Indicated hardness values are average of three readings.

TABLE 18

AGING PRACTICES FOR MATERIAL EVALUATION

Alloy	Age No. 1	Age No. 2	Age No. 3
1	18 hr @ 375°F	72 hr @ 400°F	--
2	72 hr @ 375°F	72 hr @ 400°F	18 hr @ 350°F
3	48 hr @ 375°F	72 hr @ 400°F	--
4	48 hr @ 350°F	--	--
5	36 hr @ 375°F	48 hr @ 400°F	72 hr @ 325°F
6	48 hr @ 375°F	48 hr @ 400°F	--
7	72 hr @ 300°F	--	--
8	48 hr @ 325°F	36 hr @ 400°F	--
9	72 hr @ 350°F	48 hr @ 400°F	--
10	72 hr @ 350°F	36 hr @ 400°F	--
11	72 hr @ 350°F	36 hr @ 400°F	--

NOTES: Age No. 1 selected to produce maximum or near maximum hardness.

Age No. 2 selected to produce 90 percent of maximum hardness by overaging.

Age No. 3 selected to produce high hardness by aging to initial hardness peak.

TABLE 19

TENSILE PROPERTIES OF Al-Mg-Li EXTRUSIONS

Alloy	S. No.	Mg	Li	Practice 1 Aged to Max Strength			Practice 2 Overaged			Practice 3 Aged to Max Strength-Alternate		
				Longitudinal								
				T.S., ksi	Y.S., ksi	% El. in 1.4"	T.S., ksi	Y.S., ksi	% El. in 1.4"	T.S., ksi	Y.S., ksi	% El. in 1.4"
1	427599	2.03	2.30	65.20	59.65	4.3	57.90	36.45	7.9	--	--	--
2	427600	1.99	2.76	70.70	57.90	3.6	58.30	35.70	5.7	68.80	(1)	1.8
3	427601	1.94	3.14	70.00	61.35	1.4	59.00	36.20	4.3	--	--	--
4	427602	3.51	1.80	59.75	48.95	10.0	--	--	--	--	--	--
5	427603	3.50	2.28	71.50	62.65	3.9	64.70	42.60	5.7	67.30	63.15	3.6
6	427604	3.55	2.71	76.00	66.05	2.1	67.55	44.35	3.2	--	--	--
7	427605	4.89	1.37	60.50	41.55	14.6	--	--	--	--	--	--
8	427606	4.89	1.81	69.05	53.30	9.0	63.20	37.75	7.5	--	--	--
9	427607	4.84	2.33	75.00	64.30	2.9	63.45	41.25	3.2	--	--	--
10	427608	3.44	2.26+.1 Cd	73.70	66.65	2.9	60.70	34.85	5.7	--	--	--
11	427609	3.34	2.19+.09 Cd +.007 Be	73.80	66.70	2.9	61.50	36.75	5.7	--	--	--
				Transverse								
				T.S., ksi	Y.S., ksi	% El. in 0.5"	T.S., ksi	Y.S., ksi	% El. in 0.5"	T.S., ksi	Y.S., ksi	% El. in 0.5"
1	427599	2.03	2.30	53.35	36.45	4.0	50.15	31.70	7.0	--	--	--
2	42760	1.99	2.76	60.45	43.15	3.0	53.35	32.60	5.0	55.05	40.35	4.0
3	427601	1.94	3.14	59.35	48.00	4.0	40.30	35.05	1.0	--	--	--
4	427602	3.51	1.80	52.85	33.75	7.0	--	--	--	--	--	--
5	427603	3.50	2.28	59.80	41.55	4.0	56.75	35.60	4.0	59.05	39.55	4.0
6	427604	3.55	2.71	61.10	45.55	6.0	57.45	39.05	4.0	--	--	--
7	427005	4.89	1.37	53.05	32.90	12.0	--	--	--	--	--	--
8	427606	4.89	1.81	53.25	39.30	4.0	45.95	32.70	2.0	--	--	--
9	427607	4.84	2.33	55.95	45.45	1.0	47.45	38.45	3.0	--	--	--
10	427608	3.44	2.26+.1 Cd	65.35	45.10	3.0	56.85	31.90	6.0	--	--	--
11	427609	3.34	2.19+.09 Cd +.007 Be	60.80	44.00	4.0	58.20	33.90	6.0	--	--	--

NOTE: 1. Failed before 0.2% offset was obtained.

TABLE 20

DENSITIES OF Al-Mg-Li EXTRUSIONS

Alloy	S. No.	Density grams/cm^3	Density lbs/in.^{3}	Mg	Li
1	427599	2.5217	0.0911	2.03	2.30
2	427600	2.4876	0.0899	1.99	2.76
3	427601	2.4504	0.0885	1.94	3.14
4	427602	2.5367	0.0916	3.51	1.80
5	427603	2.5027	0.0904	3.50	2.28
6	427604	2.4676	0.0891	3.55	2.71
7	427605	2.5474	0.0920	4.89	1.37
8	427606	2.5136	0.0908	4.89	1.81
9	427607	2.4680	0.0892	4.84	2.33
10	427608	2.5002	0.0903	3.44	2.26+.1 Cd
11	427609	2.5007	0.0903	3.34	2.19+.09 Cd+ .007 Be

TABLE 21

ELASTIC MODULI OF Al-Mg-Li EXTRUSIONS

Alloy	S. No.	Mg	Li	Modulus X(10^6) psi	Average
1	427599-L1	2.03	2.30	11.63	11.56
	427599-L2			11.49	
2	427600-L1	1.99	2.76	11.70	11.67
	427600-L2			11.63	
3	427601-L1	1.94	3.14	11.76	11.81
	427601-L2			11.85	
4	427602-L1	3.51	1.80	11.11	11.16
	427602-L2			11.20	
5	427603-L1	3.50	2.28	11.51	11.48
	427603-L2			11.44	
6	427604-L1	3.55	2.71	11.60	11.63
	427604-L2			11.66	
7	427605-L1	4.89	1.37	10.90	10.88
	427605-L2			10.85	
8	427606-L1	4.89	1.81	11.18	11.18
	427606-L2			11.17	
9	427607-L1	4.84	2.33	11.38	11.42
	426607-L2			11.45	
10	427608-L1	3.44	2.26	11.47	11.47
	427608-L2			11.47	
11	427609-L1	3.34	2.19	11.43	11.43
	427609-L2			11.43	

TABLE 22

NOTCH TOUGHNESS OF Al-Mg-Li EXTRUSIONS

Alloy	S. No.	Mg	Li	Practice 1 Aged to Max Strength			Practice 2 Overaged			Practice 3 Aged to Max Strength-Alternate		
				Y.S., ksi	NTS, ksi	NTS/YS	Y.S., ksi	NTS, ksi	NTS/YS	Y.S., ksi	NTS, ksi	NTS/YS
Longitudinal												
1	427599	2.03	2.30	59.65	74.05	1.25	36.95	61.55	1.67	--	--	--
2	427600	1.99	2.76	57.90	69.30	1.20	35.70	54.25	1.52	--	68.80	--
3	427601	1.94	3.14	61.35	55.65	0.91	36.20	48.75	1.35	--	--	--
4	427602	3.51	1.80	48.95	71.25	1.46	--	--	--	--	--	--
5	427603	3.50	2.28	62.65	75.60	1.21	42.60	60.00	1.41	63.15	75.10	1.19
6	427604	3.55	2.71	66.05	63.85	0.97	47.35	47.50	1.07	--	--	--
7	427605	4.89	1.37	41.55	68.95	1.66	--	--	--	--	--	--
8	427606	4.89	1.81	53.30	64.00	1.20	37.75	43.65	1.16	--	--	--
9	427607	4.84	2.33	64.30	63.05	0.98	41.25	39.35	0.95	--	--	--
10	427608	3.44	2.26+.1 Cd	66.65	75.20	1.13	34.85	53.25	1.53	--	--	--
11	427609	3.34	2.19+.09 Cd +.007 Be	66.70	77.10	1.16	36.75	53.85	1.47	--	--	--
Transverse												
1	427599	2.03	2.30	36.45	52.15	1.43	31.70	46.90	1.48	--	--	--
2	427600	1.99	2.76	43.15	39.30	0.91	32.60	36.50	1.12	40.35	58.10	1.44
3	427601	1.94	3.14	48.00	30.65	0.64	35.00	19.80	0.56	--	--	--
4	427602	3.51	1.80	33.75	57.45	1.70	--	--	--	--	--	--
5	427603	3.50	2.28	41.55	47.25	1.14	35.60	43.90	1.23	39.55	51.85	1.31
6	427604	3.55	2.71	45.55	35.30	0.77	39.05	30.90	0.79	--	--	--
7	427605	4.89	1.37	32.90	57.30	1.74	--	--	--	--	--	--
8	427606	4.89	1.81	39.30	40.10	1.02	32.70	36.05	1.10	--	--	--
9	427607	4.84	2.33	45.45	29.70	0.65	38.45	23.50	0.61	--	--	--
10	427608	3.44	2.26+.1 Cd	45.10	42.90	0.95	31.90	44.40	1.39	--	--	--
11	427609	3.34	2.19+.09 Cd +.007 Be	44.00	42.10	0.96	33.90	45.70	1.35	--	--	--

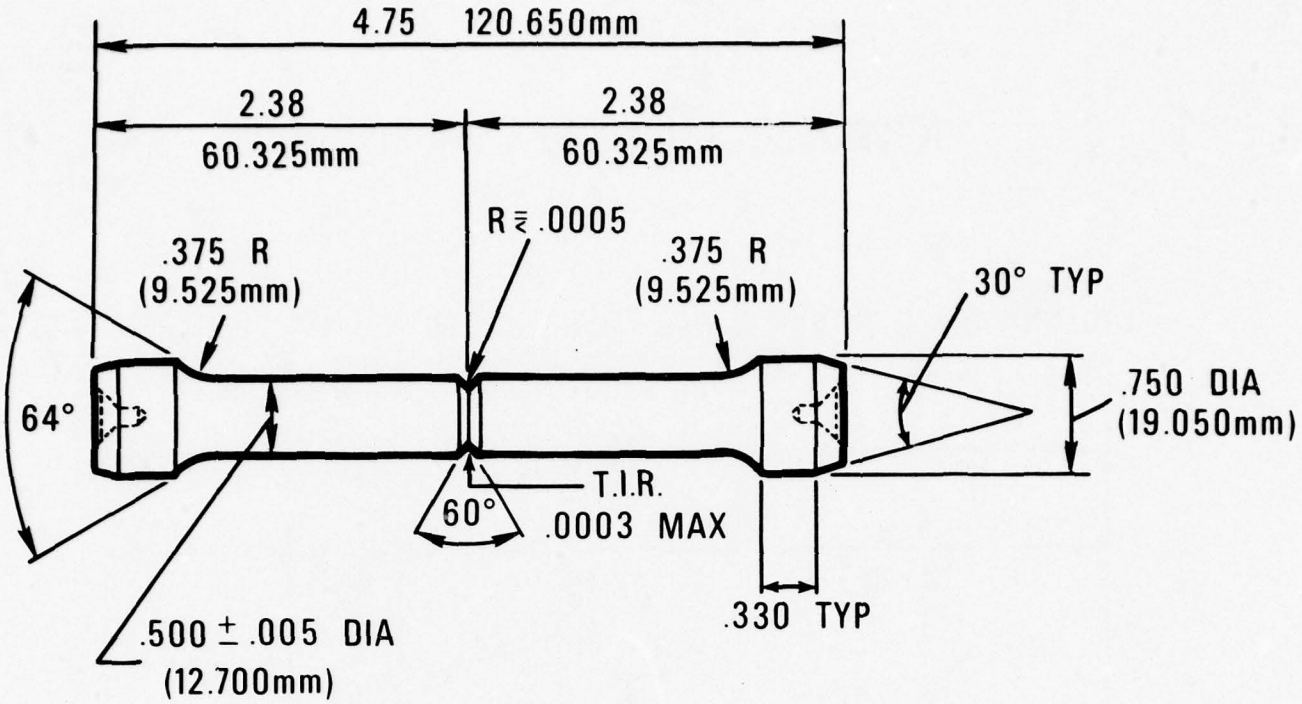

NOTE: TO OBTAIN SHORT-TRANSVERSE SPECIMENS, THE OVERALL LENGTH MAY BE REDUCED BY SHORTENING THE REDUCED SECTION

NOTCH TENSILE SPECIMEN

Figure 1

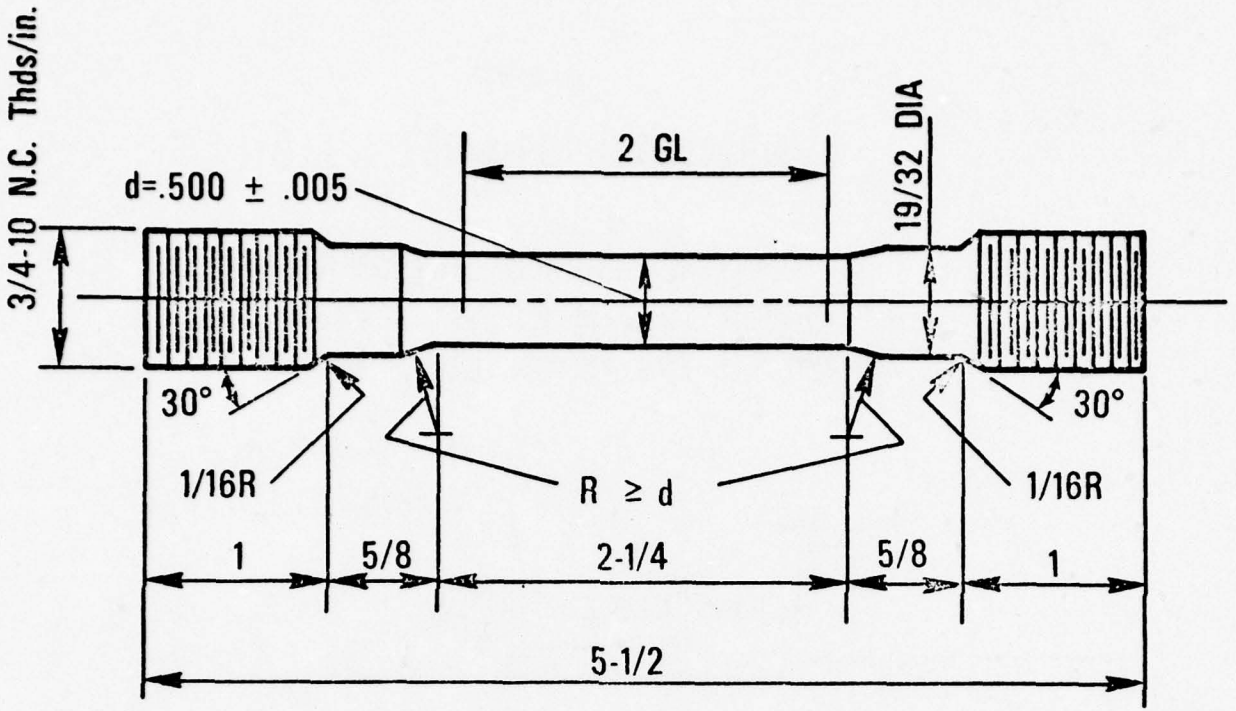

1/2" DIA THREADED END TENSILE SPECIMEN FOR MODULUS DETERMINATION

MODULUS OF ELASTICITY SPECIMEN

Figure 2

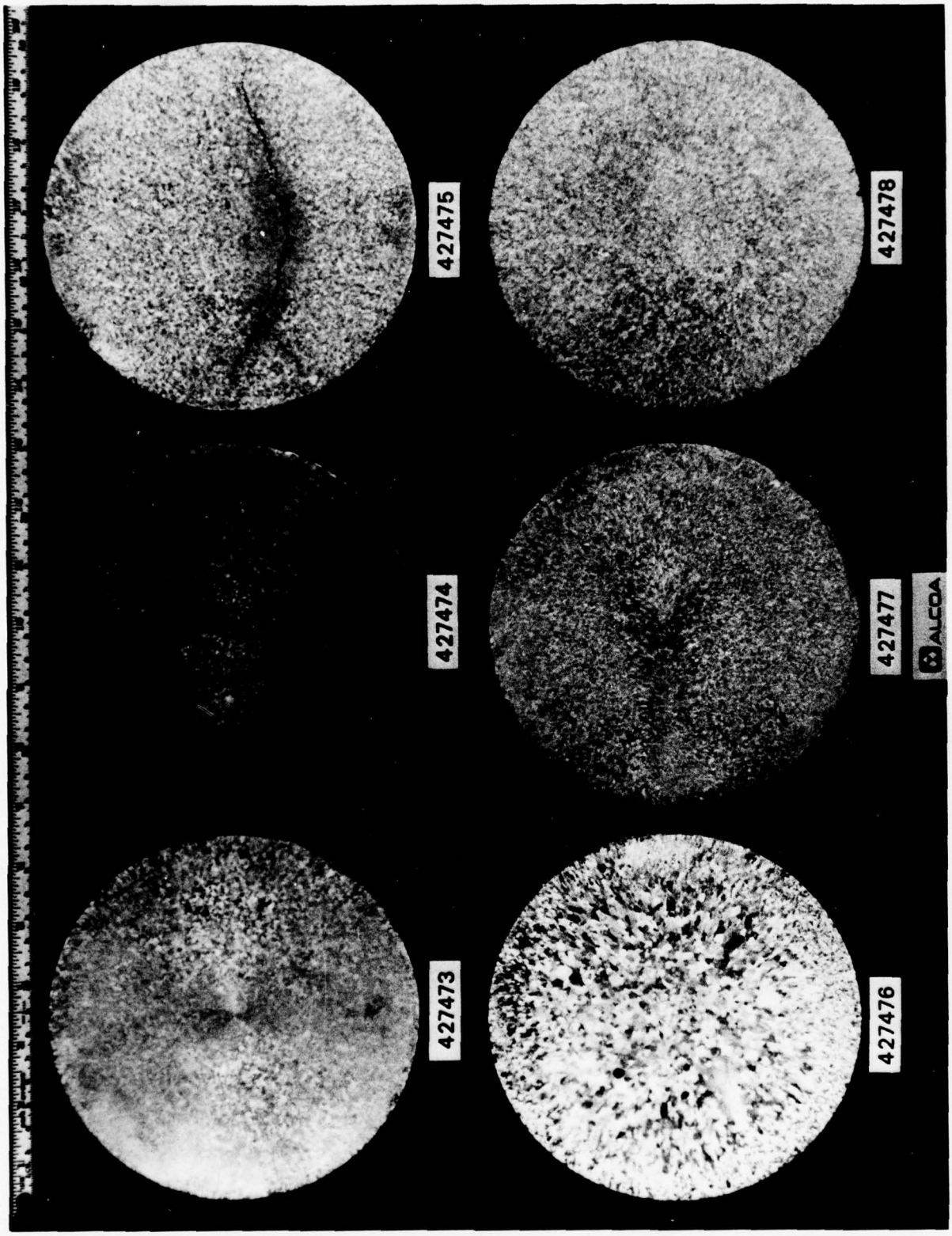

Figure 3 - Etched Ingot Slices Cut from DC Ingots of Alloys 1 (S. No. 427473) through 6 (S. No. 427478).

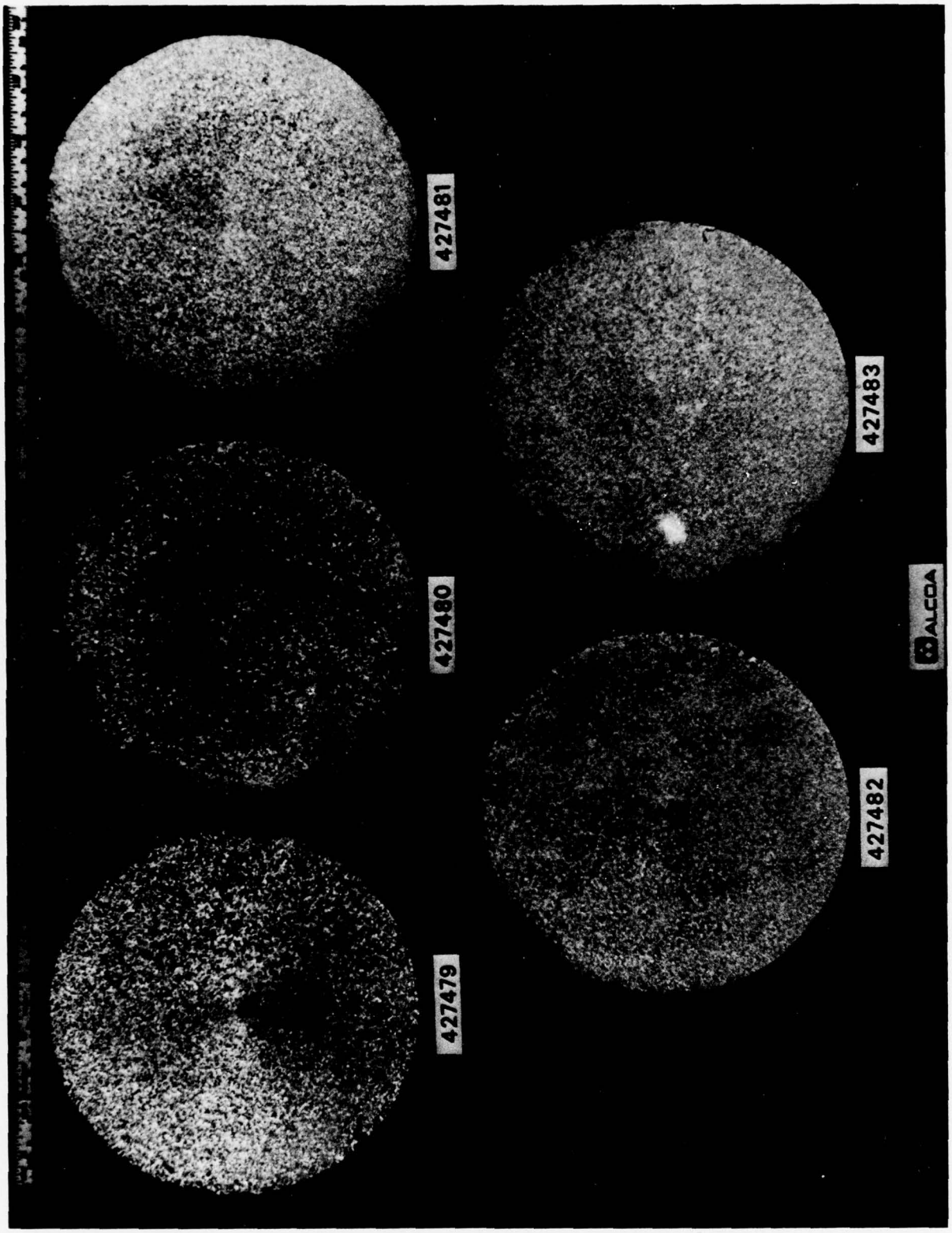

Figure 4 - Etched Ingot Slices Cut from DC Ingots of Alloys 7 (S. No. 427479) through 11 (S. No. 427483).

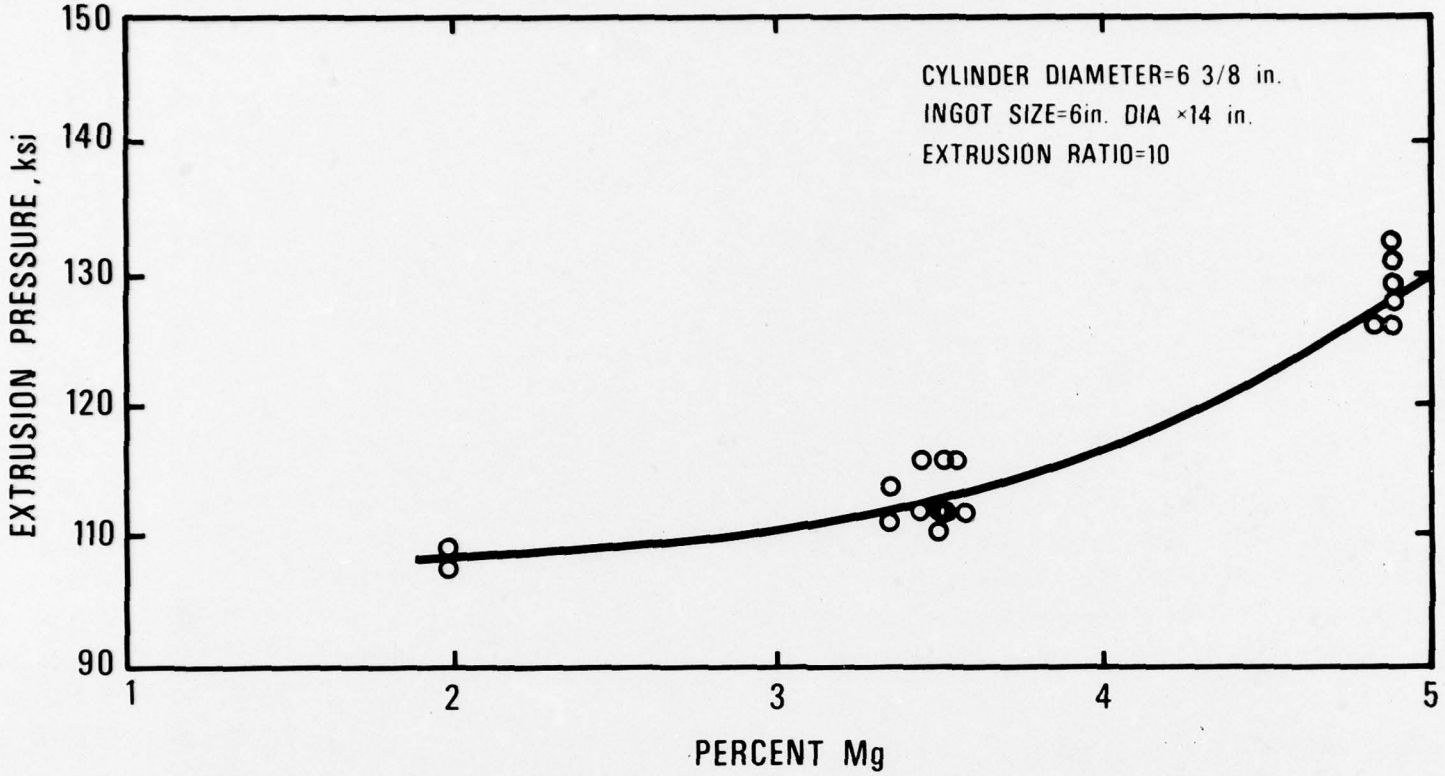

EFFECT OF Mg CONTENT ON EXTRUSION PRESSURES OF Al-Mg-Li ALLOYS

Figure 5

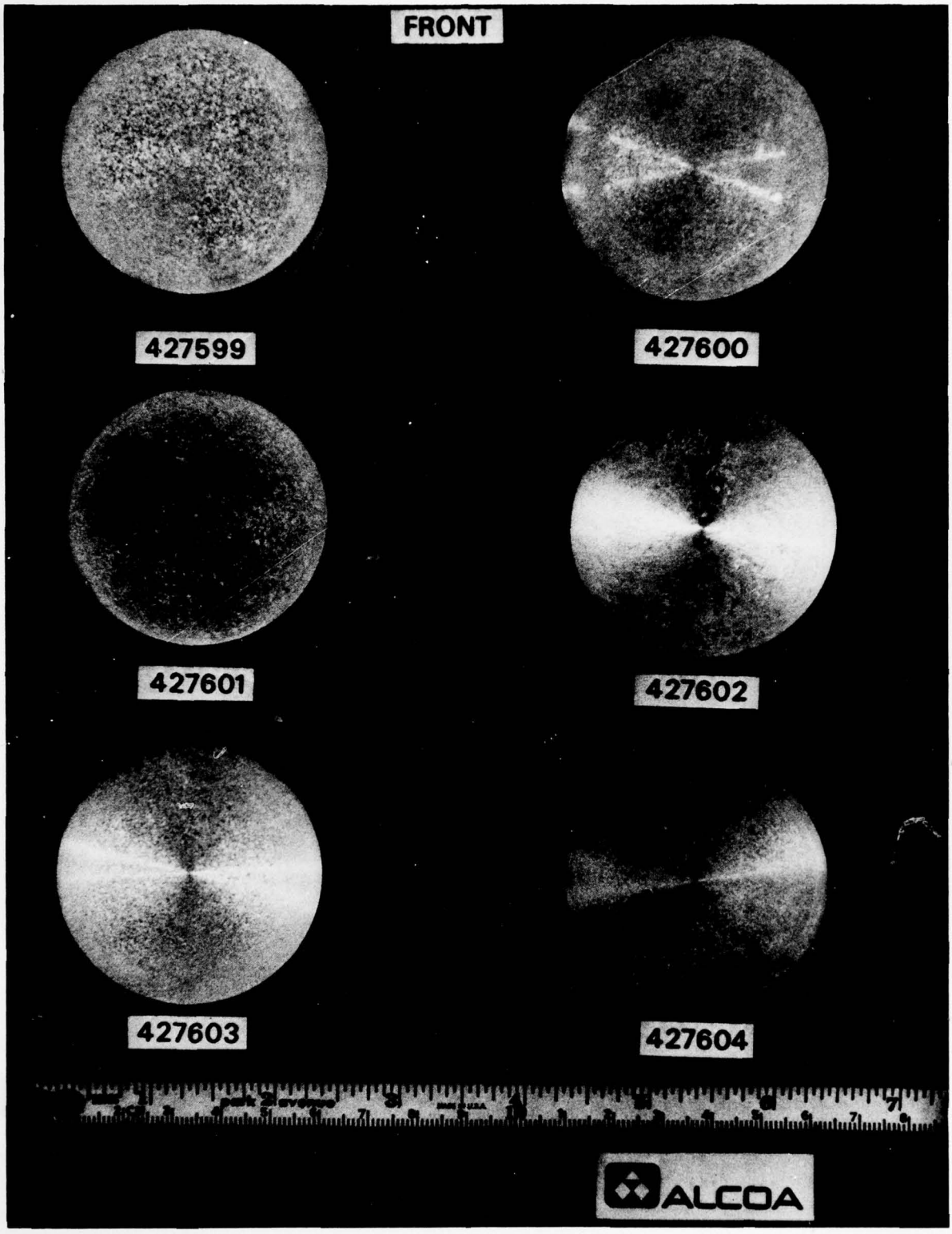

Figure 6 - Etched Slices Removed from Front of Phase II Al-Mg-Li Extrusions (S. Nos. 427599 through 427604).

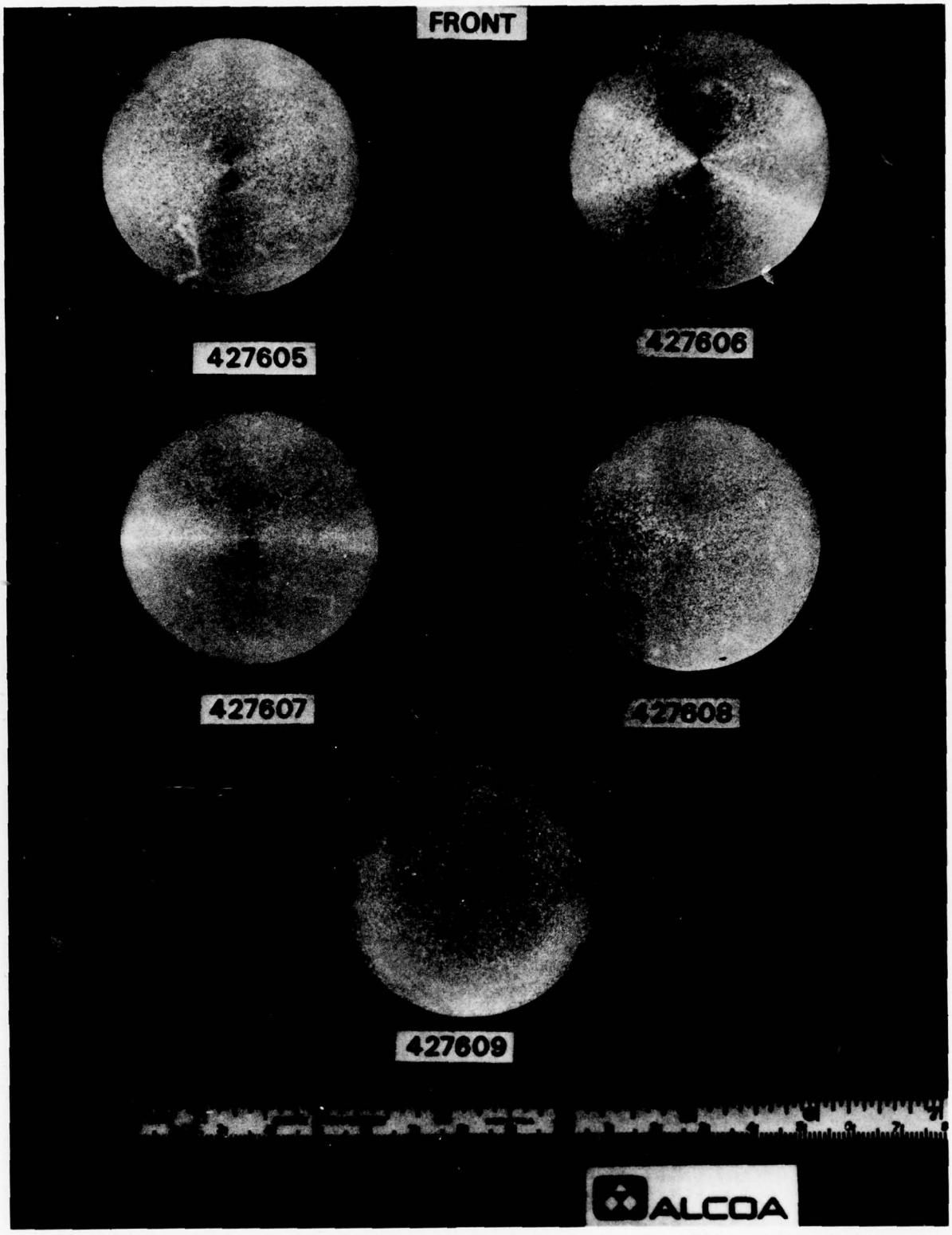

Figure 7 - Etched Slices Removed from Front of Phase II Al-Mg-Li Extrusions (S. Nos. 427605 through 427609).

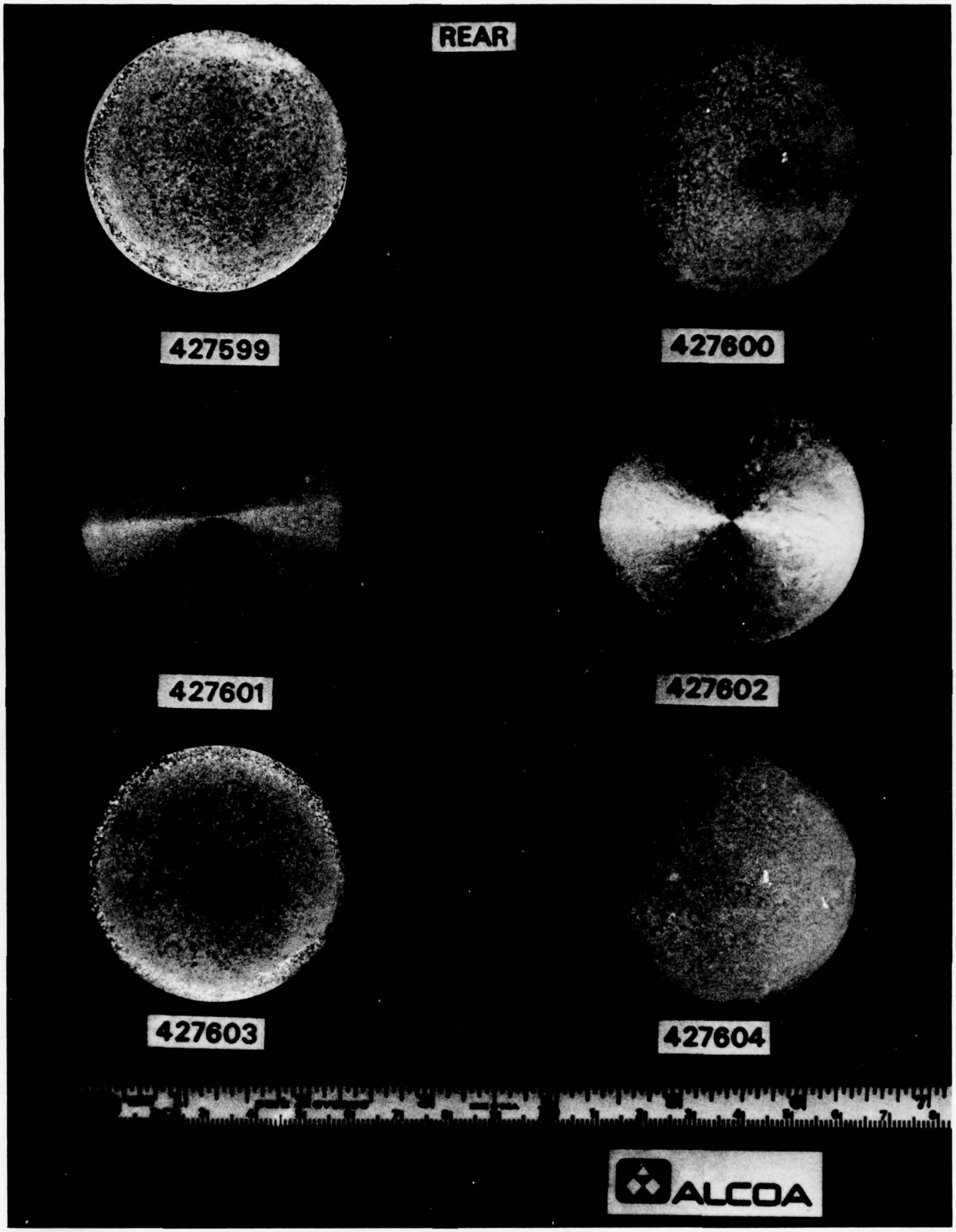

Figure 8 - Etched Slices Removed from Rear of Phase II Al-Mg-Li Extrusions (S. Nos. 427599 through 427604).

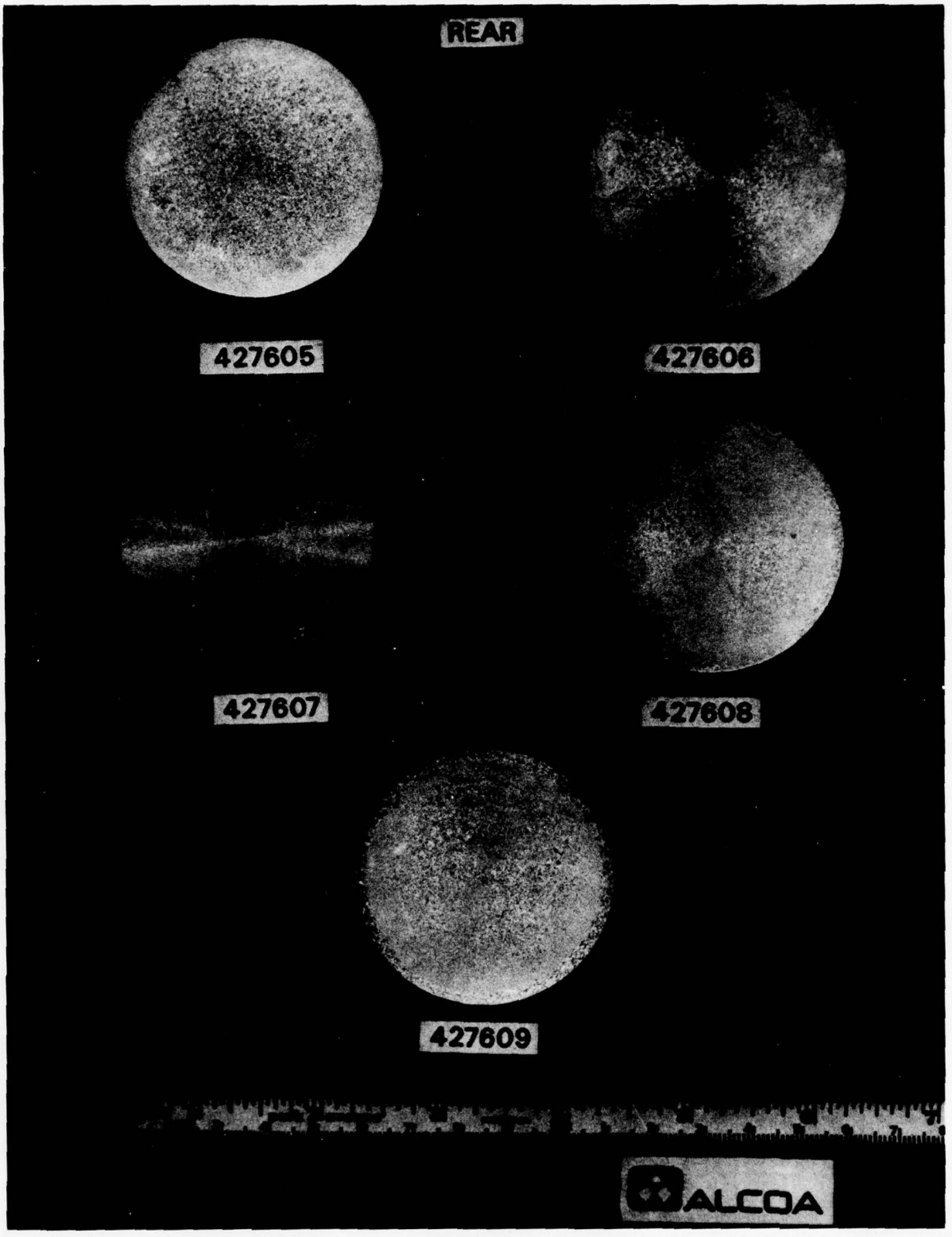

Figure 9 - Etched Slices Removed from Rear of Phase II Al-Mg-Li Extrusions (S. Nos. 427605 through 427609).

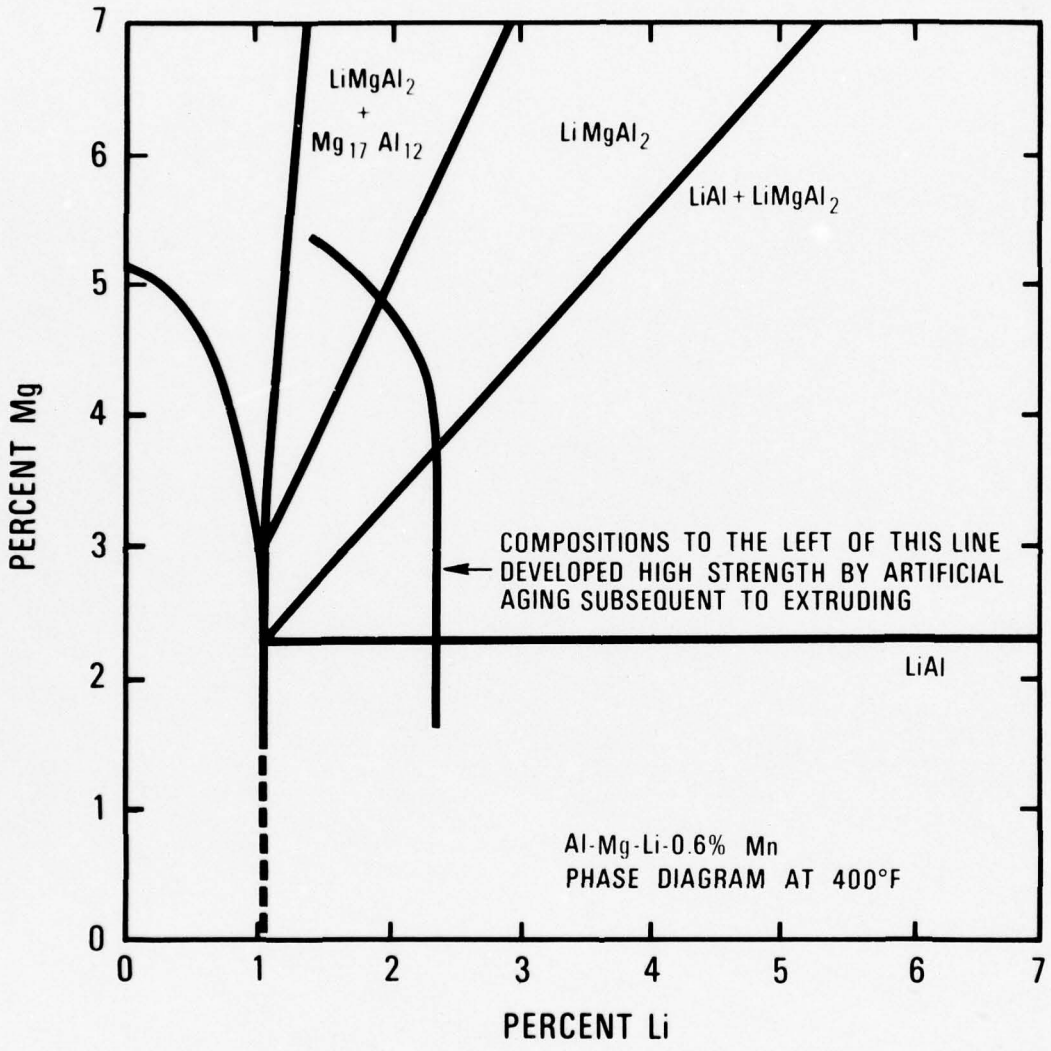

COMPOSITIONS PRODUCING HIGH STRENGTH BY AGING SUBSEQUENT TO EXTRUDING AND AIR COOLING

Figure 10

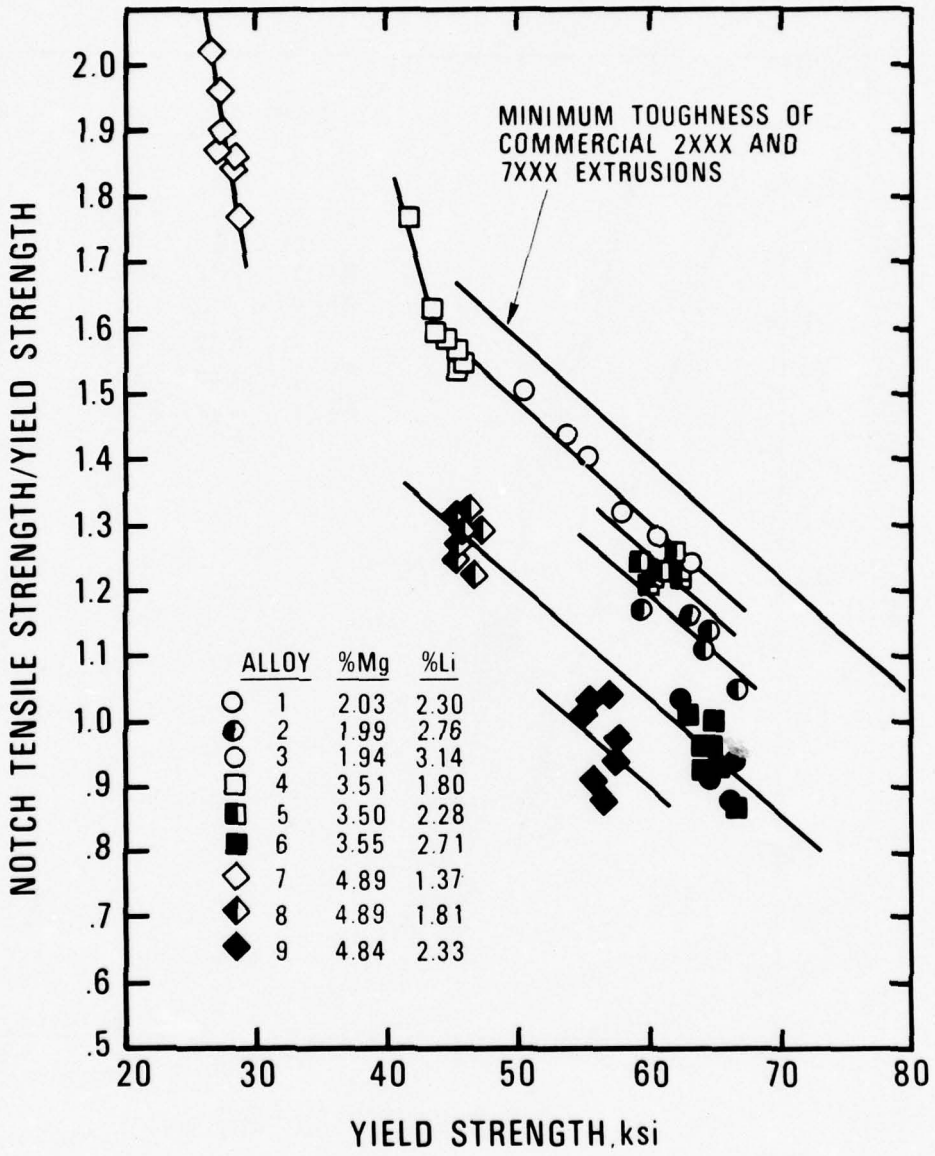

LONGITUDINAL TOUGHNESS OF
Al-Mg-Li ALLOY EXTRUSIONS

Figure 11

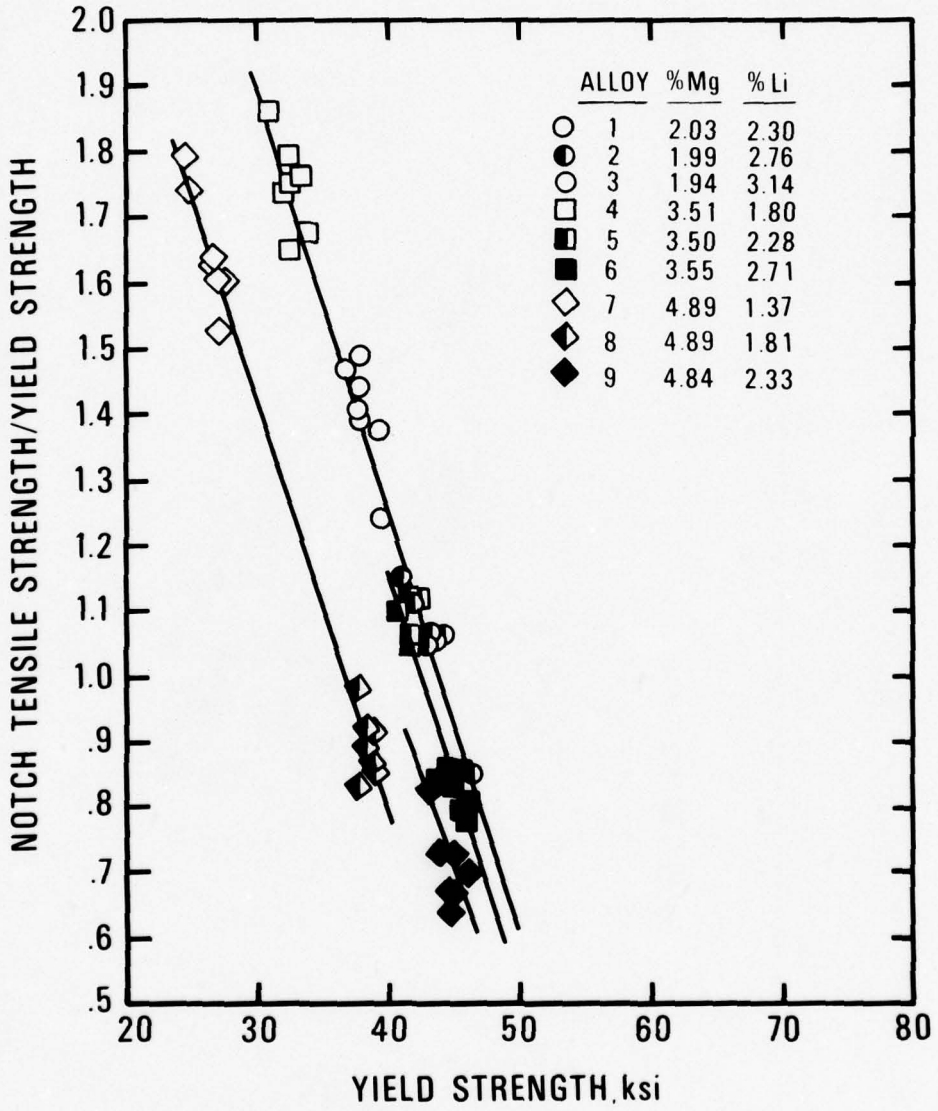

TRANSVERSE TOUGHNESS OF
Al-Mg-Li ALLOY EXTRUSIONS

Figure 12

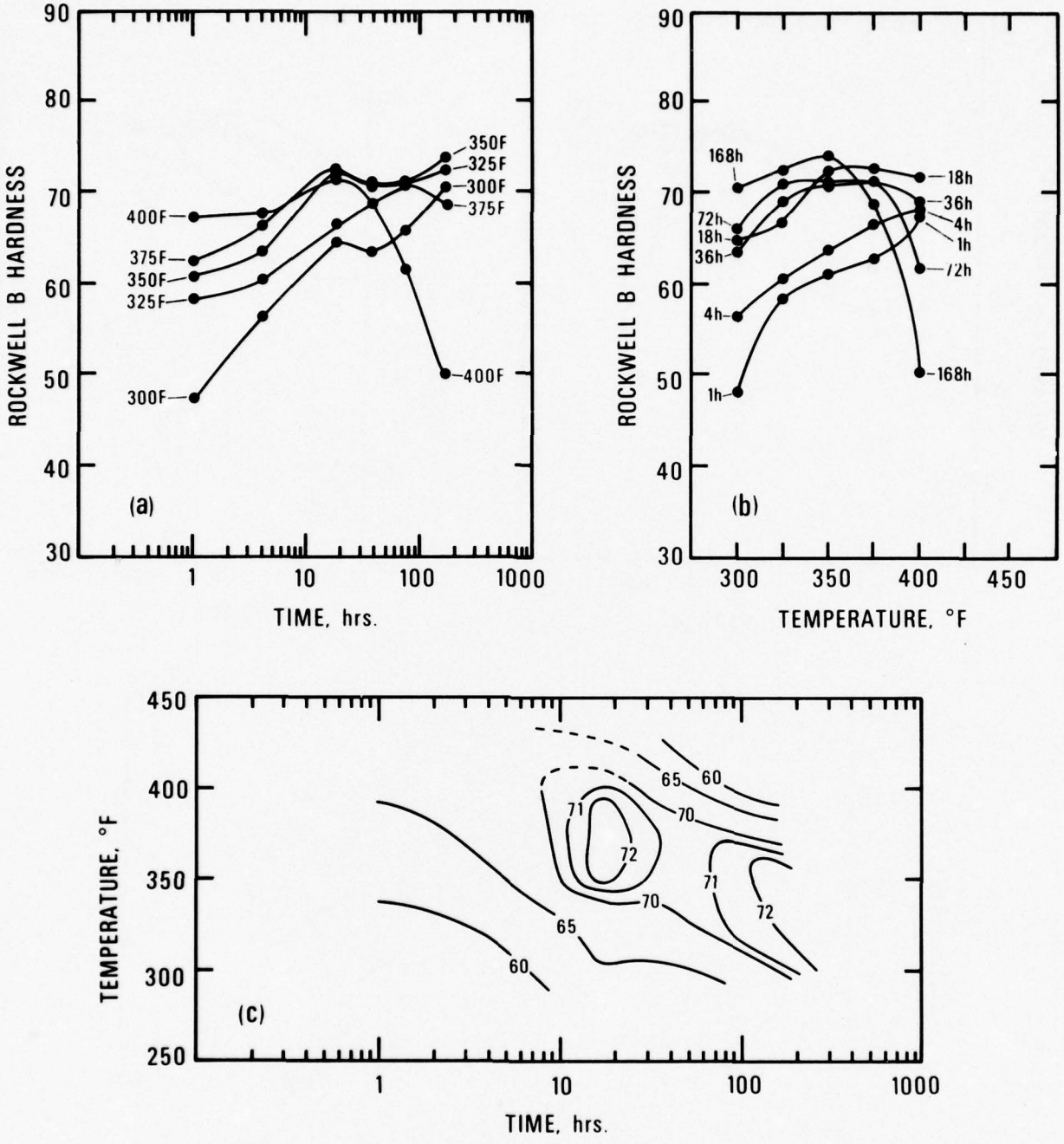

ARTIFICIAL AGING CURVES FOR ALLOY 1 (S.NO.427599)

a) ISOTHERMAL CURVES, b) ISOCHRONAL CURVES, AND C) ISO-ROCKWELL B HARDNESS CURVES

Figure 13

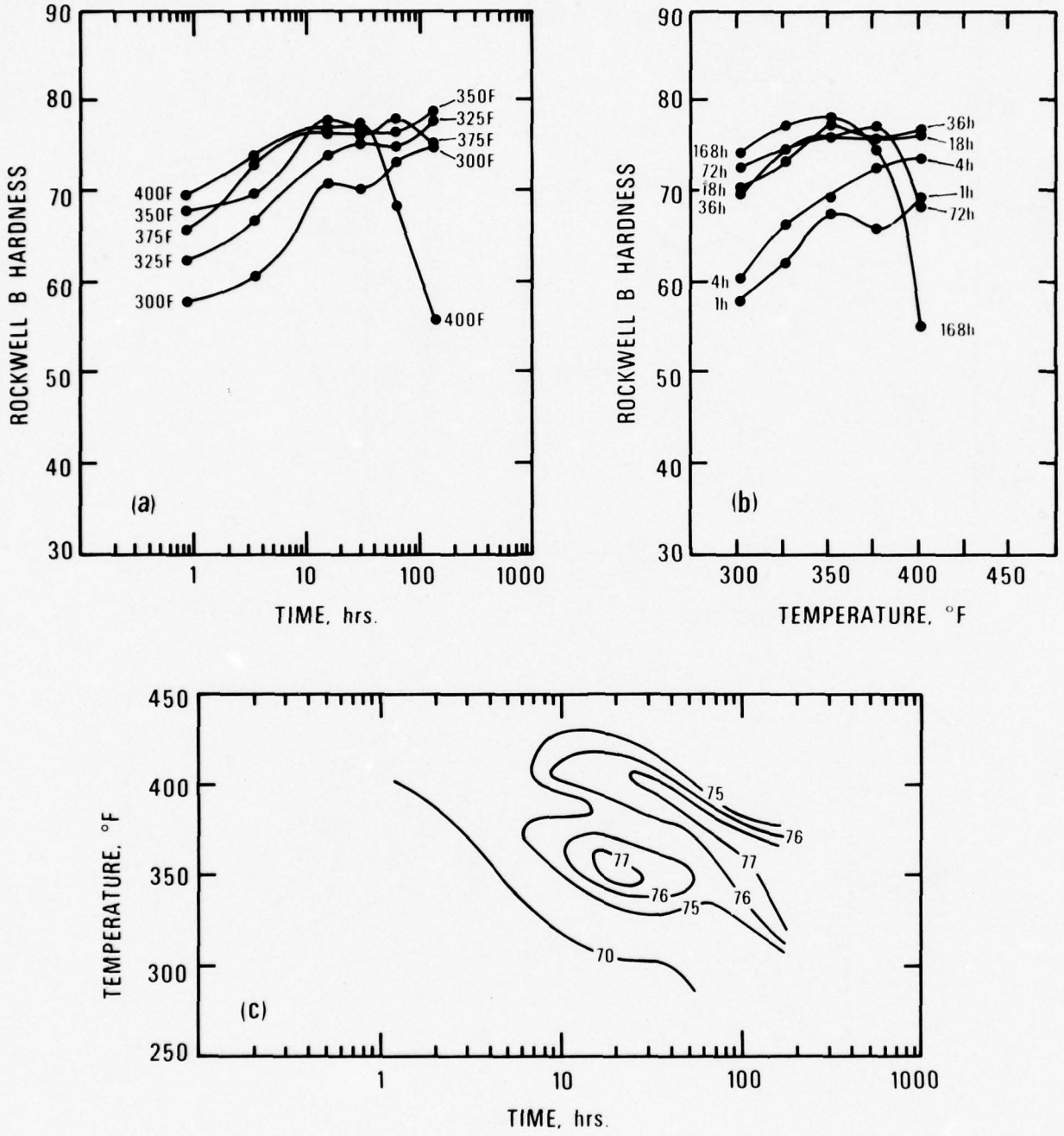

ARTIFICIAL AGING CURVES FOR ALLOY 2 (S.NO.427600)

a) ISOTHERMAL CURVES, b) ISOCHRONAL CURVES, AND C) ISO-ROCKWELL B HARDNESS CURVES

Figure 14

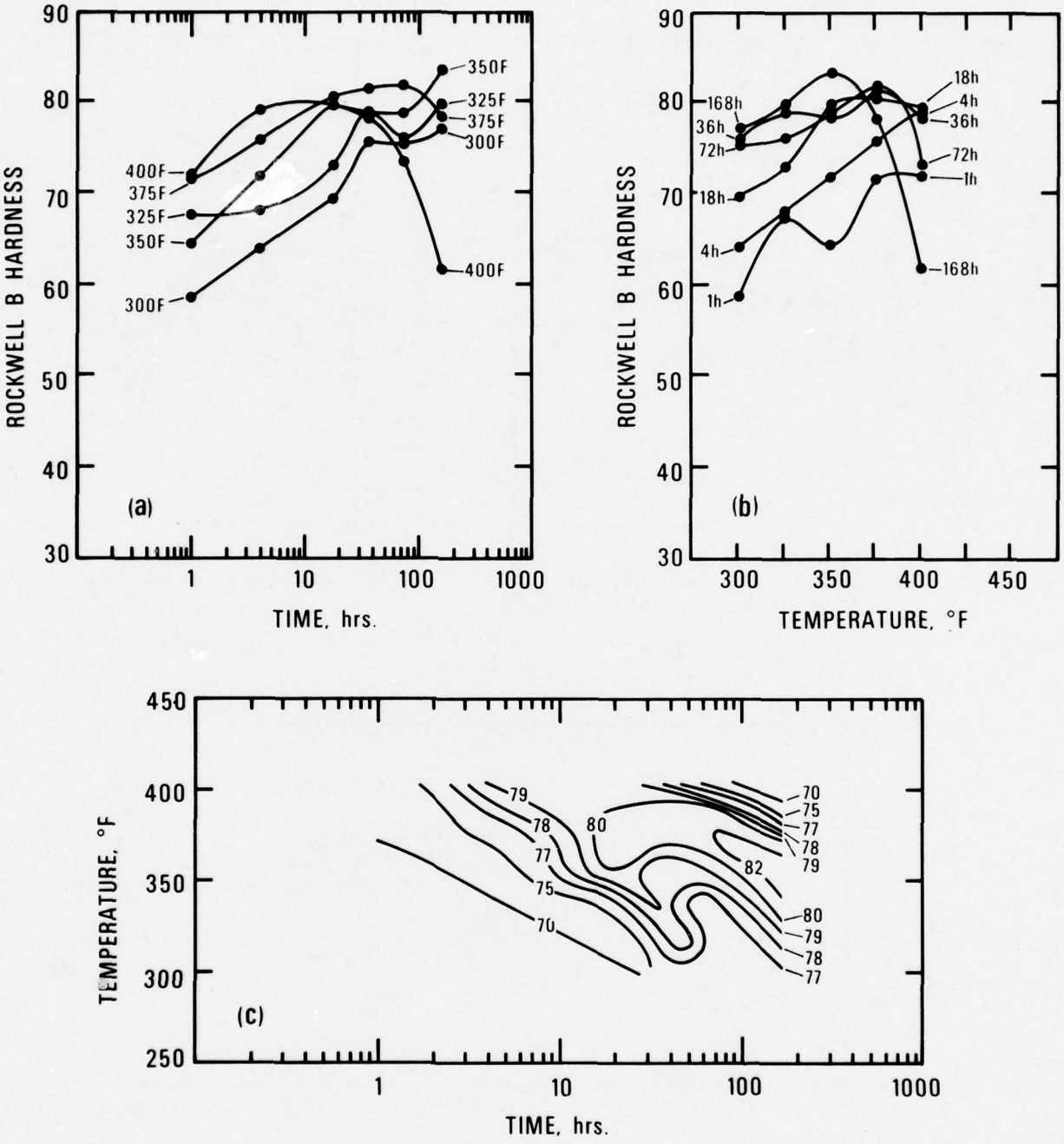

ARTIFICIAL AGING CURVES FOR ALLOY 3 (S.NO.427601)

a) ISOTHERMAL CURVES, b) ISOCHRONAL CURVES, AND C) ISO-ROCKWELL B HARDNESS CURVES

Figure 15

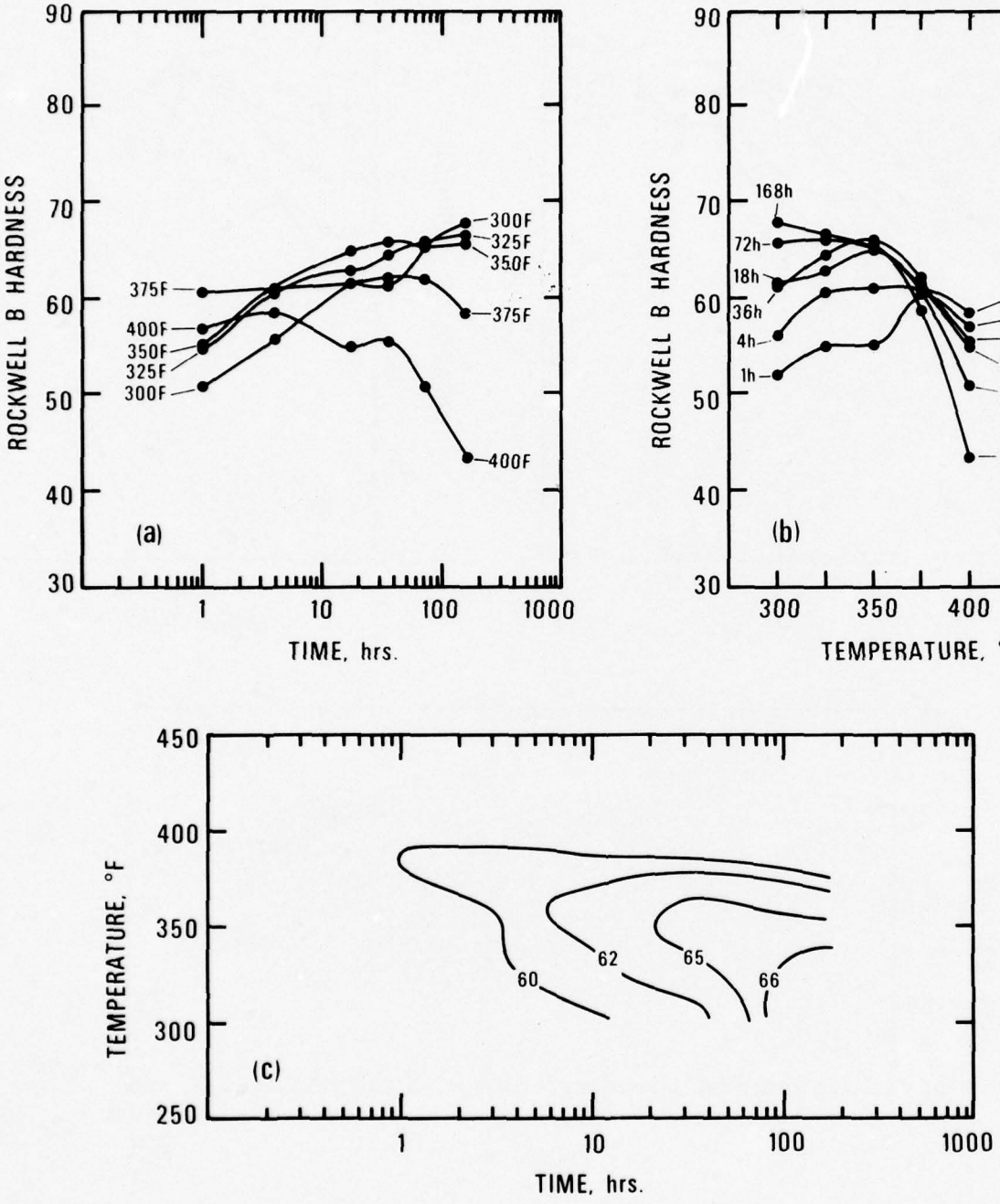

ARTIFICIAL AGING CURVES FOR ALLOY 4 (S.NO.427602)

a) ISOTHERMAL CURVES, b) ISOCHRONAL CURVES, AND C) ISO-ROCKWELL B HARDNESS CURVES

Figure 16

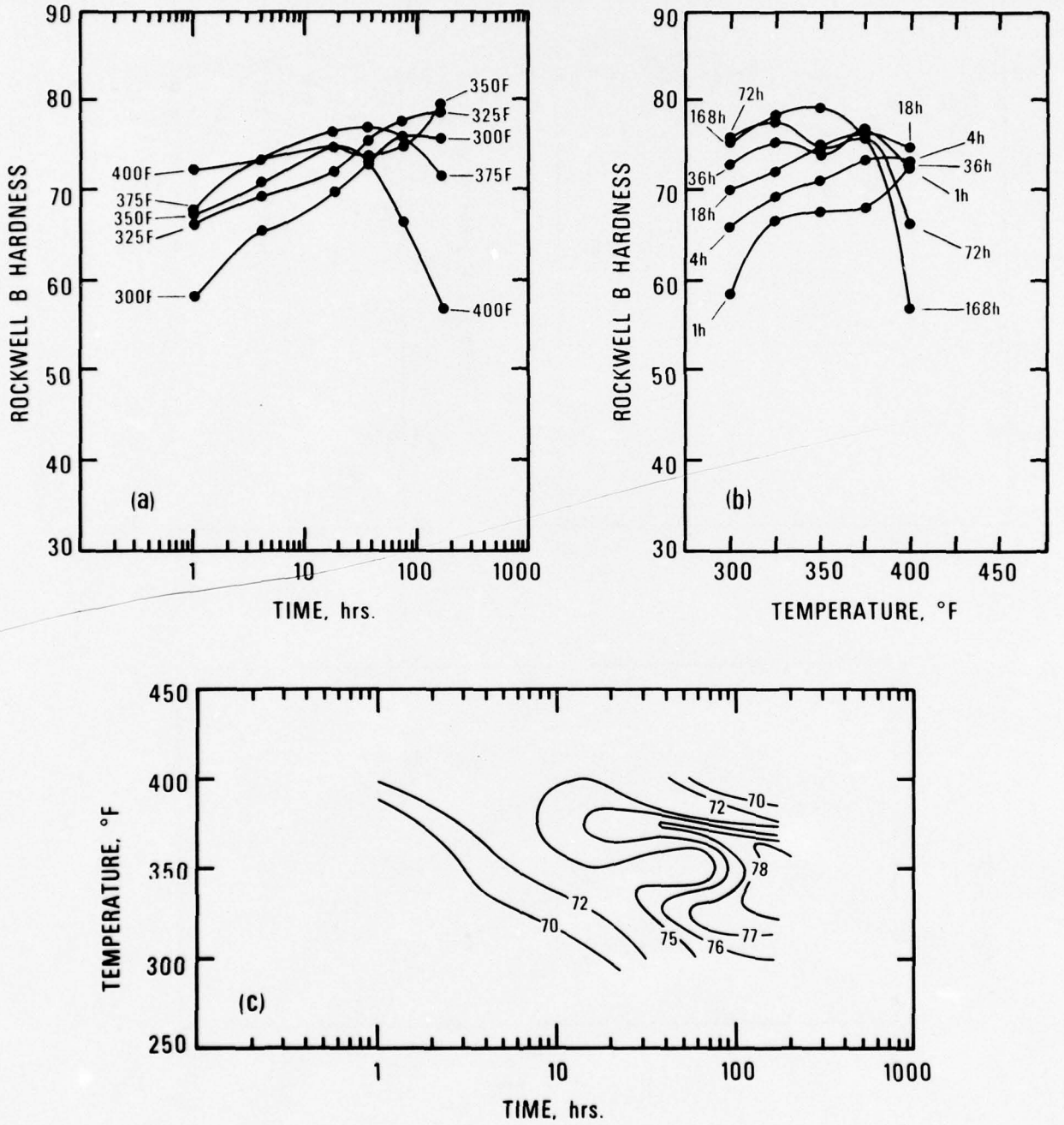

ARTIFICIAL AGING CURVES FOR ALLOY 5 (S.NO.427603)

a) ISOTHERMAL CURVES, b) ISOCHRONAL CURVES, AND C) ISO-ROCKWELL B HARDNESS CURVES

Figure 17

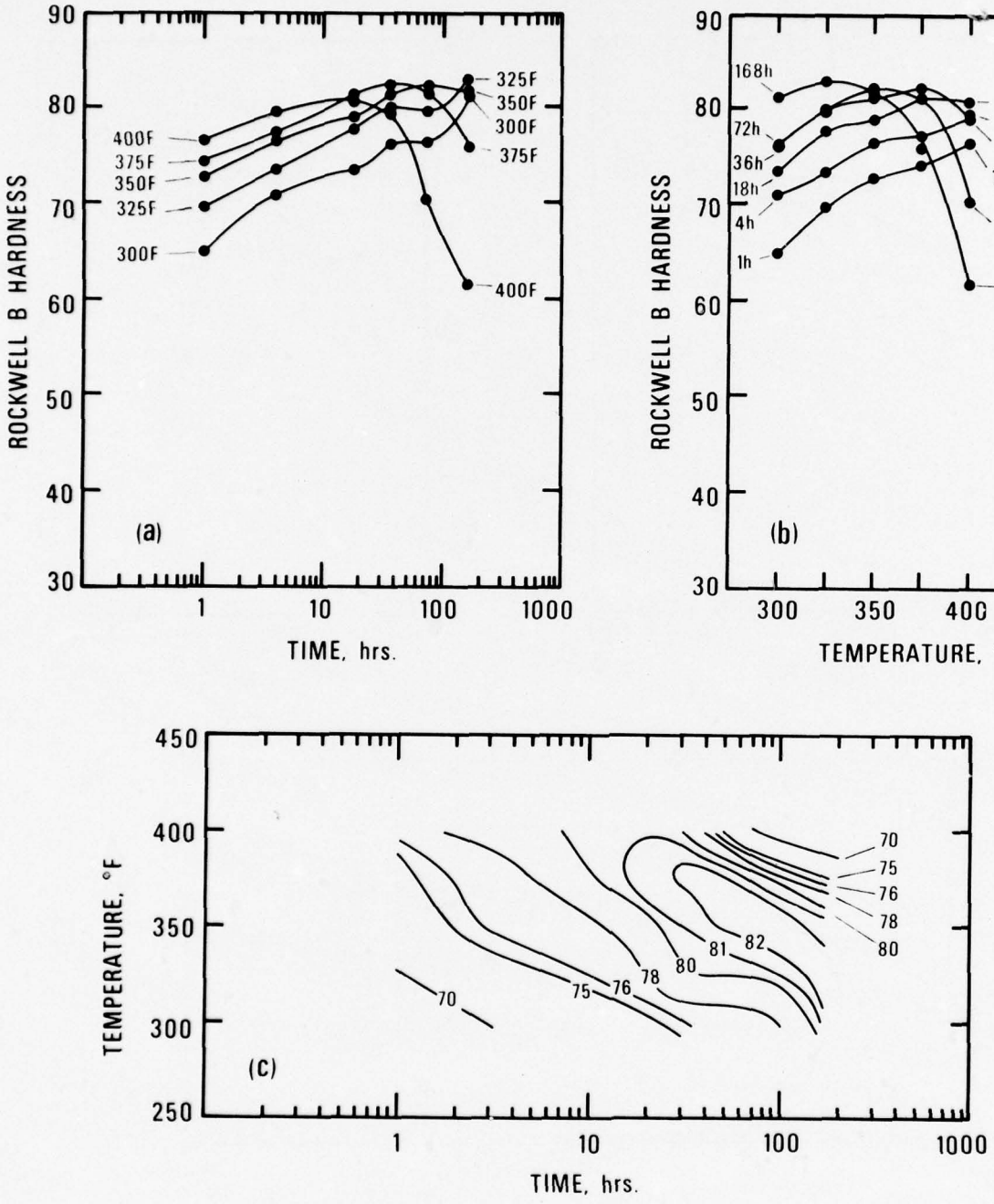

ARTIFICIAL AGING CURVES FOR ALLOY 6 (S.NO. 427604)

a) ISOTHERMAL CURVES, b) ISOCHRONAL CURVES, AND
C) ISO-ROCKWELL B HARDNESS CURVES

Figure 18

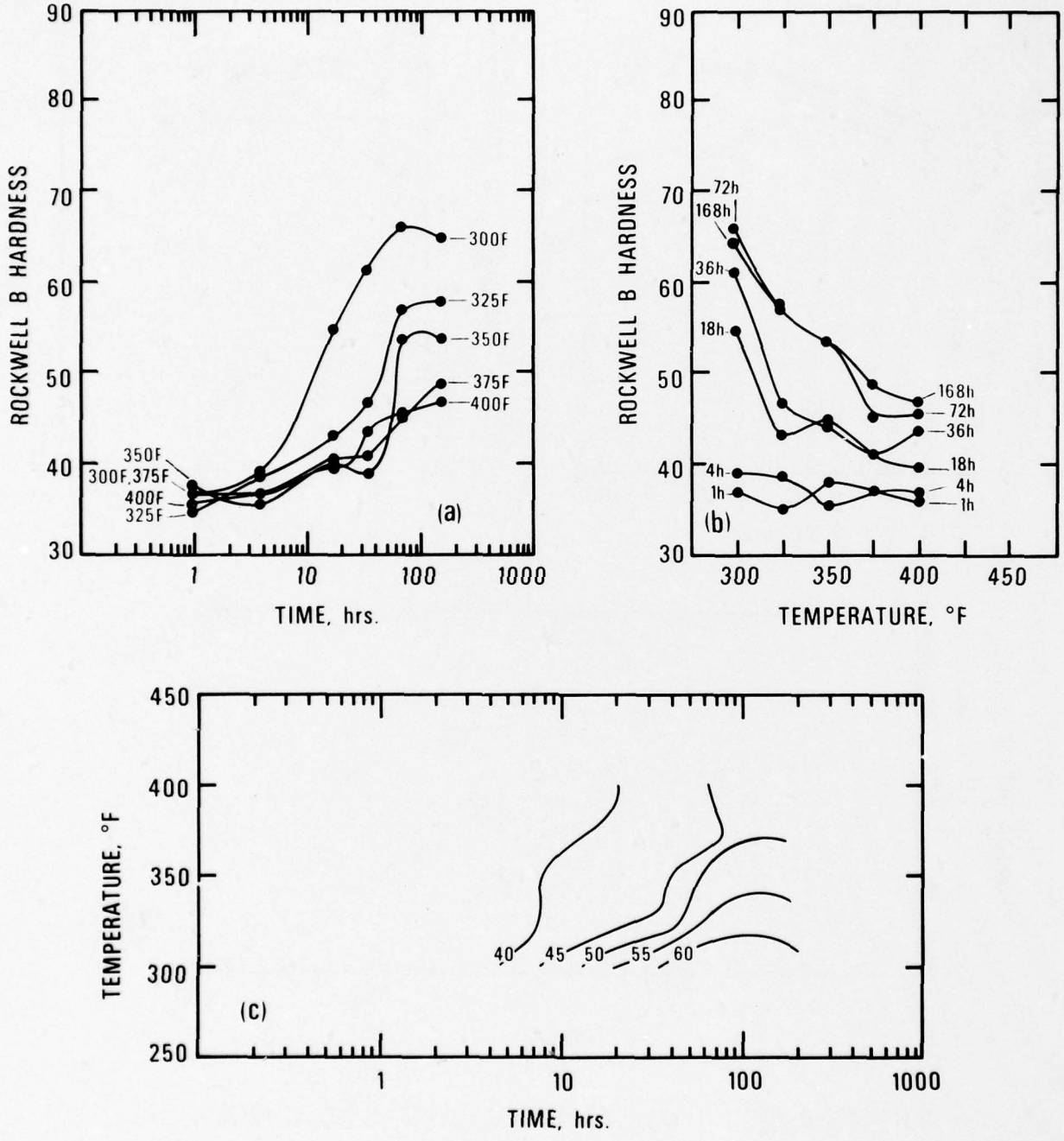

ARTIFICIAL AGING CURVES FOR ALLOY 7 (S.NO. 427605)

a) ISOTHERMAL CURVES, b) ISOCHRONAL CURVES, AND C) ISO-ROCKWELL B HARDNESS CURVES

Figure 19

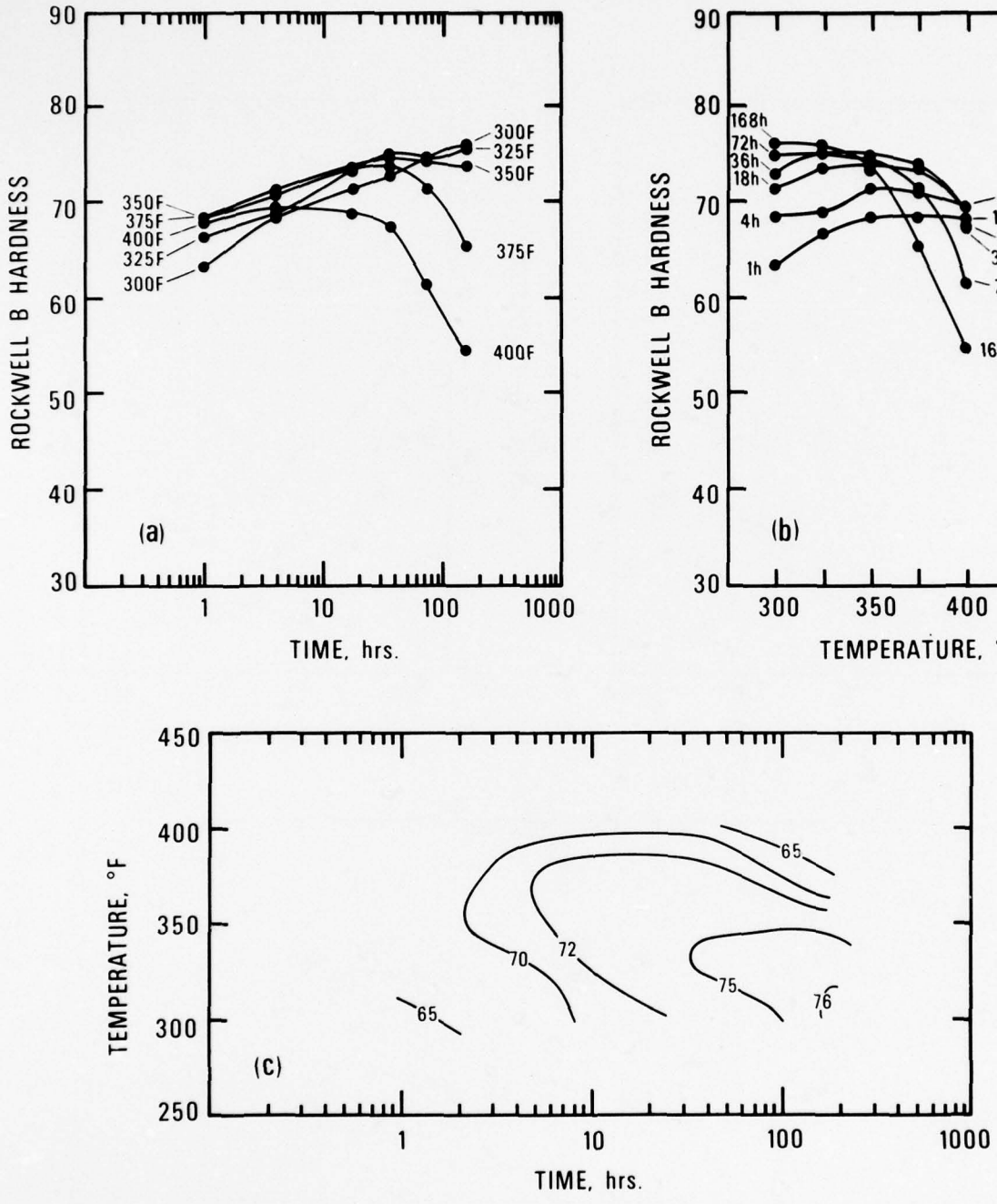

ARTIFICIAL AGING CURVES FOR ALLOY 8 (S.NO.427606)

a) ISOTHERMAL CURVES, b) ISOCHRONAL CURVES, AND C) ISO-ROCKWELL B HARDNESS CURVES

Figure 20

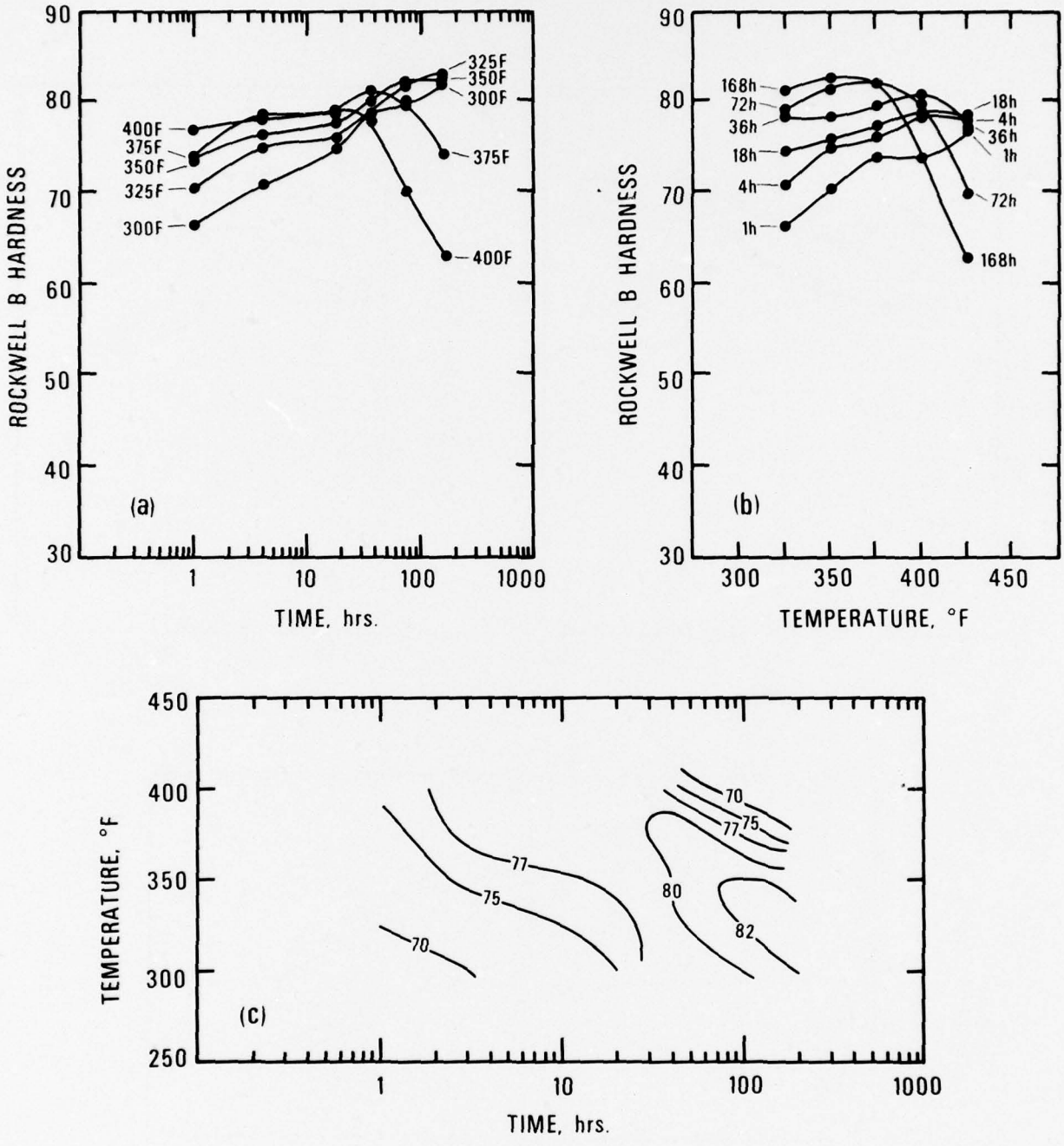

ARTIFICIAL AGING CURVES FOR ALLOY 9 (S.NO.427607)

a) ISOTHERMAL CURVES, b) ISOCHRONAL CURVES, AND C) ISO-ROCKWELL B HARDNESS CURVES

Figure 21

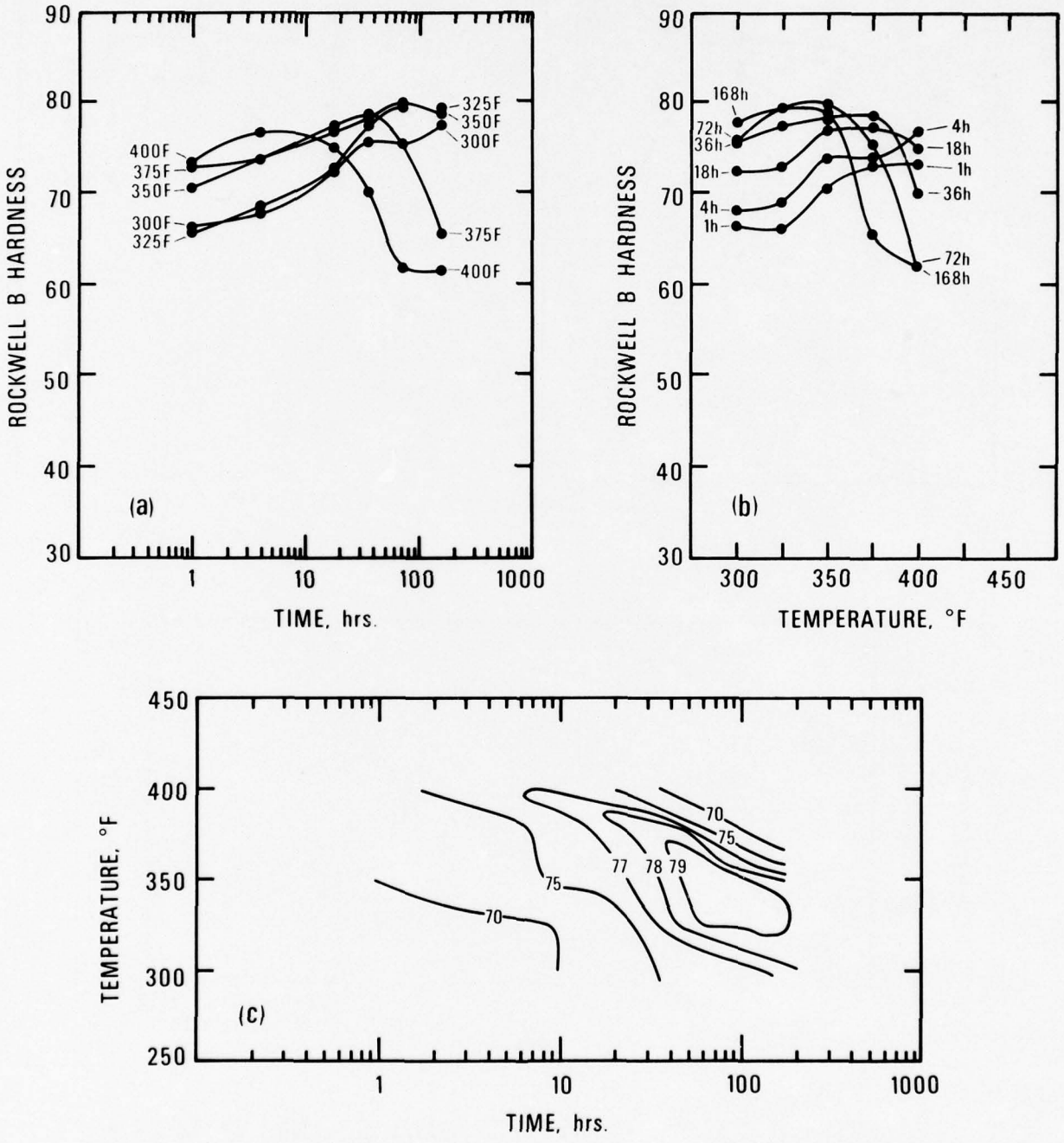

ARTIFICIAL AGING CURVES FOR ALLOY 10 (S.NO. 427608)

a) ISOTHERMAL CURVES, b) ISOCHRONAL CURVES, AND C) ISO-ROCKWELL B HARDNESS CURVES

Figure 22

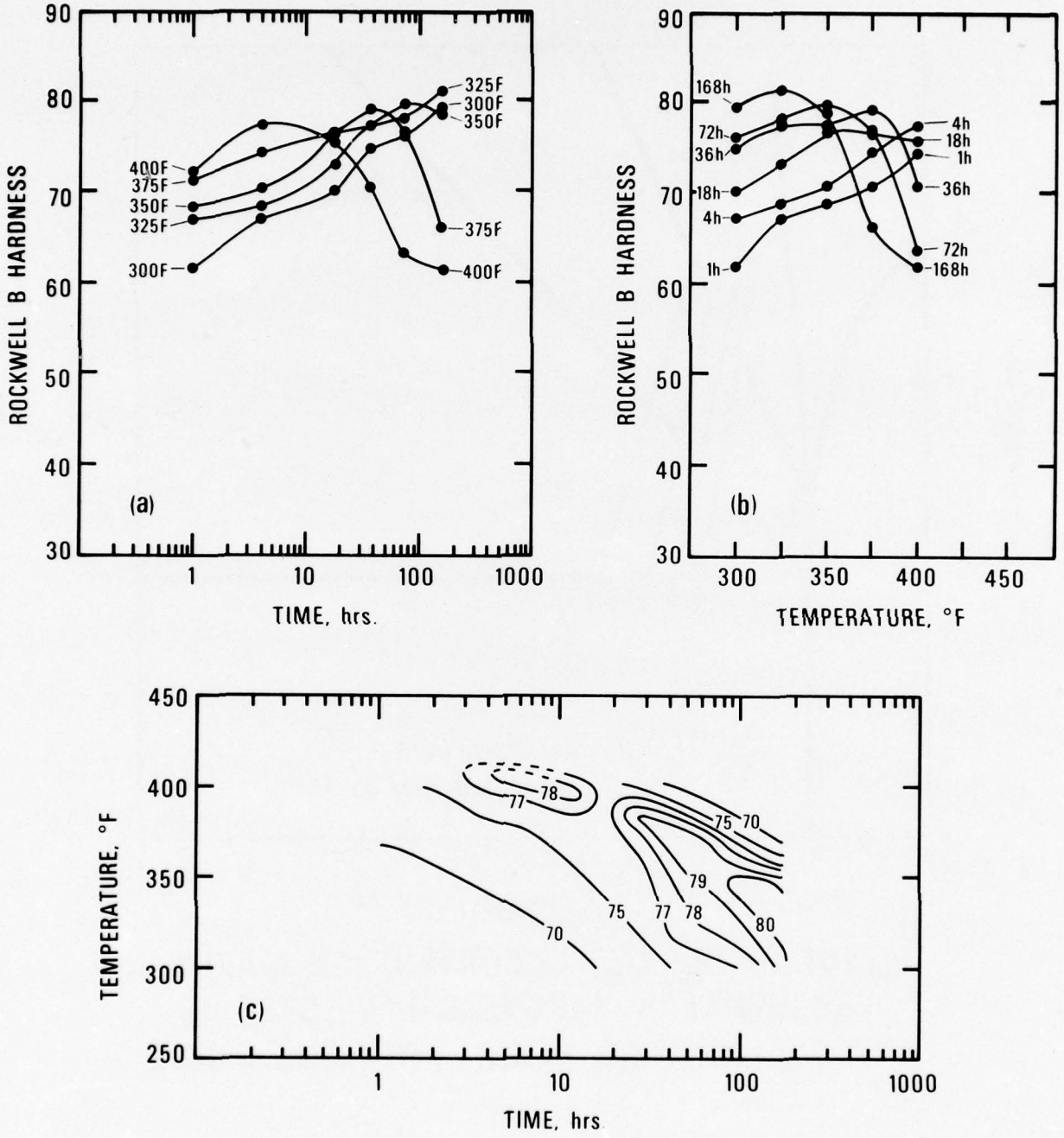

ARTIFICIAL AGING CURVES FOR ALLOY 11 (S.NO. 427609)

a) ISOTHERMAL CURVES, b) ISOCHRONAL CURVES, AND C) ISO-ROCKWELL B HARDNESS CURVES

Figure 23

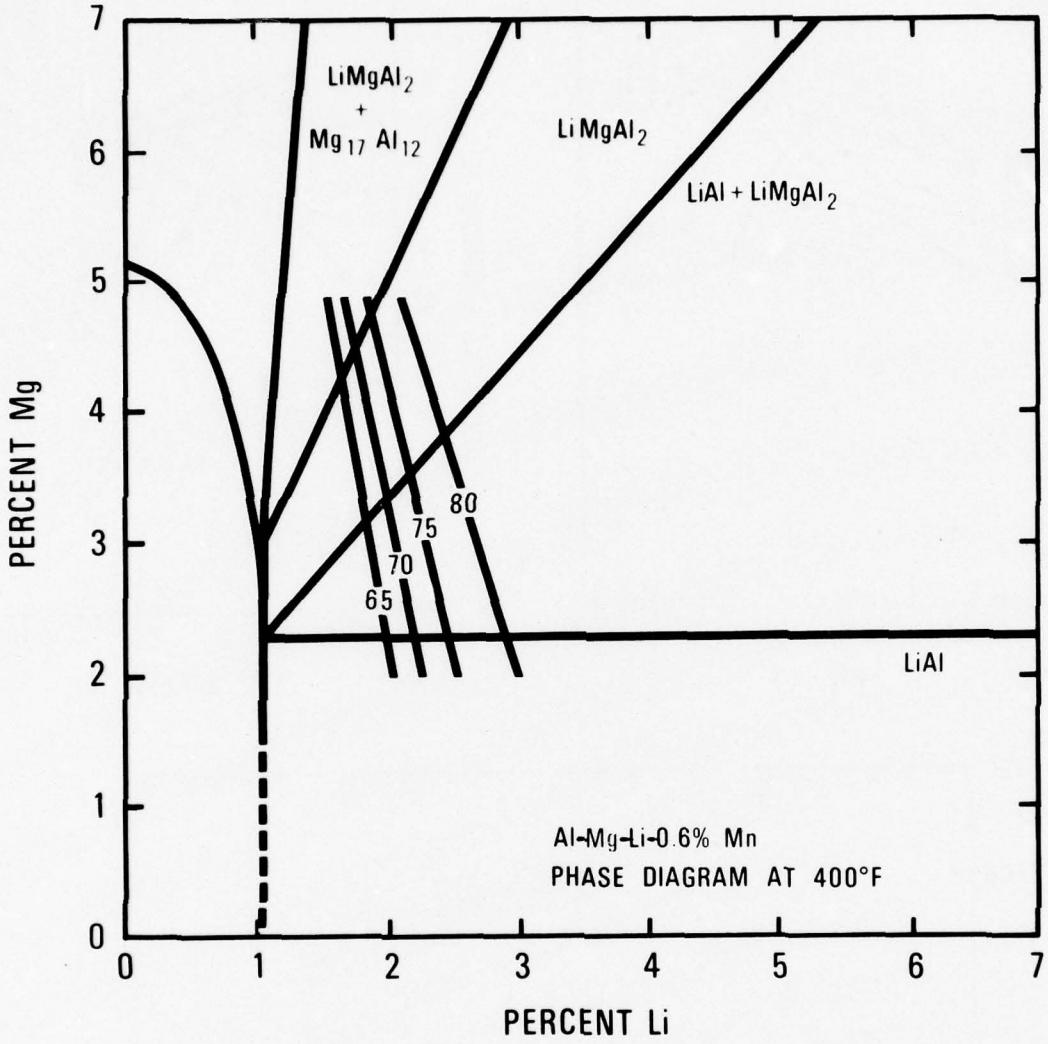

EFFECT OF Mg AND Li CONTENT ON MAXIMUM ROCKWELL B HARDNESS DEVELOPED IN Al-Mg-Li ALLOYS AFTER ARTIFICIAL AGING

Figure 24

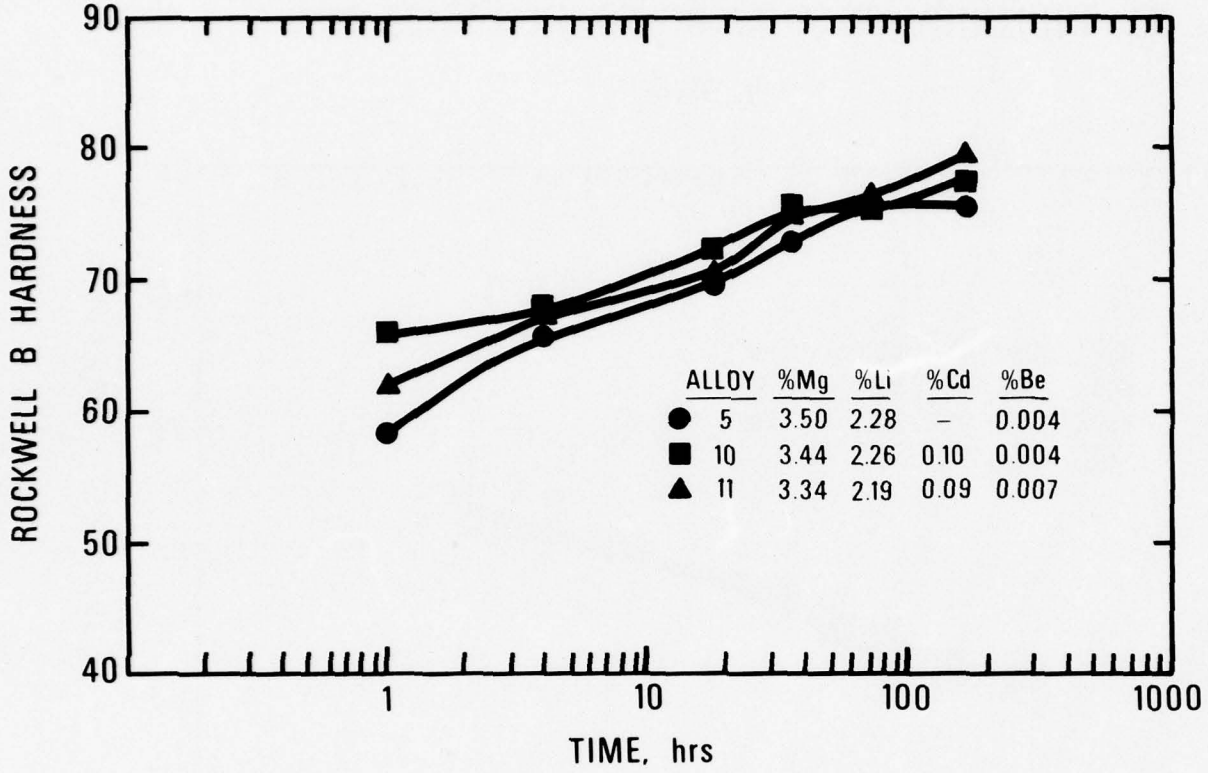

THE EFFECT OF Cd OR Cd + Be ADDITIONS TO Al-Mg-Li ALLOYS ON ARTIFICIAL AGING AT 300°F

Figure 25

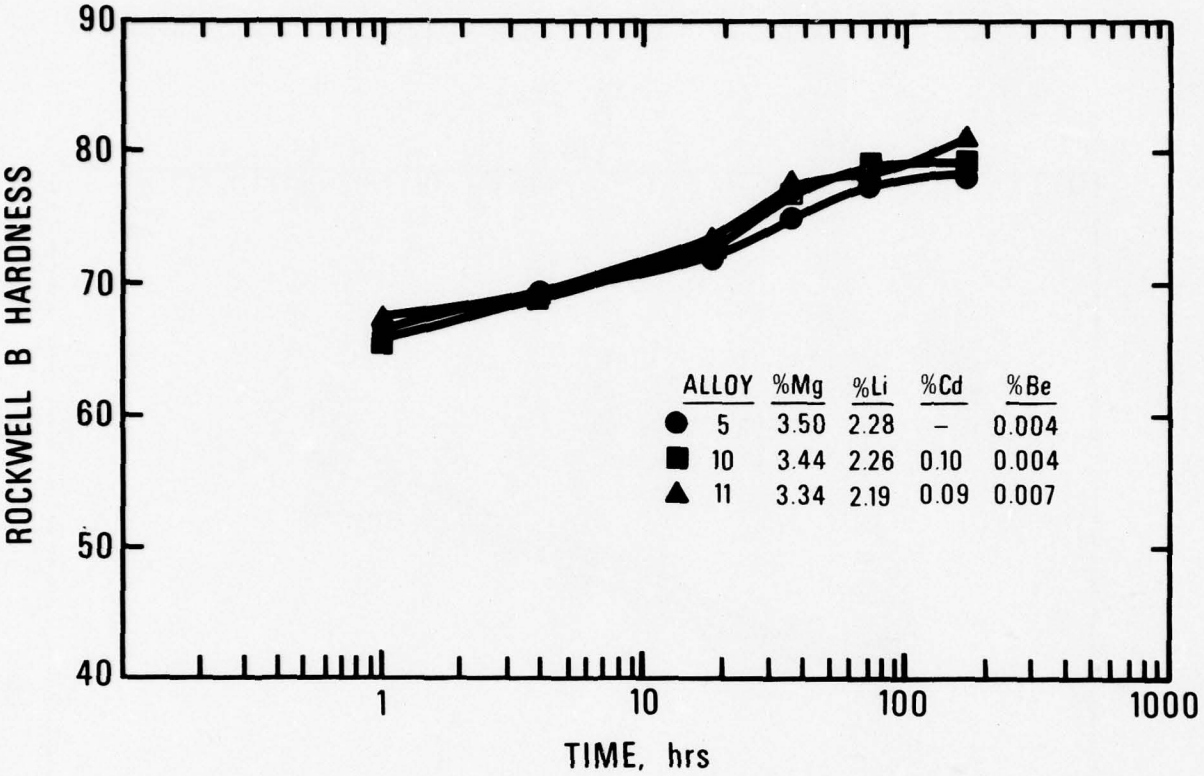

THE EFFECT OF Cd OR Cd + Be ADDITIONS TO Al-Mg-Li ALLOYS ON ARTIFICIAL AGING AT 325 °F

Figure 26

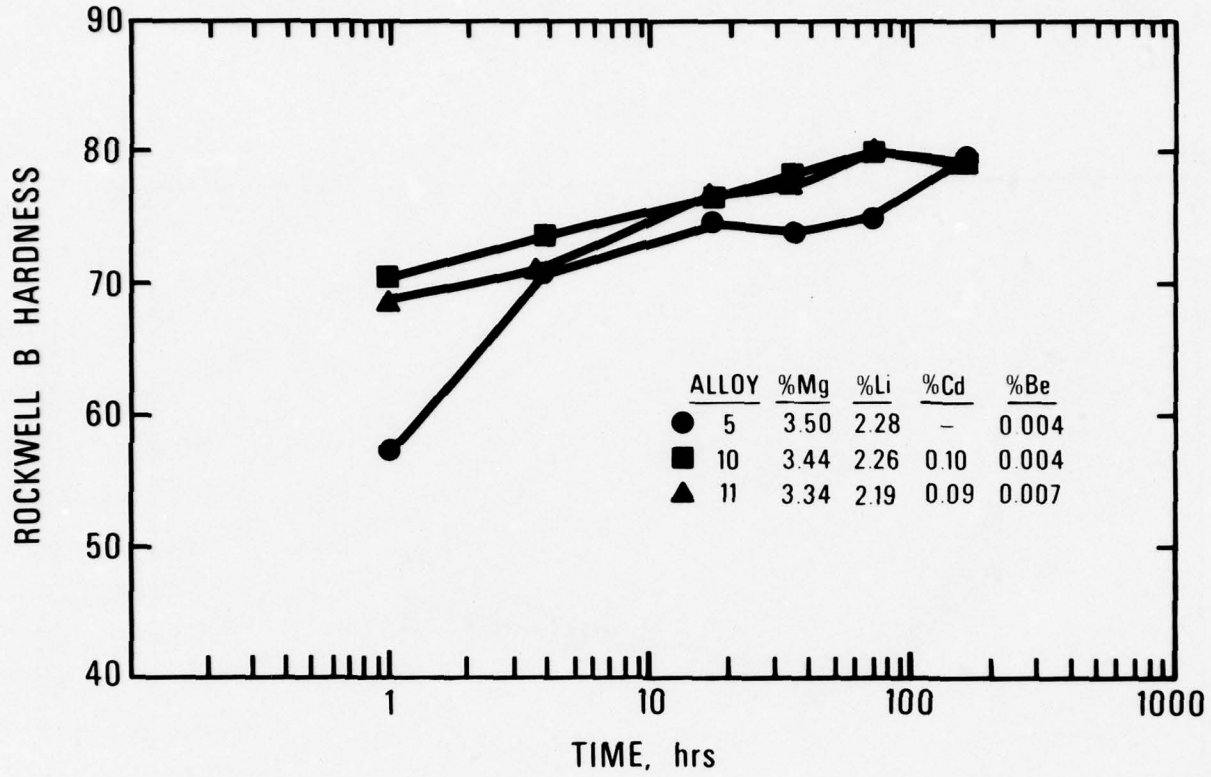

THE EFFECT OF Cd OR Cd + Be ADDITIONS TO Al-Mg-Li ALLOYS ON ARTIFICIAL AGING AT 350°F

Figure 27

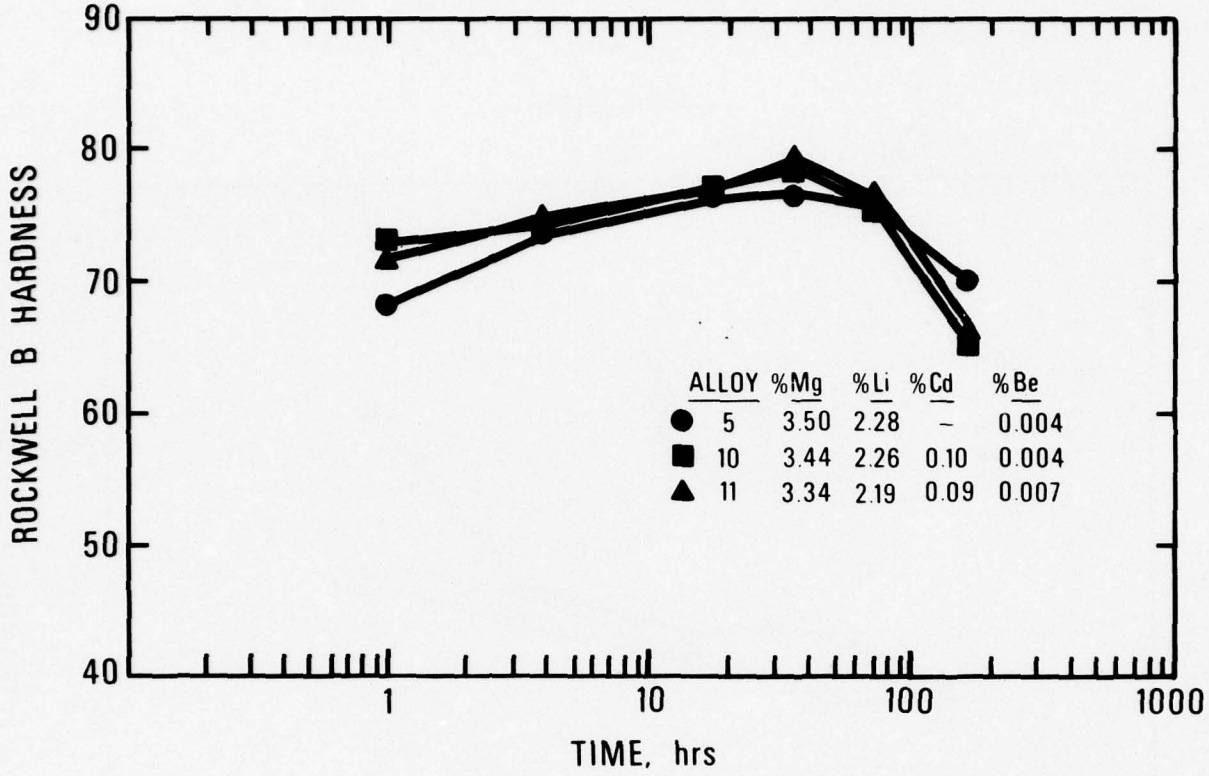

THE EFFECT OF Cd OR Cd + Be ADDITIONS TO Al-Mg-Li ALLOYS ON ARTIFICIAL AGING AT 375°F

Figure 28

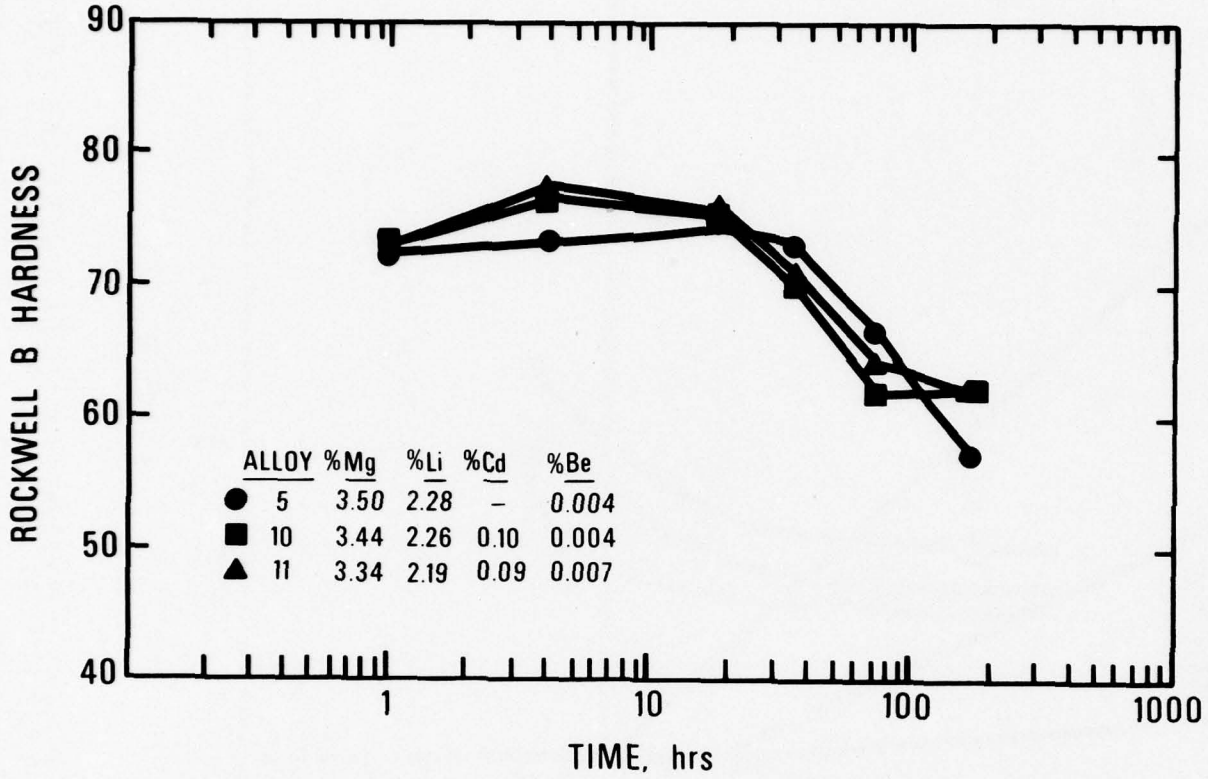

THE EFFECT OF Cd OR Cd + Be ADDITIONS TO Al-Mg-Li ALLOYS ON ARTIFICIAL AGING AT 400°F

Figure 29

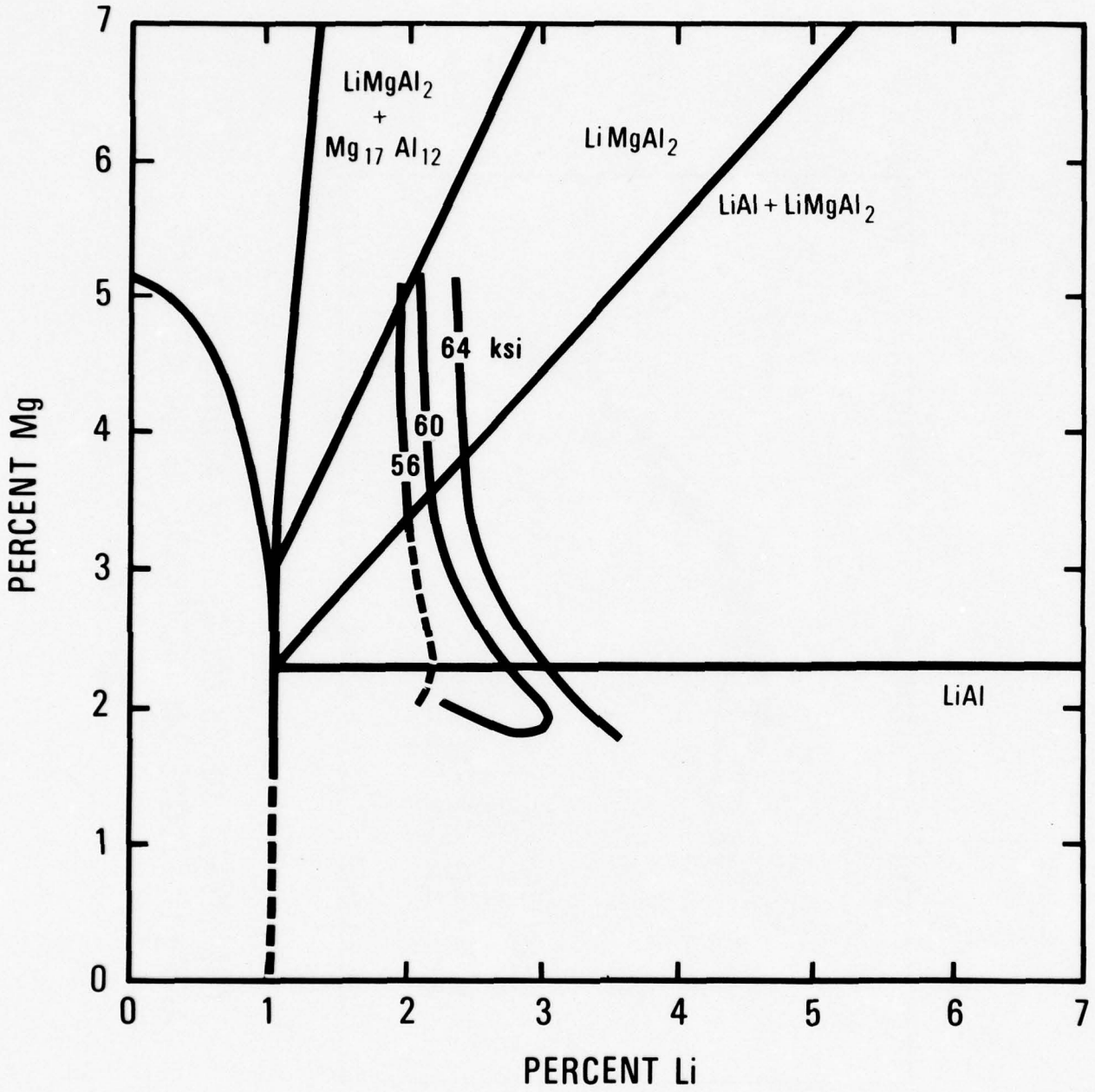

EFFECT OF COMPOSITION ON MAXIMUM LONGITUDINAL YIELD STRENGTH OF Al-Mg-Li EXTRUSIONS

Figure 30

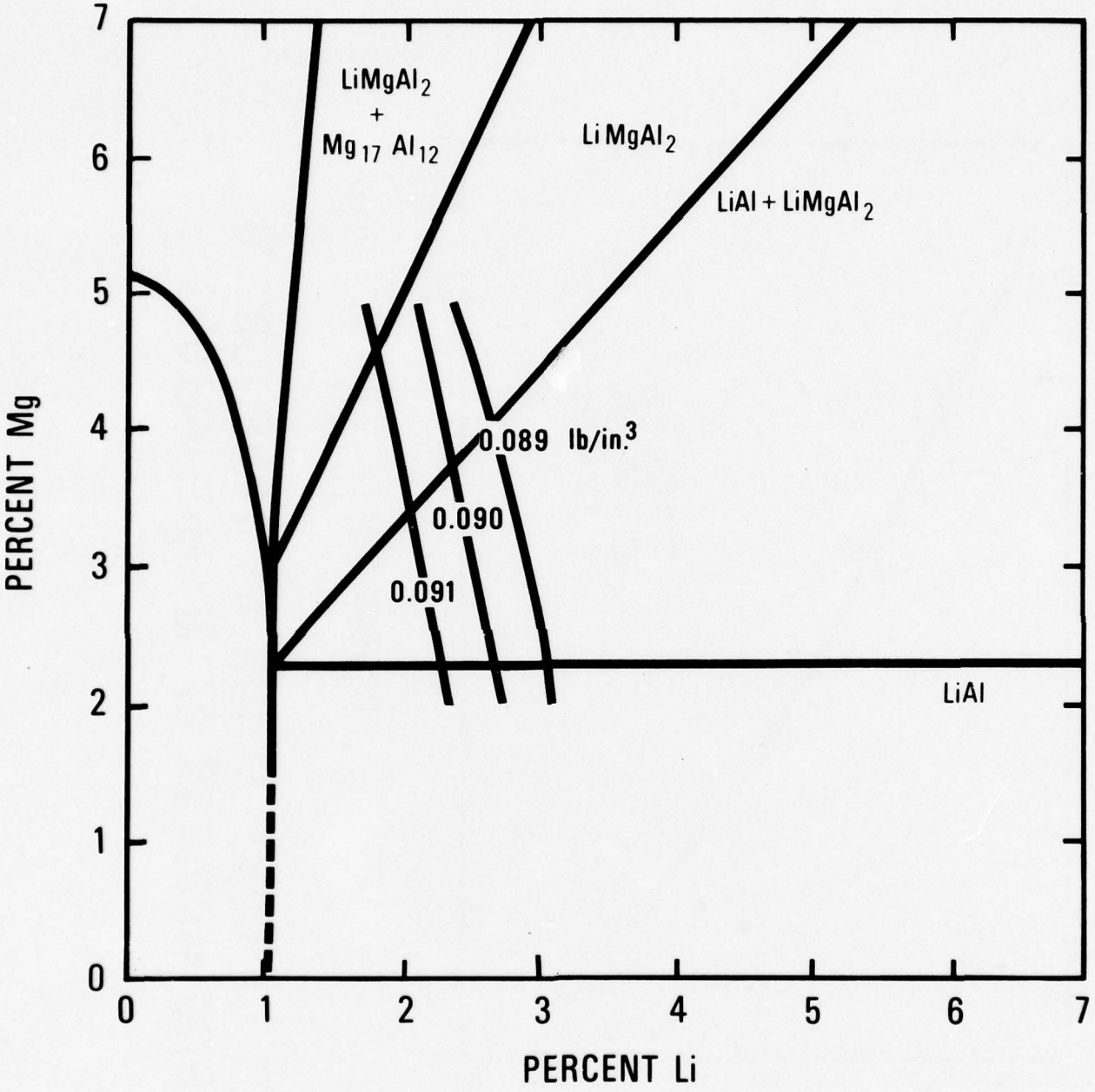

EFFECT OF COMPOSITION ON DENSITY OF Al-Mg-Li EXTRUSIONS

Figure 31

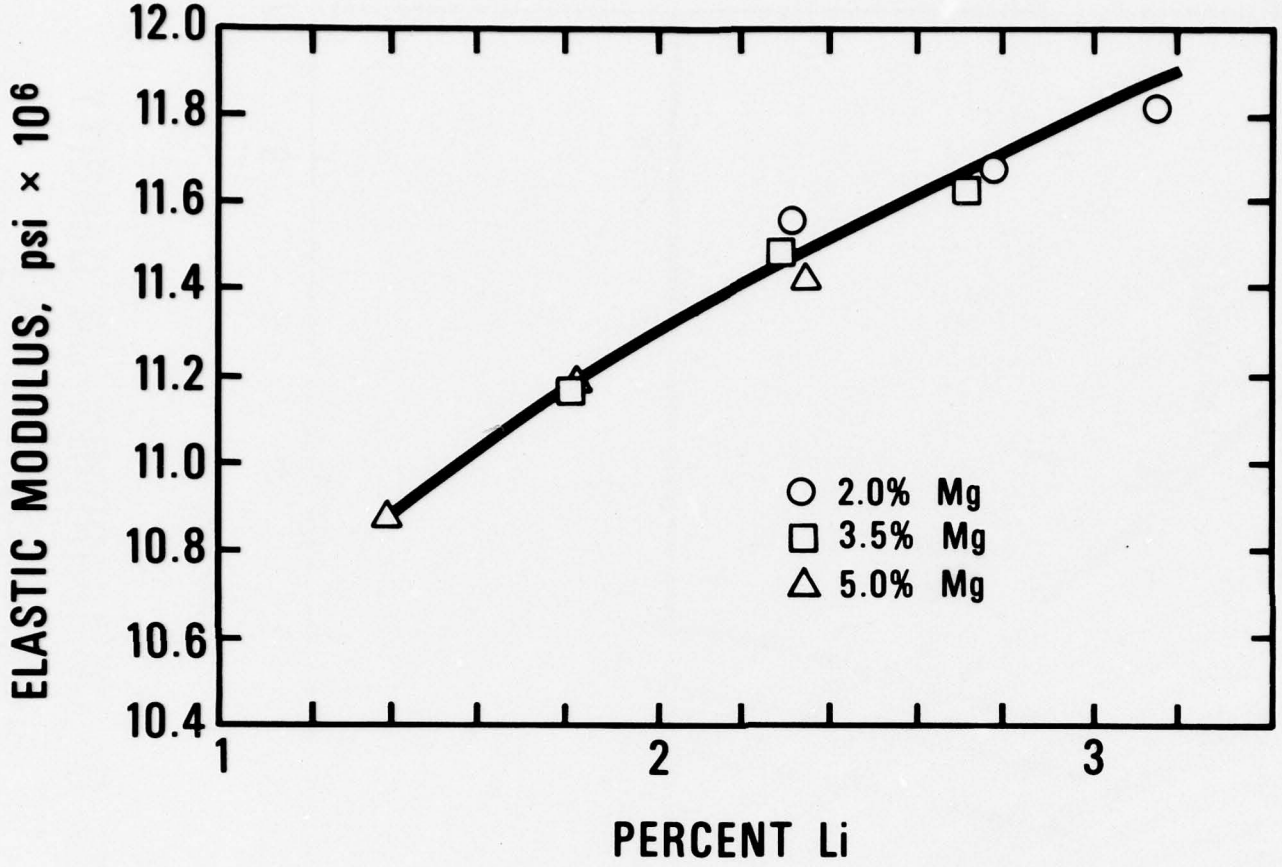

EFFECT OF COMPOSITION ON LONGITUDINAL ELASTIC MODULUS OF Al-Mg-Li ALLOYS

Figure 32

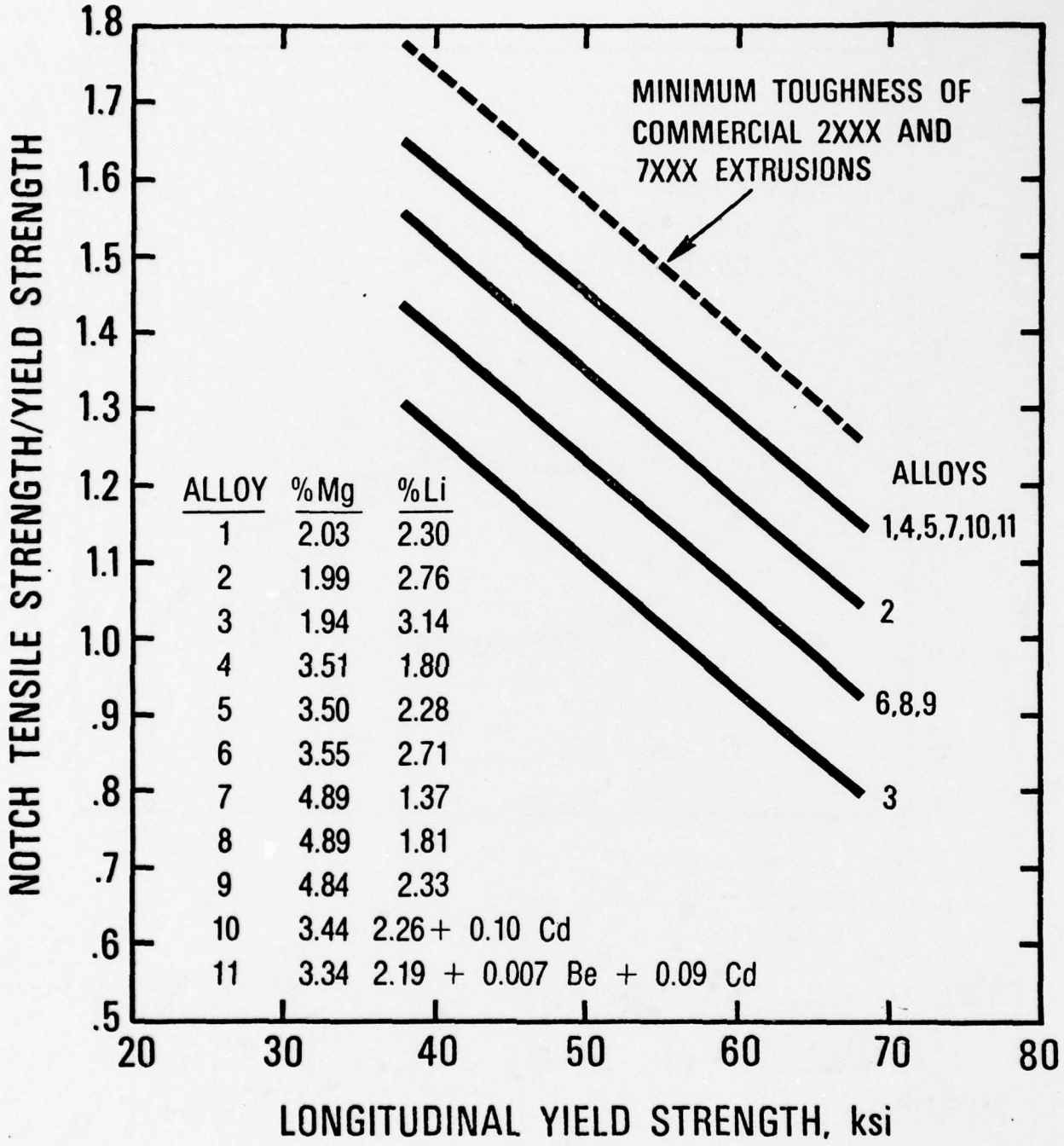

EFFECT OF YIELD STRENGTH AND COMPOSITION ON LONGITUDINAL TOUGHNESS OF Al-Mg-Li

Figure 33

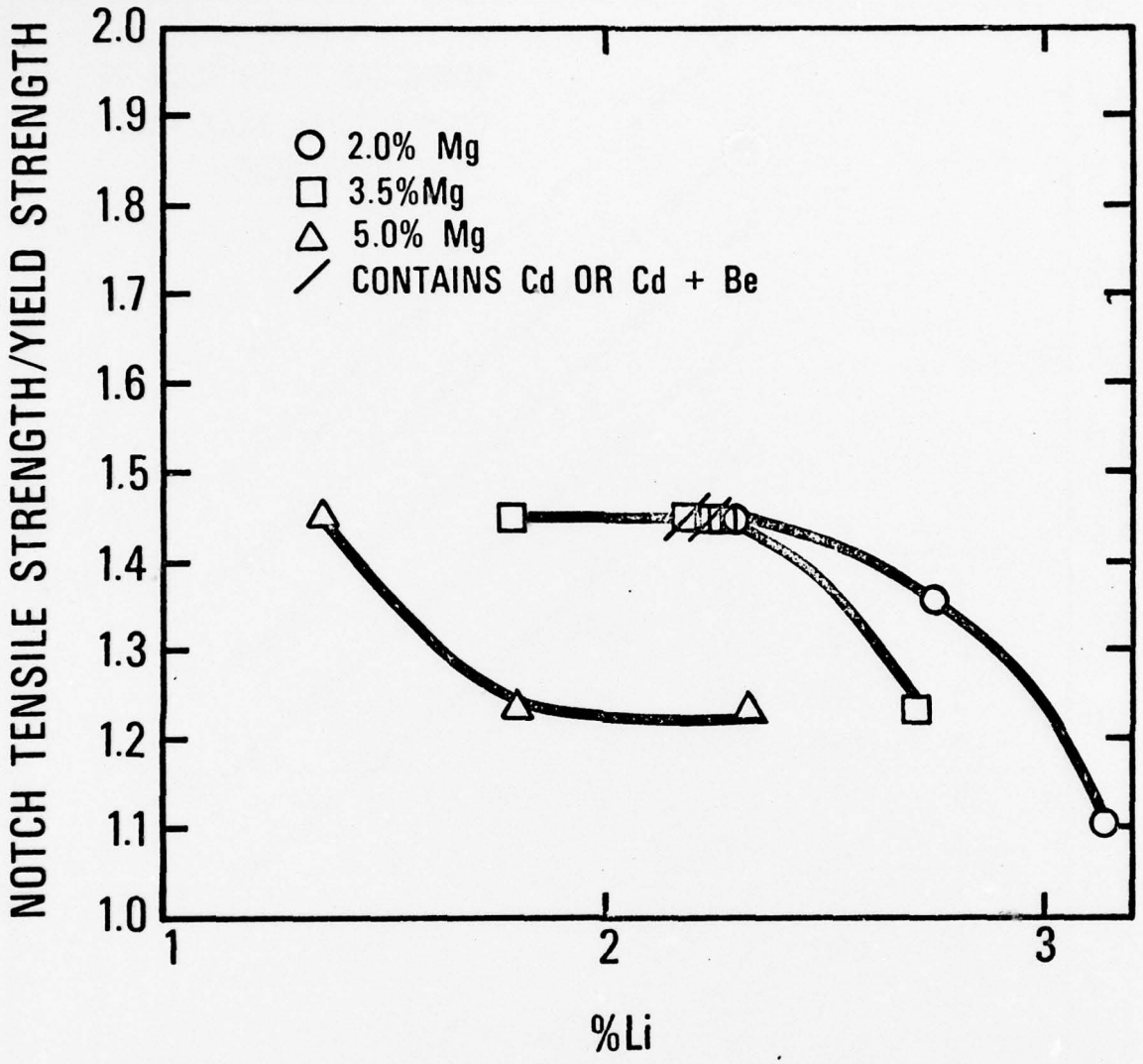

EFFECT OF COMPOSITION ON LONGITUDINAL TOUGHNESS OF Al-Mg-Li EXTRUSIONS NORMALIZED TO 50 ksi YIELD STRENGTH

Figure 34

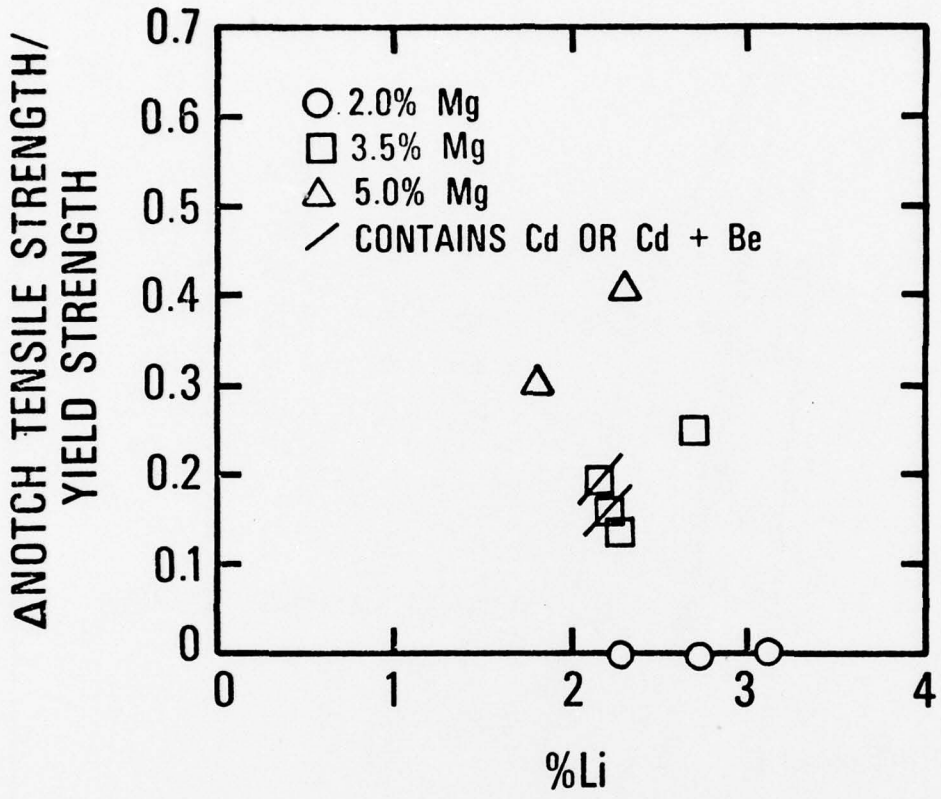

EFFECT OF COMPOSITION ON DECREASE (Δ)
IN LONGITUDINAL TOUGHNESS
OF Al-Mg-Li EXTRUSION WITH OVERAGING

Figure 35

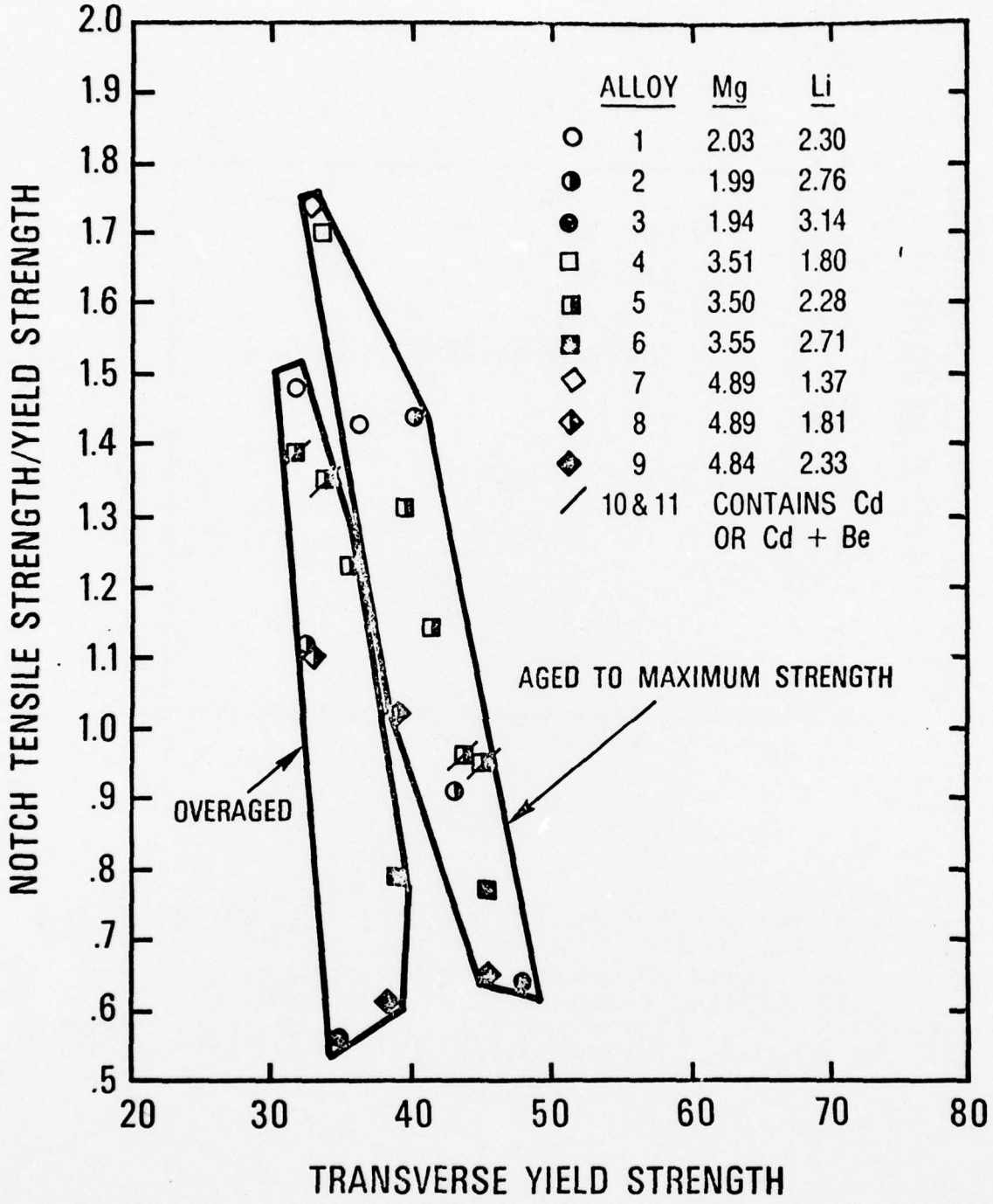

EFFECT OF YIELD STRENGTH AND AGING PRACTICE ON TRANSVERSE TOUGHNESS OF Al-Mg-Li EXTRUSIONS

Figure 36

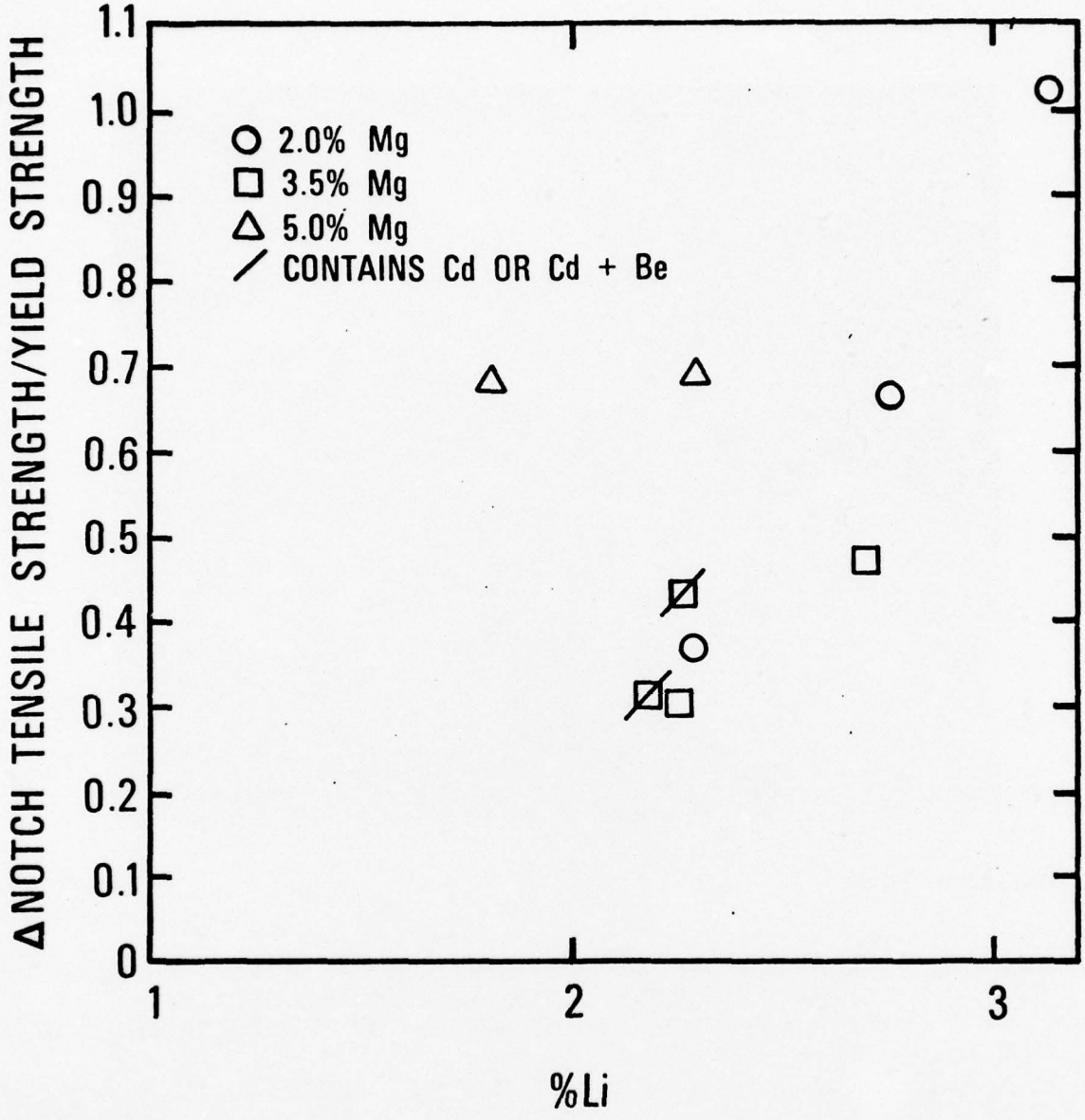

EFFECT OF COMPOSITION ON DECREASE (Δ) IN TRANSVERSE TOUGHNESS OF Al-Mg-Li EXTRUSIONS WITH OVERAGING

Figure 37

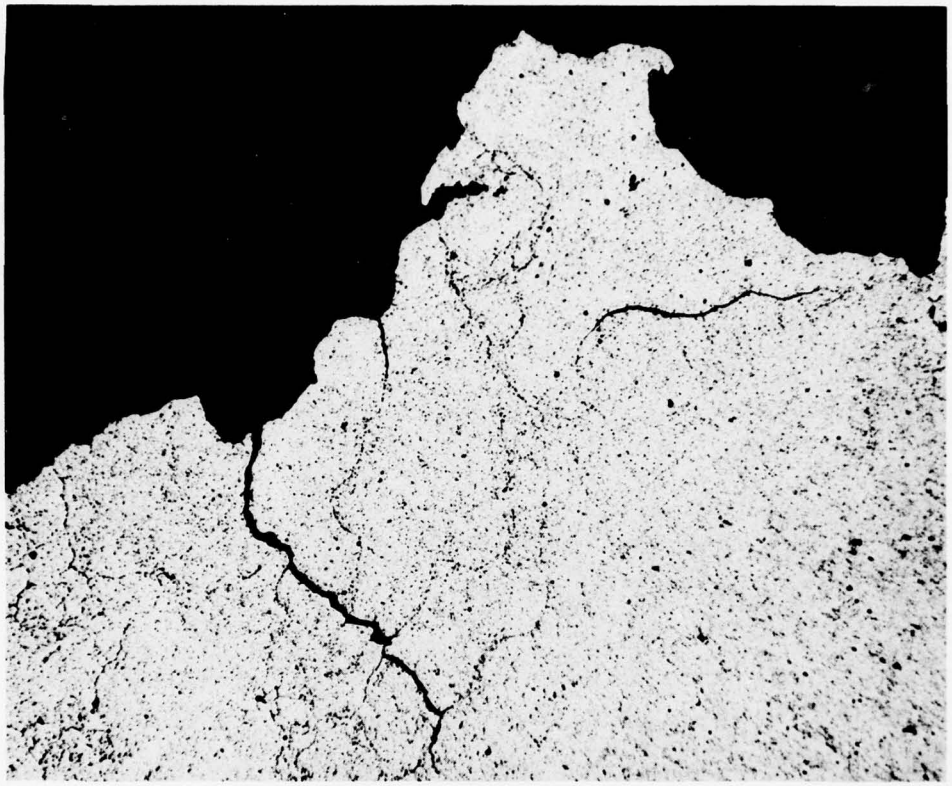

Keller's Etch 250X

FIGURE 38 - LIGHT MICROGRAPH OF PLANE NORMAL TO FRACTURED SURFACE OF NOTCHED TENSILE SPECIMEN SHOWING SECONDARY CRACKING ALONG SUB-GRAIN BOUNDARIES.

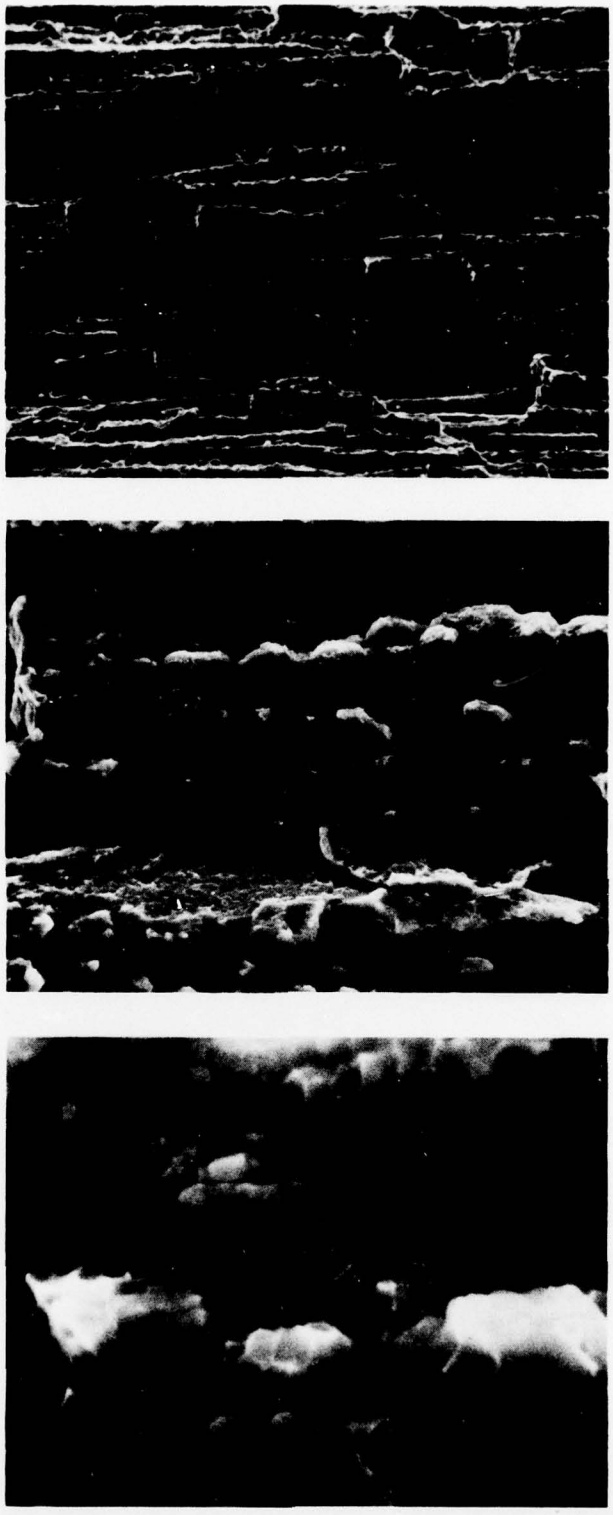

200X

1000X

5000X

FIGURE 39 - SCANNING ELECTRON MICROGRAPHS SHOWING FRACTURED SURFACE OF NOTCHED TENSILE SPECIMEN. (Al-3.59 Mg-2.9 Li-T6)

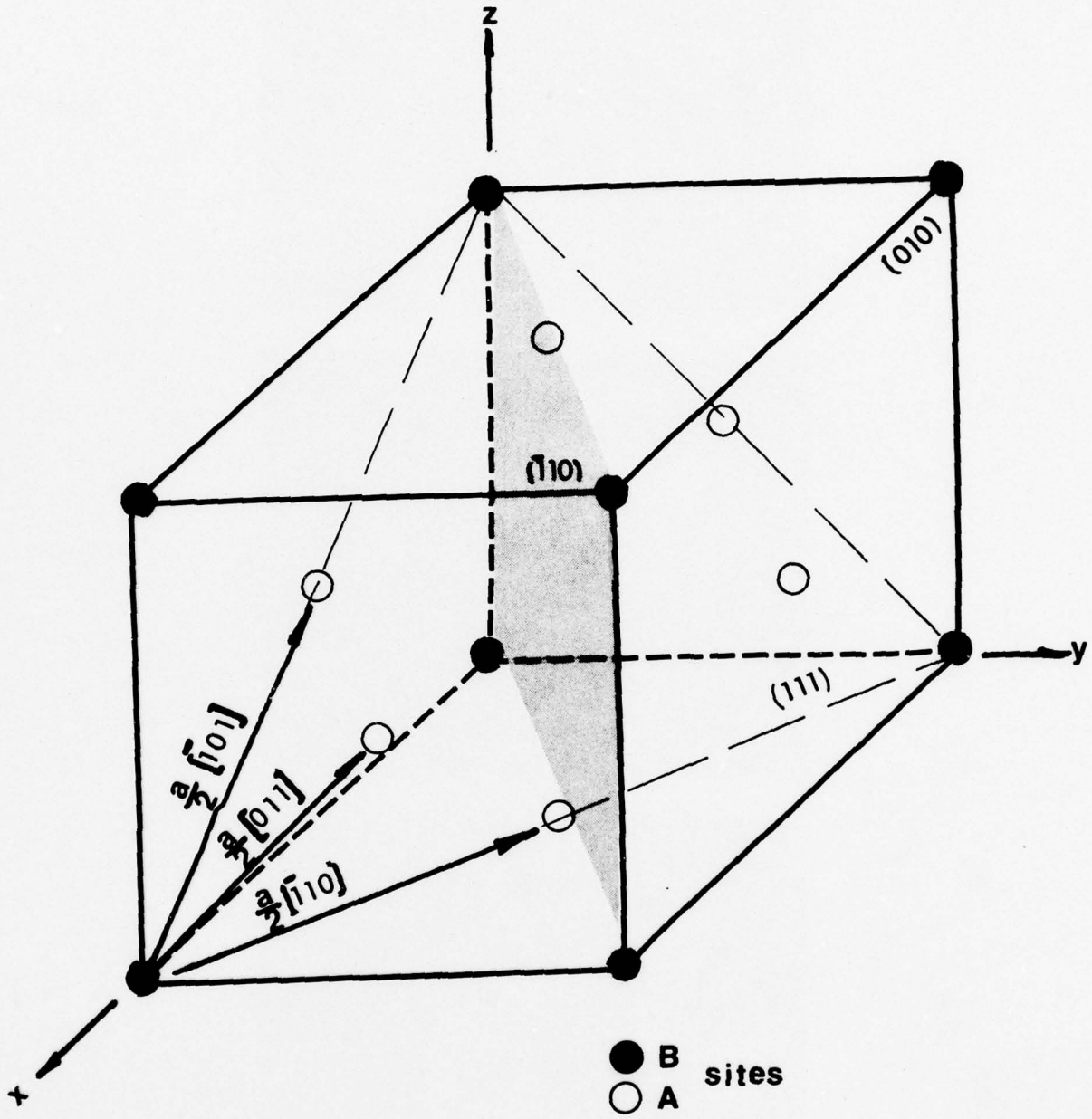

Figure 40 - Definition of Atomic Positions in the Face-Centered, Cubic (FCC) Lattice.

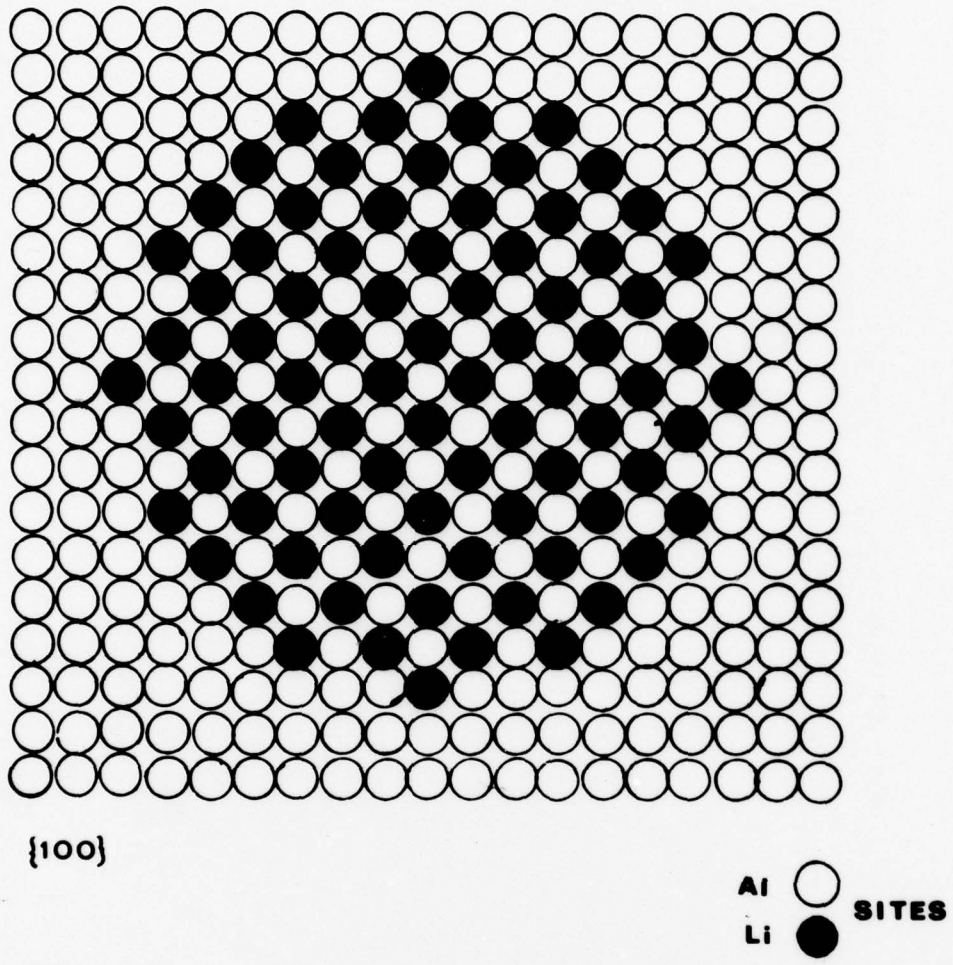

Figure 41 - A {100} Section Through a Region of Alloy Which Contains Aluminum Matrix and Al_3Li Precipitate.

Figure 42 - Spherical Precipitates of Al_3Li Produced When Al-2.86% Li is Aged at 400°F for 24 Hours.

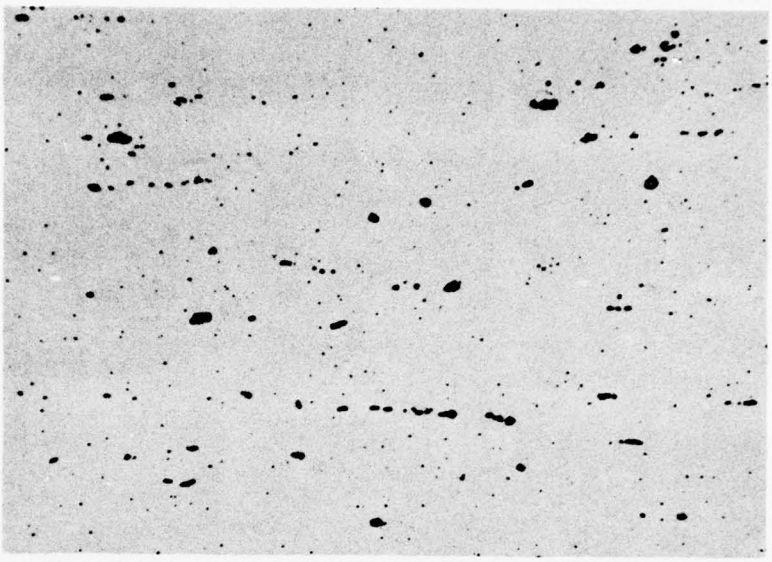

Etch: H_3PO_4 Magnification 500X

2.07 Li + 0.00 Mg (S 201202)

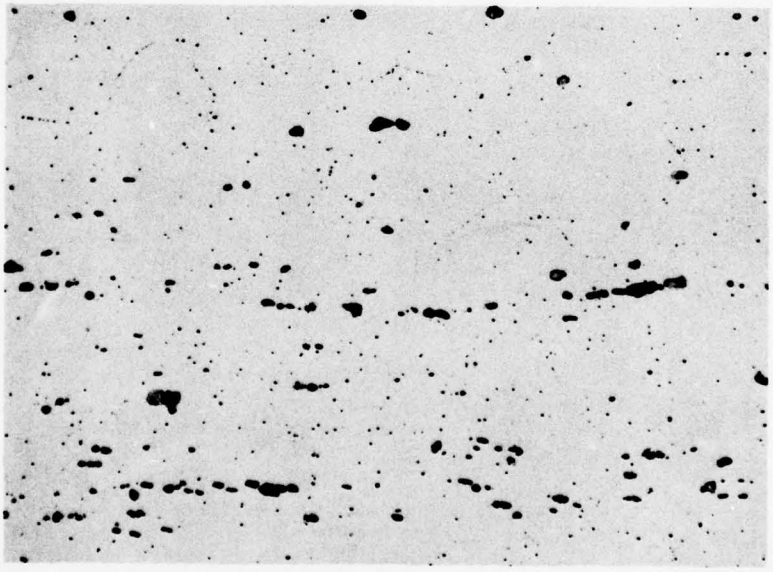

Etch: H_3PO_4 Magnification 500X

2.07 Li + 0.95 Mg (S 201203)

Figure 43a - Microstructure of Heat Treated and Aged Al-2 Li-Mg Alloys Showing Increase of Intergranular Precipitate with Increasing Magnesium Content.

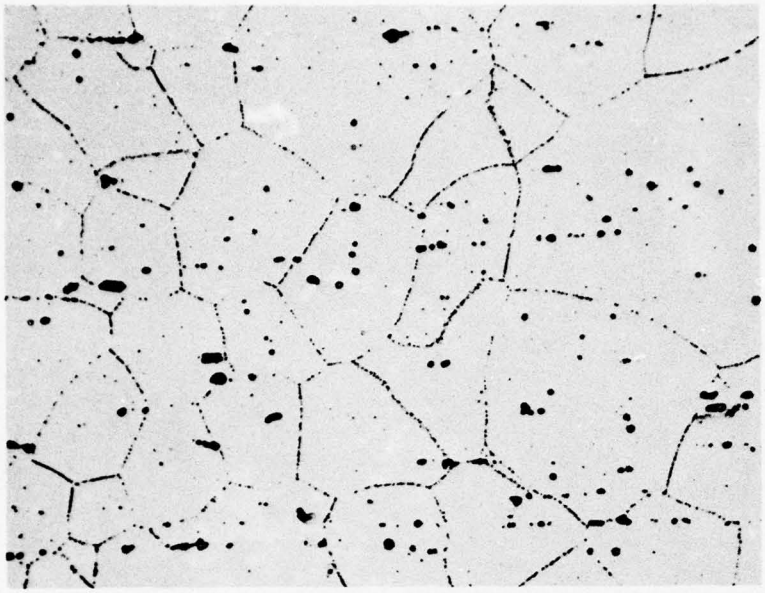

Etch: H_3PO_4 Magnification 500X

2.02 Li + 2.93 Mg (S 201205)

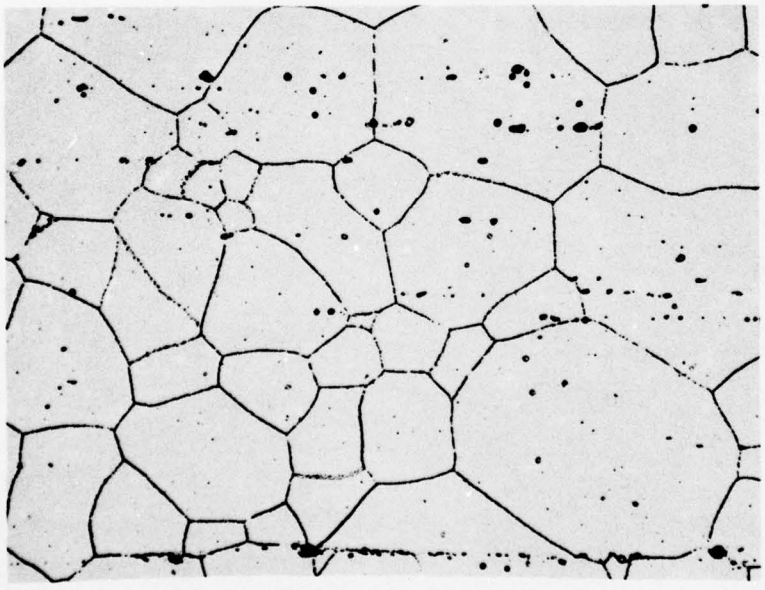

Etch: H_3PO_4 Magnification 500X

2.10 Li + 4.99 Mg (S 201207)

Figure 43b - Continued Microstructure of Heat Treated and Aged Al-2 Li Mg Alloys Showing Increase of Intergranular Precipitate with Increasing Magnesium Content.

Figure 44a - Bright Field Micrograph of 2020 Alloy in the Early Stages of Aging Showing the Fine Al_2Cu Plate-Like Precipitates.

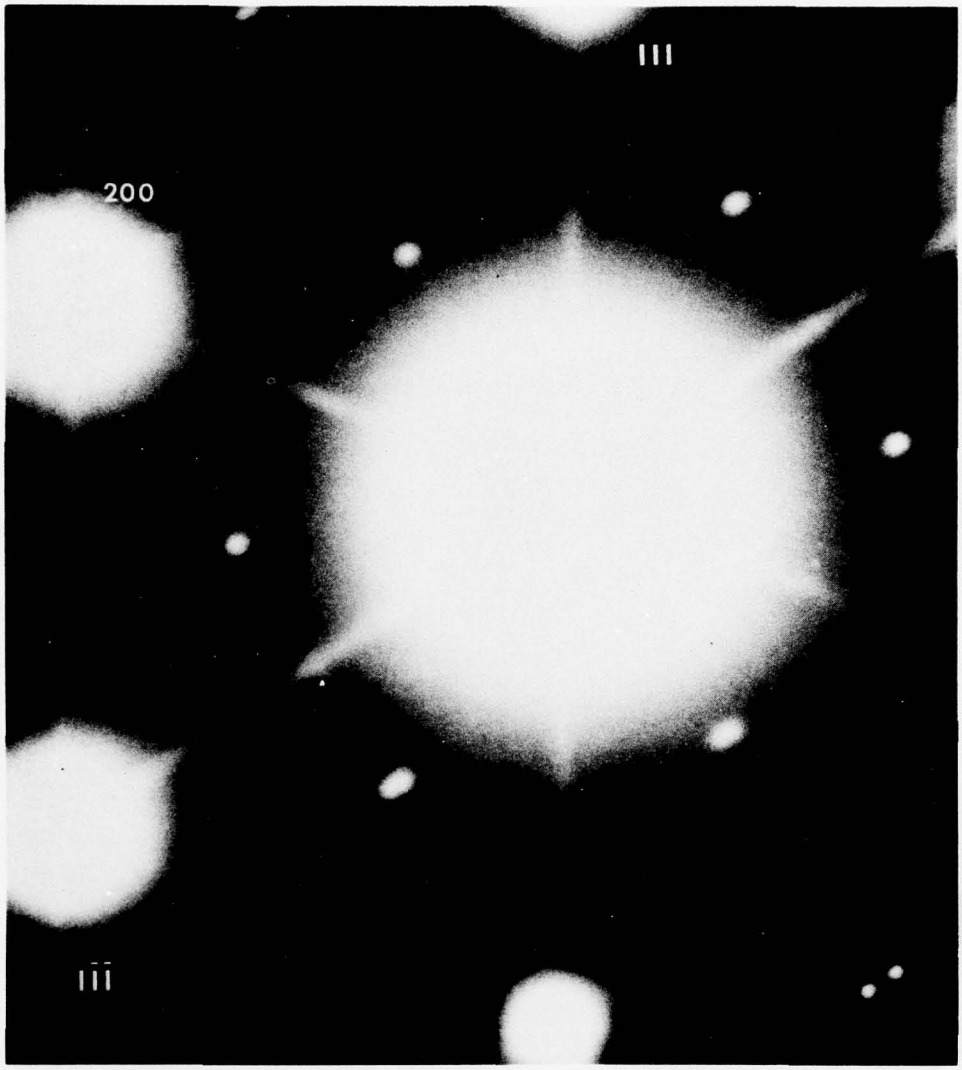

Foil Normal [$0\bar{1}1$]

Figure 44b - SAD of 44a, Showing Strong Streaking Associated with Thin Plate Al_2Cu Precipitates.

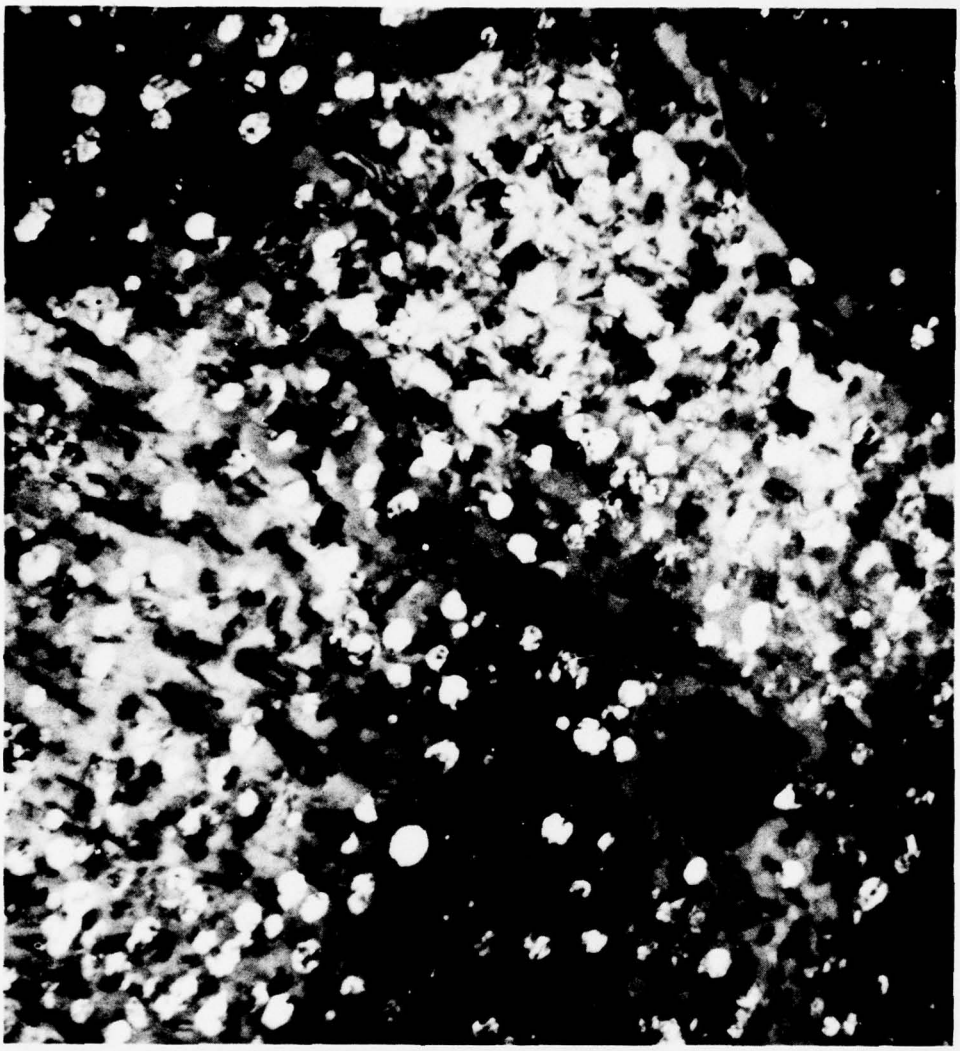

Figure 45 - Dark Field Micrograph of 2020-T651 Using (100) Superlattice Reflection. Small spherical precipitates are the metastable Al_3Li.

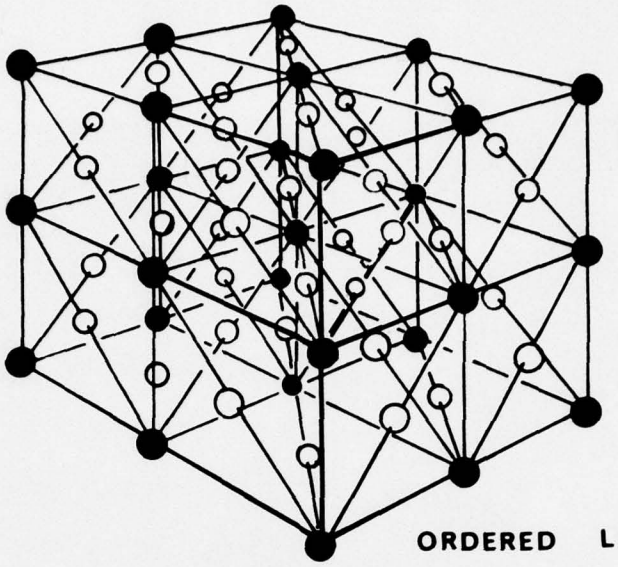

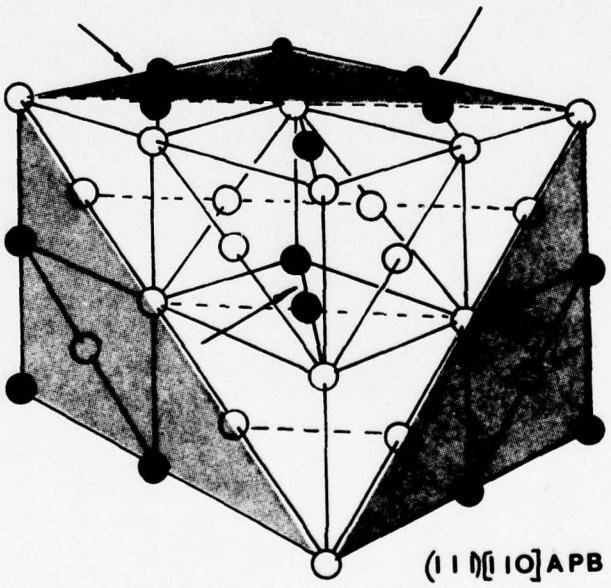

Figure 46 - (a) The Ordered Cu_3Au, $L1_2$ Structure. (b) (111)[110] Antiphase Boundary in the $L1_2$ Structure. Brackets show the creation of unlike neighbors.[26]

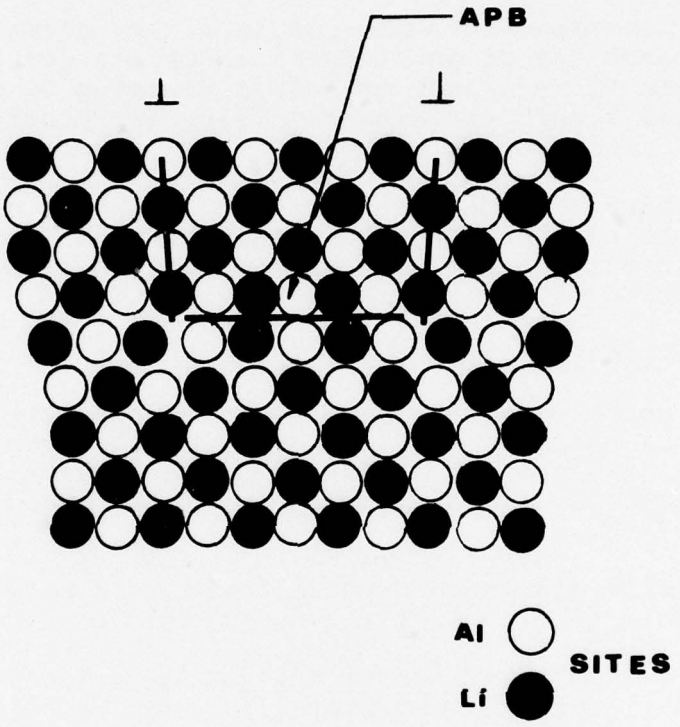

Figure 47 - A (100) Section Through a Region of Ordered Alloy Illustrating the Pair-Wise Motion of Dislocations.

APPENDIX A - SELECTION OF ANCILLARY ELEMENT ADDITION

EXPERIMENTAL

Ingot Casting and Fabrication

To determine the effect of ancillary elements on the mechanical properties of an Al-Mg-Li alloy, target compositions listed in Table A1 were cast as 6-inch diameter DC ingots and fabricated into 2-inch diameter rod using the practice described in the body of this report.

Chemical compositions of the melts were determined and are listed in Table A2. Although the analyses show little differences in Zr contents between the LoZr and HiZr ingots, the alloys will still be referred to as LoZr and HiZr.

Effect of Solution Heat Treatment Temperature

Solution heat treatment temperatures were in the range of 800 to 950°F in steps of 25°F. Samples of the as-extruded products were solution heat treated at the various temperatures for one hour, cold water quenched, and along with an "as-extruded sample" aged 48 hours at 375°F.

Tensile and notch-tensile tests were made as indicated in the body of this report.

X-ray degree of recrystallization was determined on the alloys after different solution heat treatment temperatures using unfiltered copper radiation and transmission pinhole geometry.

Density and Moduli of Elasticity

Densities and moduli of elasticity of the alloys in Table A2 were determined using procedures described in the body of this report.

RESULTS

Ingot Casting

All of the ingots were cast successfully. The surfaces of the ingots showed no deep laps, and dye-checked ingot slices showed no porosity. Etched ingot slices of LoCr, LoMn, and LoZr are shown in Figures A1-A3, respectively. The dramatic effect of Zr on the cast grain structure is readily evident.

Fabrication

Extrusion data for the different alloys are given in Table A3. Inspection of the ingots revealed that the defects were confined to the rear three feet of all the extrusions. Slices were also removed from locations two feet from the front and three feet from the rear and etched to reveal the macro-grain structure. Photographs of the etched slices are shown in Figures A4 and A5. The extremely fine grain structure of the ingots containing Zr was retained in the extruded structure. Remelt chemical analyses of the extrusions are listed in Table A4.

Effects of Solution Heat Treatment Temperature

Tensile properties for the different alloys and solution heat treatment temperatures are given in Tables A5, A6, and A7, and notch tensile strength and notch tensile strength/yield strength ratios (an indicator of the ability to plastically deform in the presence of a stress raiser) are listed in Tables A8, A9, and A10.

The longitudinal yield and tensile strengths decreased as solution heat treat temperature increased for the Lo and HiCr-containing alloys, and was constant for the Mn-containing alloys. A slight increase as solution heat treatment temperature increased was observed in the alloys which contained the Zr.

The type of ancillary element affected notch toughness. Figure A6 is a plot of the longitudinal notch toughness of the different Al-Mg-Li extrusions. For comparison, the minimum toughness of commercial 2XXX and 7XXX extrusions is given. Considering the importance of the combination of strength and toughness, the alloy containing Mn as the ancillary element appeared to have the most promise. Figure A7 is a plot in the transverse direction. Because sufficient transverse data for commercial alloy extrusions were not available, a comparison of the 2XXX and 7XXX alloys could not be given. But one could speculate that in the transverse direction, the fracture toughness of these alloys is probably lower than in other commercial medium-strength alloys.

Densities and Elastic Moduli

The densities are listed in Table A11; although alloy LoMn showed the lowest densities, densities among the alloys varied very little. The average density of all six alloys was 2.500 grams/cm^3, which is lower than the average density of either 2024 or 7075, 2.803 and 2.781, respectively.

The moduli of elasticity are listed in Table A12. The moduli for the three alloys were similar.

DISCUSSION OF RESULTS

Reviewing the tensile data given in Tables A5-A7, one can speculate as to the cause of the reduction in yield and tensile strengths with increased solution heat treatment temperature in the alloys which contained Cr. X-ray degree of recrystallization revealed that as temperature increased, there was a corresponding increase in the degree of recrystallization (Figure A8a). The loss in strength can be explained on the basis of a reduction in the duplex extrusion texture as a consequence of recrystallization during solution heat treatment. The difference in the notch toughness of the HiCr and LoCr alloys can be explained on the basis of the development of coarse Cr constituent in the alloy containing the high Cr.

The yield and tensile strengths of the Mn alloys changed little with increasing solution heat treatment temperature. No detectable change in degree of recrystallization between 800 and 900°F was observed (Figure A8b). A comparison between the notch tensile strength and yield strength data suggests that the LoMn alloy provides a better combination of these properties (Tables A6 and A9).

An increase in yield and tensile strengths resulted when the solution heat treatment temperature increased in the Zr alloys (Table A7). There was no apparent change in the degree of recrystallization as a function of solution heat treatment temperature (Figure A8c). The mechanism which is responsible for the increase in strength with increased solution heat treatment temperature is unknown at this time.

A comparison of notch tensile strength, yield strength ratio as a function of yield strength for the different alloys suggests a slight advantage can be realized by using Mn instead of Zr and a significant advantage by using Mn instead of Cr.

CONCLUSION

On the basis of the combination of strength and toughness, an addition of 0.3% Mn should be used in the work to determine the optimum Li and Mg content.

TABLE A1

TARGET COMPOSITIONS OF ALLOYS FOR DETERMINATION OF ANCILLARY ELEMENT

Alloy	Mg	Li	Cr	Mn	Zr	Ti	Be
LoCr	3.5	2.5	0.1	--	--	0.02	0.005
HiCr	3.5	2.5	0.3	--	--	0.02	0.005
LoMn	3.5	2.5	--	0.3	--	0.02	0.005
HiMn	3.5	2.5	--	0.5	--	0.02	0.005
LoZr	3.5	2.5	--	--	0.1	0.02	0.005
HiZr	3.5	2.5	--	--	0.2	0.02	0.005

TABLE A2

MELT ANALYSES OF INGOTS FOR DETERMINATION OF ANCILLARY ELEMENT

Alloy	S. Number	Si	Fe	Cu	Mn	Mg	Cr	Ni	Zn	Ti	Be	Zr	Li
LoCr	427083A	0.04	0.06	0.00	0.00	3.51	0.10	0.00	0.00	0.02	0.005	0.00	2.50
HiCr	427084B	0.05	0.06	0.00	0.00	3.51	0.31	0.00	0.00	0.02	0.004	0.00	2.46
LoMn	427085A	0.03	0.05	0.00	0.28	3.54	0.00	0.00	0.00	0.02	0.004	0.00	2.49
HiMn	427086A	0.04	0.05	0.00	0.47	3.49	0.00	0.00	0.00	0.02	0.005	0.00	2.46
LoZr	427087A	0.04	0.05	0.00	0.01	3.49	0.00	0.00	0.00	0.02	0.005	0.12	2.47
HiZr	427088A	0.04	0.06	0.00	0.01	3.45	0.00	0.00	0.00	0.02	0.005	0.14	2.44

TABLE A3

EXTRUSION DATA FOR 6-INCH DIAMETER Al-Mg-Li DC INGOTS

Alloy	Ingot S. Number	Reheat Temperature, °F	Extrusion Temperature, °F	Extrusion Speed, in./min	Breakout Pressure, ksi	Butt Length, inch	Extrusion S. Number
LoCr	427083A	700	698	2-4	148	2-1/2	427089
HiCr	427084B	700	709	4	141	2-1/2	427090
LoMn	427085A	700	704	4	130	2-1/2	427091
HiMn	427086A	700	700	4	150	2-1/2	427092
LoZr	427087A	700	700	4	137	2-1/2	427093
HiZr	427088A	700	707	4	145	2-1/2	427094

TABLE A4

REMELT ANALYSES OF EXTRUSIONS FOR DETERMINATION OF ANCILLARY ELEMENT

Alloy	S. Number	Si	Fe	Cu	Mn	Mg	Cr	Ni	Zn	Ti	Be	Zr	Li	Na
LoCr	427089	0.05	0.07	0.00	0.00	3.54	0.10	0.00	0.00	0.02	0.004	--	2.43	0.003
HiCr	427090	0.05	0.08	0.00	0.00	3.47	0.28	0.00	0.00	0.02	0.004	--	2.45	0.003
LoMn	427091	0.04	0.06	0.00	0.30	3.59	0.00	0.00	0.00	0.02	0.004	--	2.50	0.003
HiMn	427092	0.04	0.07	0.00	0.49	3.54	0.00	0.00	0.00	0.02	0.005	--	2.50	0.002
LoZr	427093	0.04	0.07	0.00	0.00	3.53	0.00	0.00	0.00	0.02	0.004	0.14	2.50	0.003
HiZr	427094	0.04	0.06	0.00	0.00	3.53	0.00	0.00	0.00	0.02	0.004	0.14	2.57	0.003

TABLE A5

THE EFFECTS OF SOLUTION HEAT TREATMENT TEMPERATURES ON TENSILE PROPERTIES OF Al-Mg-Li ALLOY EXTRUSIONS CONTAINING Cr

Solution Heat Treatment Temperature, °F	Sample Number	Longitudinal T.S., ksi	Y.S., ksi	% El. in 2"	R of A, %	Transverse T.S., ksi	Y.S., ksi	% El. in 0.64"	R of A, %
		LoCr - S. No. 427089							
As Extruded	1	54.8	30.6	7.5[1]	7	44.5	19.8	12.5	12
As Extruded/Artificially Aged	2	62.0	40.8	4.0	4	52.5	32.1	4.7	4
800	3	69.2	54.8	2.0[1]	2	47.5	36.6	1.6	6
825	4	68.1	53.4	3.5	6	58.5	35.4	4.7	5
850	5	68.0	52.2	2.5	2	57.2	35.4	4.7	5
875	6	67.5	50.9	2.5	2	57.5	36.2	4.7	5
900	7	65.7	46.9	3.5	3	58.2	36.6	6.2	5
925	8	66.7	47.9	3.5	3	56.7	36.6	3.1	5
950	9	64.4	44.6	3.5	3	56.2	35.1	6.2	6
		HiCr - S. No. 427090							
As Extruded	1	57.8	36.9	7.5	7	33.7	21.5	1.6	3
As Extruded/Artificially Aged	2	63.9	36.0	4.5	5	32.3	30.6	1.6	0
800	3	([2])	([2])	2.5[1]	2	34.6	34.0	1.6	0
825	4	64.4	49.7	2.5	3	36.0	36.1	1.6	1
850	5	63.4	47.1	3.5	3	38.9	37.3	1.6	1
875	6	64.7	46.1	2.5	2	40.0	37.9	1.6	0
900	7	59.9	40.8	3.5	6	40.0	37.2	1.6	0
925	8	58.8	41.3	4.0	4	39.3	36.9	1.6	0
950	9	59.8	38.2	4.0	6	38.4	36.1	1.6	0

Samples 3 through 9 solution heat treated 1 hour at temperatures indicated, quenched in cold water, and artificially aged 48 hours at 375°F.

NOTES: 1. Failed outside of gauge length.
2. Recorder malfunctioned; tensile and yield loads not recorded.

TABLE A6

THE EFFECTS OF SOLUTION HEAT TREATMENT TEMPERATURES ON TENSILE PROPERTIES OF Al-Mg-Li ALLOY EXTRUSIONS CONTAINING Mn

Solution Heat Treatment Temperature, °F	Sample Number	Longitudinal T.S., ksi	Y.S., ksi	% El. in 2"	R of A, %	Transverse T.S., ksi	Y.S., ksi	% El. in 0.64"	R of A, %
		LoMn - S. No. 427091							
As Extruded	1	59.9	38.8	4.5[1]	4	51.8	25.7	7.8	10
As Extruded/Artificially Aged	2	67.8	54.5	3.0	5	59.7	37.3	4.7	5
800	3	71.1	61.6	2.0	4	55.6	37.9	3.1	6
825	4	70.5	63.4	1.0[1]	1	57.5	38.4	3.1	6
850	5	69.3	63.9	0.05[1]	1	56.0	38.4	3.1	4
875	6	70.8	62.9	0.05[1]	1	59.5	38.7	3.1	2
900	7	70.6	61.9	0.05[1]	1	60.0	38.7	4.7	6
925	8	71.0	60.9	1.5	2	60.0	39.0	4.7	2
950	9	70.5	62.2	1.0[1]	2	58.0	38.2	2.1	4
		HiMn - S. No. 427092							
As Extruded	1	60.1	40.2	6.0[1]	6	53.7	23.7	12.5	18
As Extruded/Artificially Aged	2	69.0	46.8	2.5	5	59.7	39.3	3.1	1
800	3	72.3	61.9	2.0[1]	2	59.5	39.4	3.1	4
825	4	70.8	59.9	1.5[1]	2	59.5	39.4	3.1	2
850	5	70.3	57.8	1.5[1]	2	60.0	39.6	4.7	2
875	6	69.8	57.6	1.5[1]	2	61.4	39.0	4.7	4
900	7	70.0	57.1	2.5	3	60.7	39.3	4.7	5
925	8	71.3	58.3	2.5	4	60.9	39.6	3.1	4
950	9	70.1	57.2	1.5[1]	2	60.7	39.3	4.7	4

Samples 3 through 9 solution heat treated 1 hour at temperatures indicated, quenched in cold water, and artificially aged 48 hours at 375°F.

NOTE: 1. Failed outside of gauge length.

TABLE A7

THE EFFECTS OF SOLUTION HEAT TREATMENT TEMPERATURE ON TENSILE PROPERTIES OF Al-Mg-Li ALLOY EXTRUSIONS CONTAINING Zr

Solution Heat Treatment Temperature, °F	Sample Number	Longitudinal T.S., ksi	Y.S., ksi	% El. in 2"	R of A, %	Transverse T.S., ksi	Y.S., ksi	% El. in 0.64"	R of A, %
		LoZr - S. No. 427093							
As Extruded	1	59.6	40.4	9.0	11	47.2	29.4	6.2	5
As Extruded/Artificially Aged	2	66.7	47.4	5.5[1]	5	52.7	39.1	3.1	2
800	3	70.3	53.2	5.5	6	59.7	40.7	3.1	5
825	4	71.3	54.5	5.0	5	57.7	41.0	3.1	4
850	5	72.3	55.8	4.0[1]	3	55.5	41.5	1.6	1
875	6	72.9	56.7	4.0[1]	4	55.7	41.5	3.1	1
900	7	73.3	57.1	3.5[1]	4	51.7	41.3	3.1	2
925	8	73.6	57.8	3.5	5	50.2	42.1	1.6	4
950	9	76.7	57.5	7.0[3]	9	52.5	42.2	1.6	4
		HiZr - S. No. 427094							
As Extruded	1	64.2	46.8	8.0	10	49.1	31.8	4.7	4
As Extruded/Artificially Aged	2	69.0	49.3	6.0	8	55.5	40.4	3.1	4
800	3	71.3	53.0	6.5	5	57.4	41.0	3.1	4
825	4	71.8	54.0	4.0[2]	4	56.1	41.5	3.1	4
850	5	72.3	56.0	3.5[1]	3	56.8	41.8	3.1	4
875	6	73.6	57.0	5.0[1]	3	55.2	41.9	3.1	1
900	7	73.8	58.3	4.0[1]	4	55.7	41.9	3.1	2
925	8	77.5	61.4	7.0[3]	9	50.7	42.2	1.6	0
950	9	77.9	59.3	1.0[3]	5	—	--	-	-

Samples 3 through 9 solution heat treated 1 hour at temperatures indicated, quenched in cold water, and artificially aged 48 hours at 375°F.

NOTES:
1. Failed outside of gauge length.
2. Failed near end of gauge length.
3. Elongation in 1.0-in. gauge length.

TABLE A8

THE EFFECTS OF SOLUTION HEAT TREATMENT TEMPERATURE ON NOTCH TOUGHNESS OF Al-Mg-Li ALLOY EXTRUSIONS CONTAINING Cr

Solution Heat Treatment Temperature, °F	Sample Number	Longitudinal Y.S., ksi	Longitudinal N.T.S., ksi	Longitudinal NTS/YS	Transverse Y.S., ksi	Transverse N.T.S., ksi	Transverse NTS/YS
		LoCr - S. No. 427089					
As Extruded	1	30.6	56.2	1.84	19.8	46.5	2.35
As Extruded/Artificially Aged	2	40.8	60.3	1.48	32.1	50.1	1.56
800	3	54.8	69.5	1.27	36.6	51.6	1.41
825	4	53.4	71.0	1.33	35.4	53.1	1.50
850	5	52.2	67.9	1.30	35.4	53.6	1.51
875	6	50.9	66.9	1.31	36.2	51.6	1.43
900	7	46.9	65.9	1.41	36.6	51.1	1.40
925	8	47.9	65.9	1.38	36.6	54.1	1.48
950	9	44.6	63.8	1.43	35.1	53.6	1.53
		HiCr - S. No. 427090					
As Extruded	1	36.9	59.8	1.62	21.5	37.3	1.73
As Extruded/Artificially Aged	2	36.0	53.1	1.48	30.6	35.8	1.17
800	3	--	62.8	--	34.0	40.3	1.19
825	4	49.7	61.3	1.23	36.0	36.8	1.02
850	5	47.1	61.3	1.30	37.3	38.3	1.03
875	6	46.1	57.2	1.24	37.9	41.9	1.11
900	7	40.8	59.8	1.47	37.2	37.3	1.00
925	8	41.3	60.3	1.46	36.9	41.9	1.14
950	9	38.2	57.7	1.51	36.1	49.5	1.37

Samples 3 through 9 solution heat treated 1 hour at temperatures indicated, quenched in cold water, and artificially aged 48 hours at 375°F.

TABLE A9

THE EFFECTS OF SOLUTION HEAT TREATMENT TEMPERATURE ON NOTCH TOUGHNESS OF Al-Mg-Li ALLOY EXTRUSIONS CONTAINING Mn

Solution Heat Treatment Temperature, °F	Sample Number	Longitudinal Y.S., ksi	Longitudinal N.T.S., ksi	Longitudinal NTS/YS	Transverse Y.S., ksi	Transverse N.T.S., ksi	Transverse NTS/YS
		LoMn - S. No. 427091					
As Extruded	1	38.0	58.2	1.53	25.7	47.0	1.83
As Extruded/Artificially Aged	2	54.5	69.5	1.28	37.3	49.0	1.31
800	3	61.6	71.5	1.16	37.9	46.5	1.27
825	4	63.4	71.5	1.13	38.4	47.0	1.22
850	5	63.9	72.0	1.13	38.4	41.9	1.09
875	6	62.9	70.5	1.12	38.7	37.8	0.98
900	7	61.9	71.0	1.15	38.7	44.4	1.15
925	8	60.9	71.5	1.17	39.0	42.4	1.09
950	9	62.2	74.1	1.19	38.2	46.5	1.22
		HiMn - S. No. 427092					
As Extruded	1	40.2	64.4	1.60	23.7	51.1	2.16
As Extruded/Artificially Aged	2	56.8	67.9	1.20	39.3	44.9	1.14
800	3	61.9	71.0	1.15	39.4	46.5	1.18
825	4	59.9	71.5	1.19	39.4	43.9	1.11
850	5	57.8	70.5	1.22	39.6	44.9	1.13
875	6	57.6	68.9	1.20	39.0	45.5	1.17
900	7	57.1	68.9	1.21	39.3	42.9	1.09
925	8	58.3	68.4	1.17	39.6	46.5	1.17
950	9	57.2	70.5	1.23	39.3	49.5	1.26

Samples 3 through 9 solution heat treated 1 hour at temperatures indicated, quenched in cold water, and artificially aged 48 hours at 375°F.

TABLE A10

THE EFFECTS OF SOLUTION HEAT TREATMENT TEMPERATURE ON NOTCH TOUGHNESS OF Al-Mg-Li ALLOY EXTRUSIONS CONTAINING Zr

Solution Heat Treatment Temperature, °F	Sample Number	Longitudinal Y.S., ksi	Longitudinal N.T.S., ksi	Longitudinal NTS/YS	Transverse Y.S., ksi	Transverse N.T.S., ksi	Transverse NTS/YS
		LoZr - S. No. 427093					
As Extruded	1	40.4	57.2	1.42	29.4	42.4	1.44
As Extruded/Artificially Aged	2	47.4	62.3	1.31	39.1	32.7	0.84
800	3	53.2	70.5	1.33	40.7	38.8	0.95
825	4	54.5	70.5	1.29	41.0	38.8	0.95
850	5	55.8	67.4	1.21	41.5	39.3	0.95
875	6	56.7	74.1	1.31	41.5	41.4	1.00
900	7	57.1	66.4	1.16	41.3	30.6	0.74
925	8	57.8	59.2	1.02	42.1	28.1	0.67
950	9	57.5	60.3	1.05	42.2	30.1	0.71
		HiZr - S. No. 427094					
As Extruded	1	46.8	61.8	1.32	31.8	42.4	1.33
As Extruded/Artificially Aged	2	49.3	61.3	1.24	40.4	30.1	0.75
800	3	53.0	69.5	1.31	41.0	34.2	0.83
825	4	54.0	71.0	1.31	41.5	35.8	0.86
850	5	56.0	72.5	1.29	41.8	37.3	0.89
875	6	57.0	76.1	1.34	41.9	39.3	0.94
900	7	58.3	74.6	1.28	41.9	36.8	0.88
925	8	61.4	60.1	0.98	42.2	26.6	0.63
950	9	59.3	60.8	1.03	--	--	--

Samples 3 through 9 solution heat treated 1 hour at temperatures indicated, quenched in cold water, and artificially aged 48 hours at 375°F.

TABLE A11

DENSITIES OF Al-Mg-Li ALLOYS CONTAINING Cr, Mn, OR Zr

Alloy	S. Number	grams/cm^3	lb/in.^{3}
LoCr	427089	2.4966	0.0902
HiCr	427090	2.5081	0.0906
LoMn	427091	2.4926	0.0900
HiMn	427092	2.4970	0.0902
LoZr	427093	2.5081	0.0906
HiZr	427094	2.5002	0.0903

TABLE A12

MODULI OF ELASTICITY OF Al-Mg-Li ALLOYS CONTAINING Cr, Mn, OR Zr

Alloy	S. Number	Dash Number	Modulus of Elasticity psix10^6	
LoCr	427089	1	11.04	
		2	10.83	
			10.94	Avg
LoMn	427091	1	10.90	
		2	11.23	
			11.07	Avg
HiMn	427092	1	11.13	
		2	11.13	
			11.13	Avg

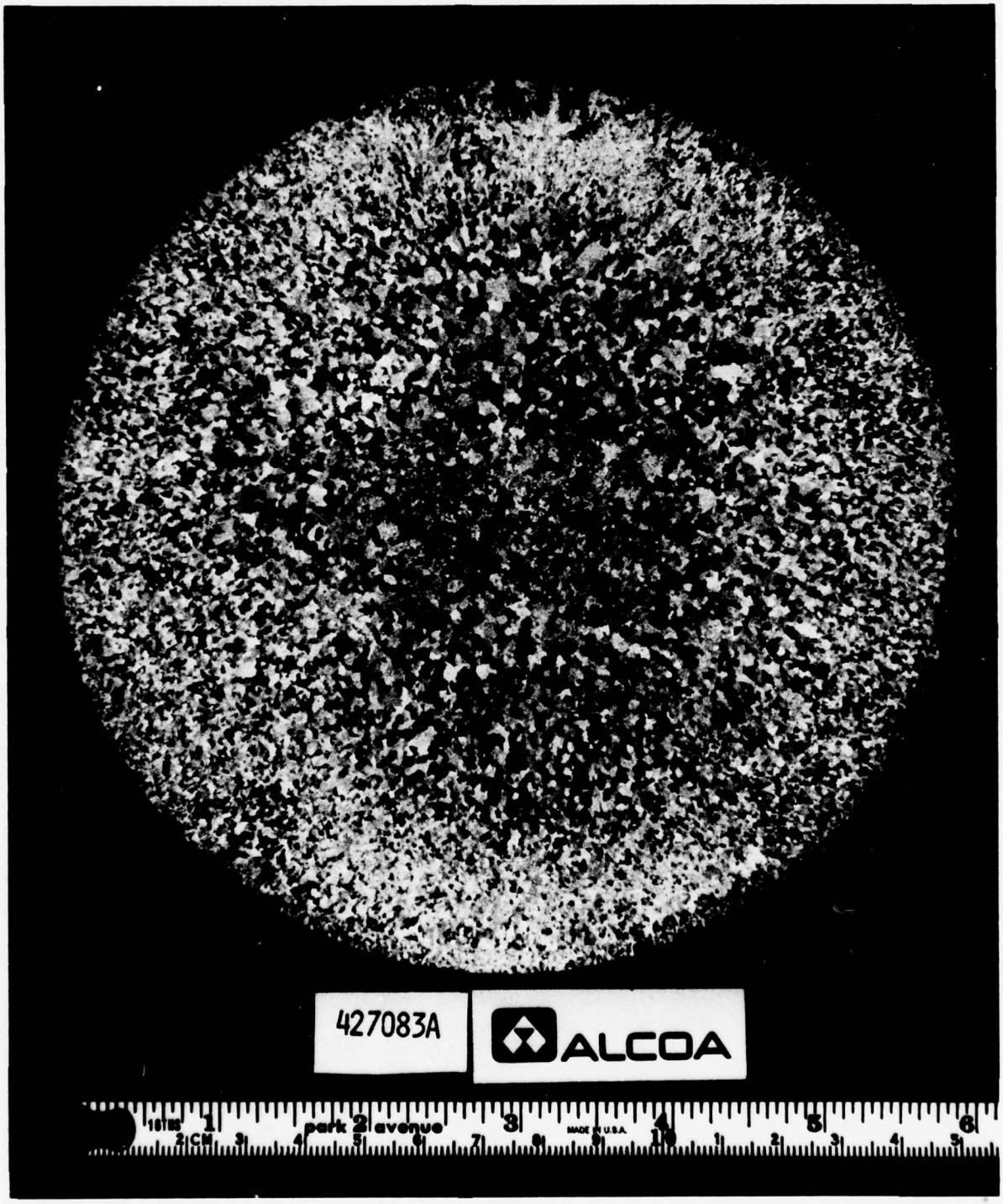

Figure A1 - Etched Ingot Slice Cut from LoCr DC Ingot
S. No. 427083A

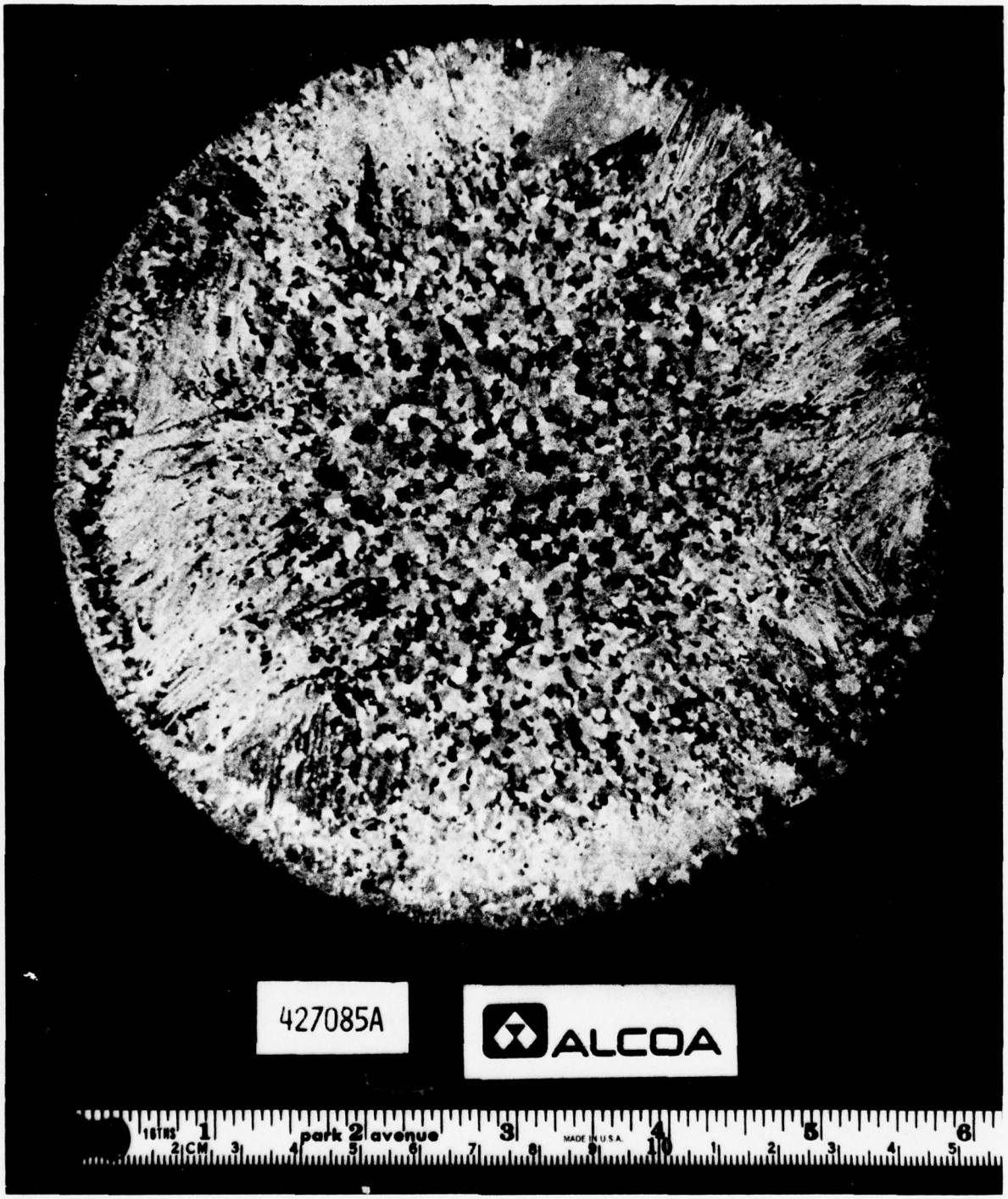

Figure A2 - Etched Ingot Slice Cut from LoMn DC Ingot
S. No. 427085A

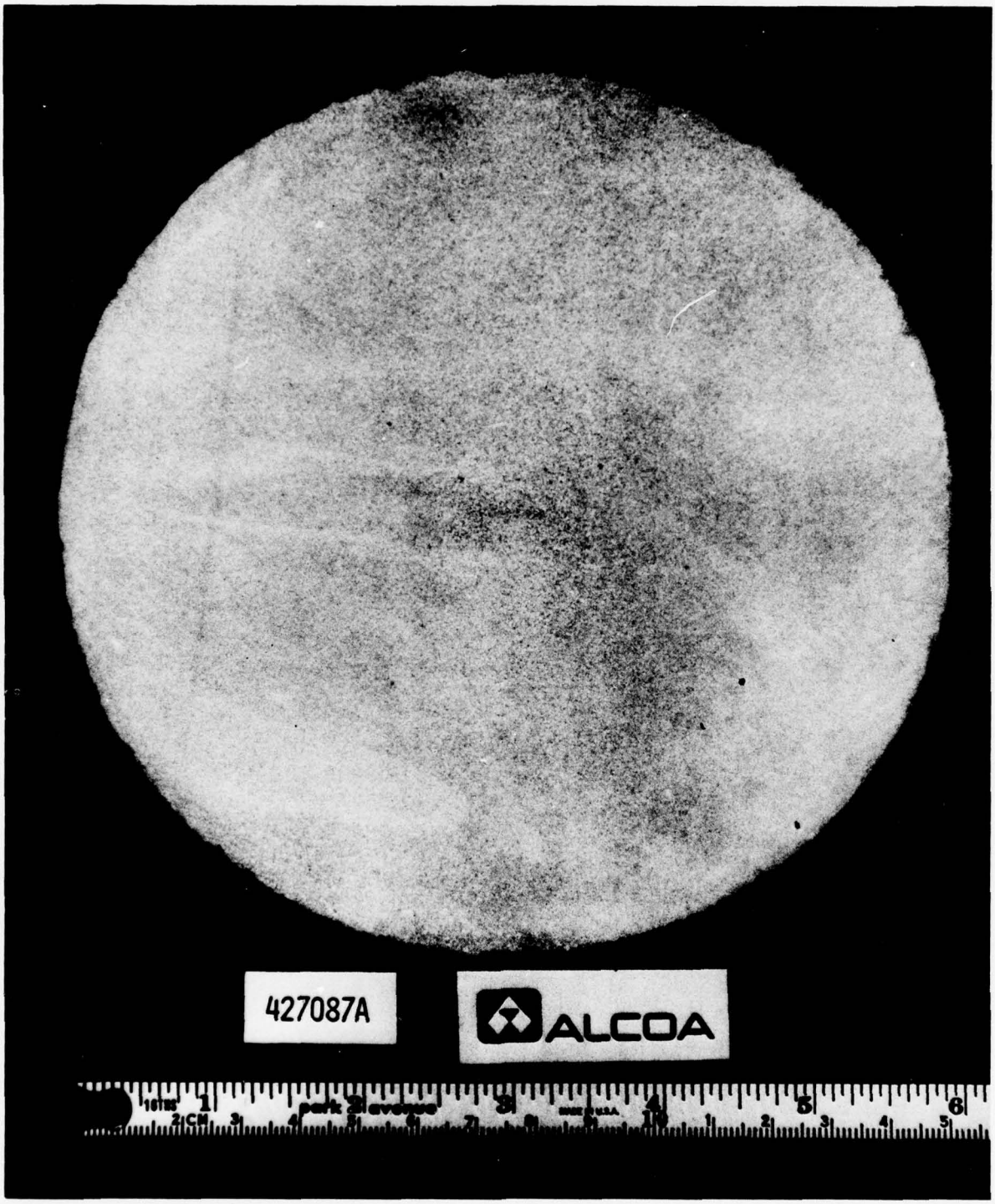

Figure A3 - Etched Ingot Slice Cut from LoZr DC Ingot
S. No. 427087A

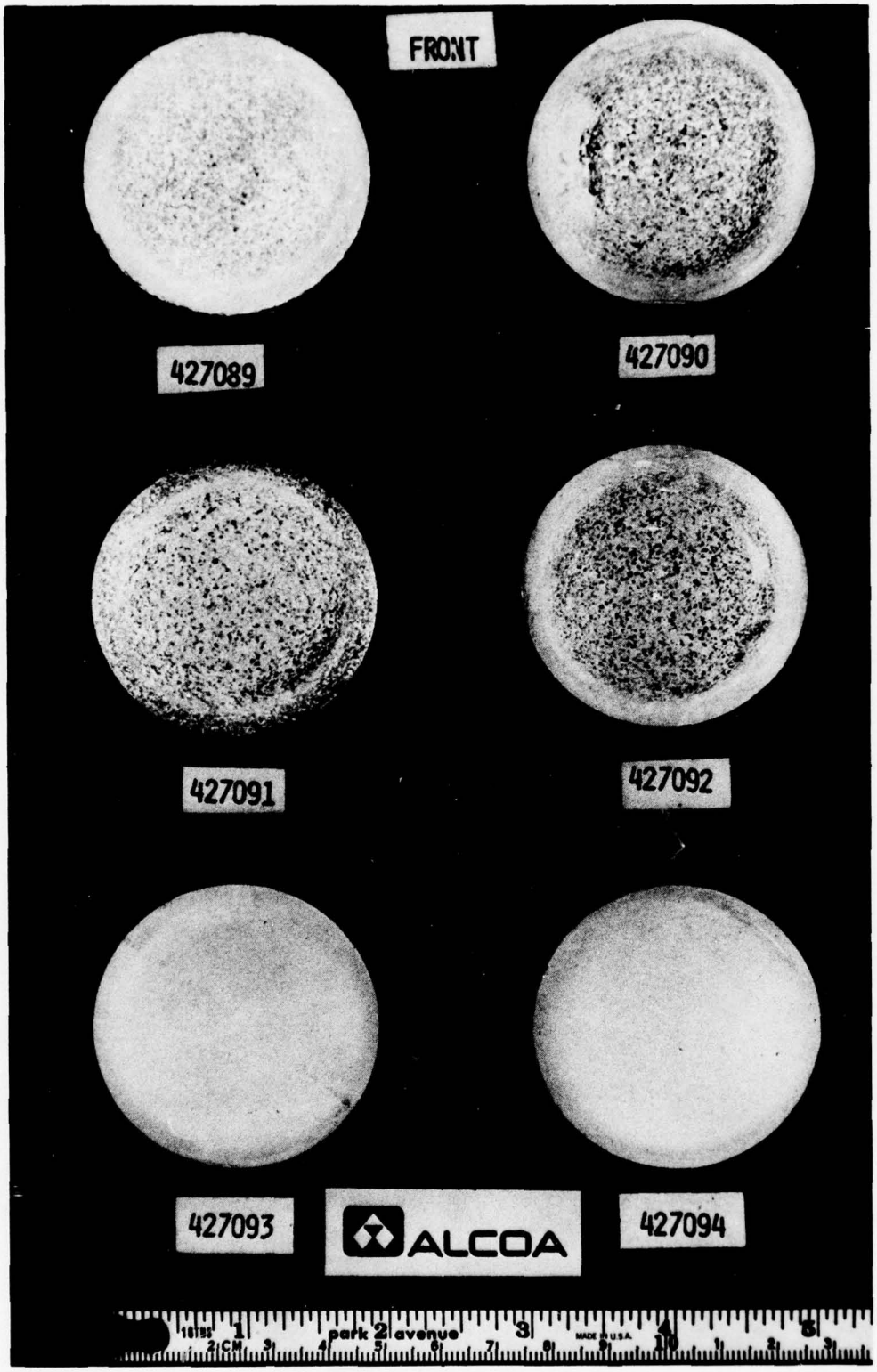

Figure A4 - Etched Slices Removed from Front of Al-Mg-Li Extrusions

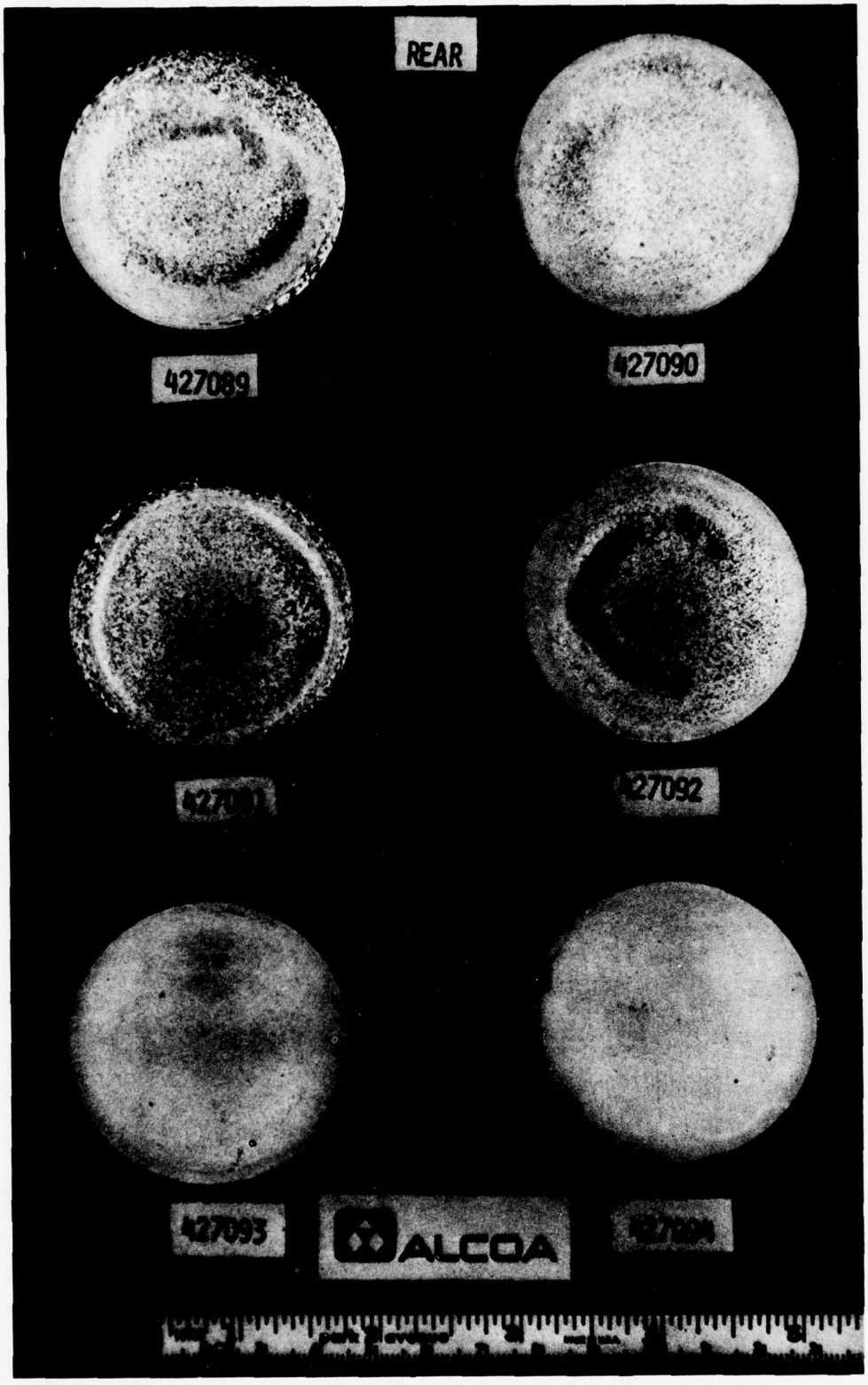

Figure A5 - Etched Slices Removed from Rear of Al-Mg-Li Extrusions

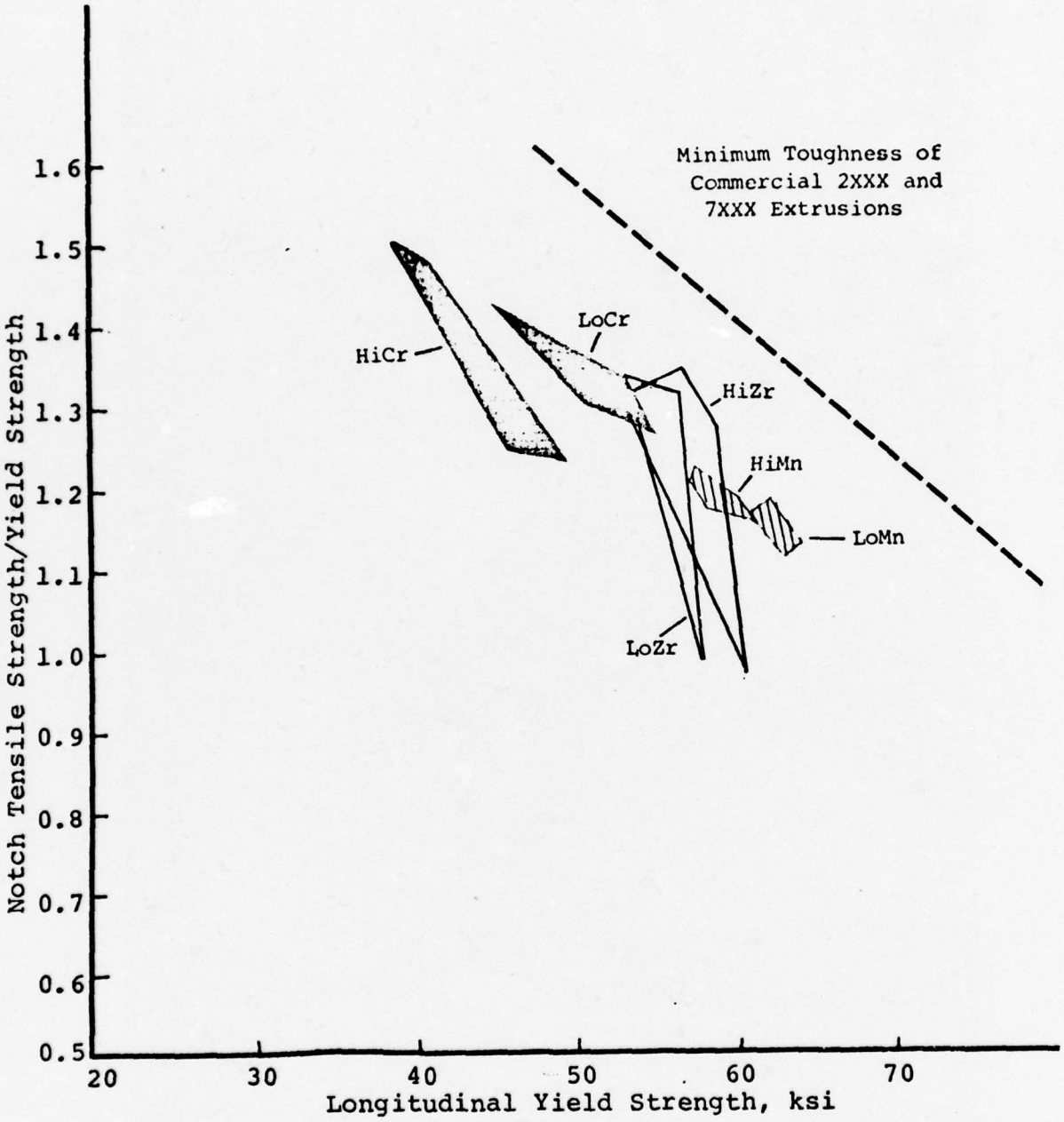

Figure A6 - Longitudinal Notch Toughness of Al-Mg-Li Extrusions Containing Different Ancillary Elements.

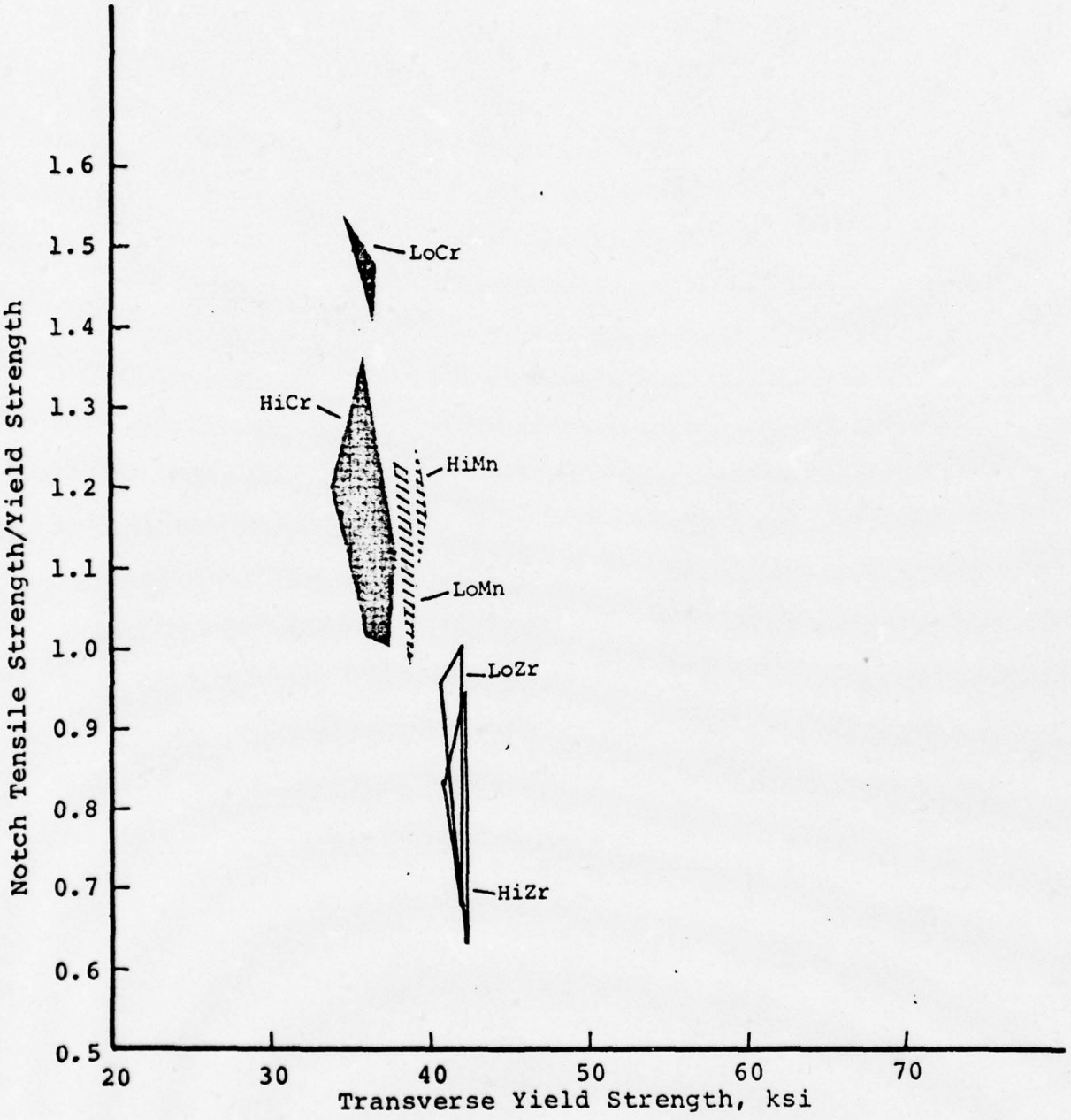

Figure A7 - Transverse Notch Toughness of Al-Mg-Li Extrusions Containing Different Ancillary Elements.

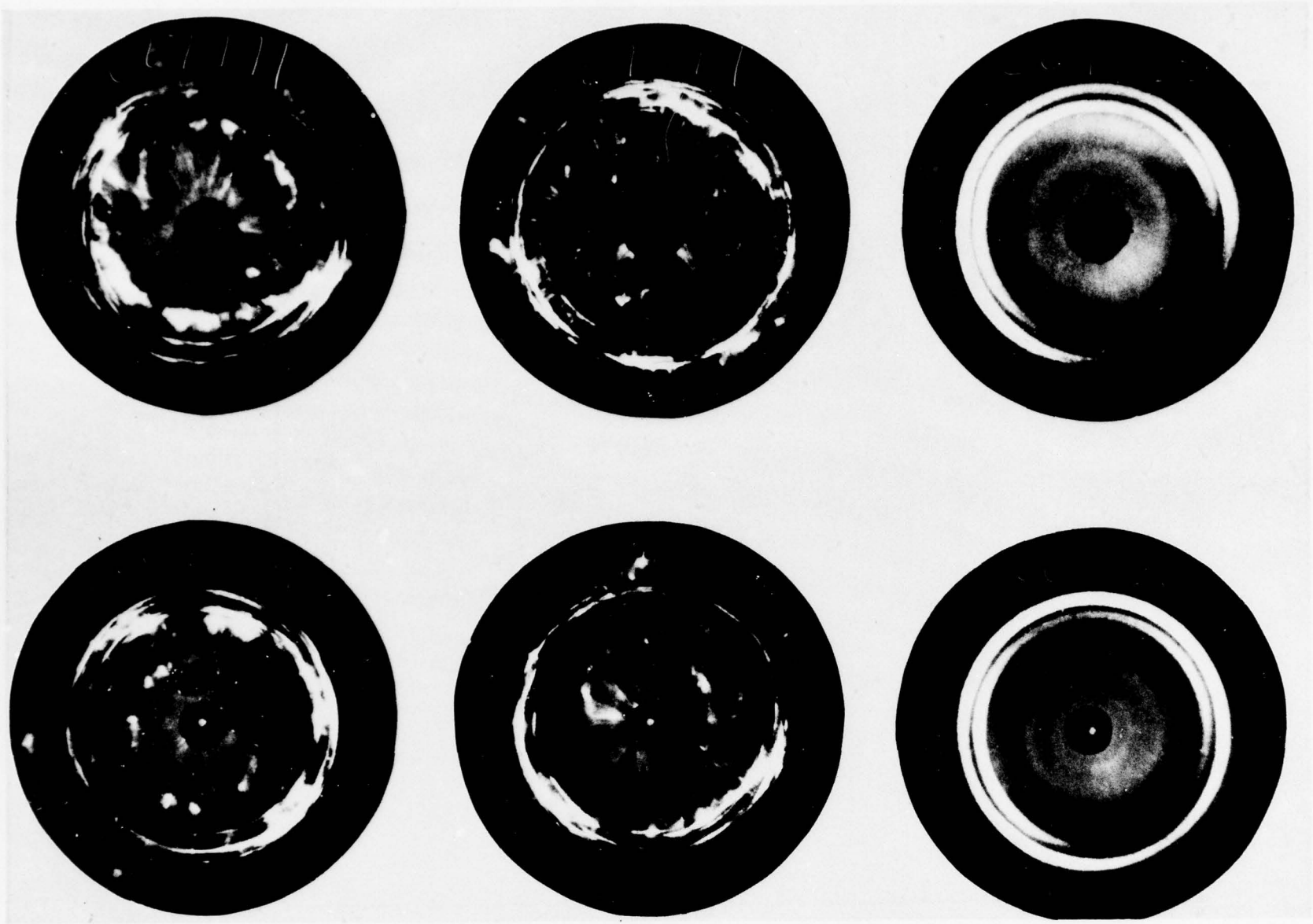

Figure A8 - X-ray Pinhole Photographs After Solution Heat Treatments at 800°F and 950°F, (a) Al-Mg-Li-Cr, (b) Al-Mg-Li-Mn, and (c) Al-Mg-Li-Zr.

APPENDIX B - THERMAL ANALYSIS OF Al-Mg-Li ALLOYS

EXPERIMENTAL

Wafers, weighing approximately 48 mg, were prepared from as-extruded material for differential scanning calorimetry (DSC). Temperature scans were run on each alloy using a DuPont 990 Thermal Analyzer in a flowing oxygen-free nitrogen atmosphere using the differential scanning calorimeter cell. Temperature scans (10°C/min) were run on each alloy. Based on solvus temperature information from this data, additional DSC specimens were solution heat treated for six hours in vacuum at 525°C (997°F) and cold-water quenched. Thermograms were recorded for each of the alloys, and scanning electron microscopy (SEM) and transmission electron microscopy (TEM) were performed at salient points on other specimens quenched from points on some of the thermograms to identify the reactions.

RESULTS

DSC curves for the different alloys are shown in Figures B1 to B9, and Table B1 is a compilation of the approximate solvus and solidus temperatures. Qualitatively, the magnitude of the exotherms (precipitation reactions) and endotherms (redissolution reactions) increased with increasing Mg and Li.

TEM and SEM on particular alloys were done on specimens quenched from the positions indicated on Figures B7 and B9. TEM micrographs are given in Figures B10 and B11. SEM of methanol-bromine etch specimens are shown in Figure B12.

DISCUSSION OF RESULTS

Precipitation reactions in the range of 25°C-200°C appear to be the result of precipitation of Al_3Li. TEM of Al-3.5 Mg-2.71 Li alloy after heatup to 200°C with a 10°C/min heatup rate shows the typical, spherical metastable precipitates of Al_3Li (Figure B10).

A number of competing reactions appear to be occurring between room temperature and 200°C. The complexity of the reactions may be attributed to:

1. dissolution of Al_3Li that forms during quenching, and
2. discontinuous precipitation reactions observed by Williams and Edington.[30]

The exothermic peak in the vicinity of 300°C is attributed to the precipitation of Al_2MgLi. Thompson and Noble[23] have shown

that, with prolonged aging of Al-Mg-Li alloys, Al_2MgLi begins to form. Observation of TEM foils prepared from DSC samples removed after they experienced the 300°C exotherm shows "rod-like" precipitates with growth directions parallel to <110> of the matrix (Figure B11). These precipitates have the same orientation relationships as found by Thompson and Noble.

In all of the alloys, a small dissolution reaction was observed to begin at approximately 450°C. This is most apparent in Figure B7, high sensitivity scan. This temperature corresponds closely with the solvus temperature of an Al-0.3% Mn alloy. The Mn dispersoid phases are visible when examined in the SEM after a bromine-methanol etch. Figure B12 shows a sample of Al-3.51 Mg-1.80 Li-0.28 Mn alloy heated up to 450°C (a) and one heated up to 550°C (b) at 10°C/min and cold-water quenched. The decrease in the number of fine particles is consistent with the suggestion that the endotherm is associated with Mn dissolution.

CONCLUSIONS

1. Precipitation in Al-Mg-Li alloys can be described by the general reaction:

   supersaturated solid solution → δ' → Al_2MgLi.

2. The metastable δ' phase is the ordered, Al_3Li, spherical precipitate.

3. The rod-like Al_2MgLi precipitate forms at elevated temperatures with growth directions parallel to <110> of the matrix.

FUTURE WORK

This section represents an initial attempt at studying the precipitation in Al-Li alloys by the combined techniques of DSC and TEM. More work will be undertaken during the next contract period.

TABLE BI

SOLVUS AND SOLIDUS TEMPERATURES FOR DIFFERENT Al-Mg-Li ALLOYS

Composition		Solvus	Solidus
Mg	Li	T, °C	T, °C
2.03	2.30	407	592
1.99	2.76	475	583
1.94	3.14	523	572
3.51	1.80	415	572
3.50	2.28	435	565
3.55	2.71	473	558
4.89	1.37	400	558
4.89	1.81	408	550
4.84	2.33	457	540

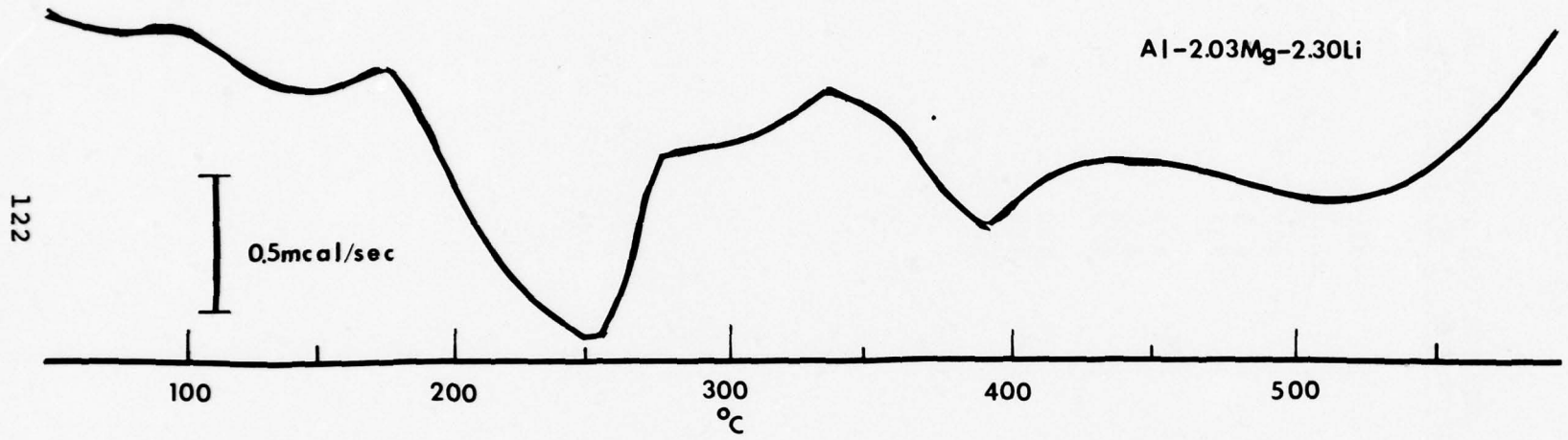

Figure B1 - DSC Thermogram of Al-Mg-Li Alloy

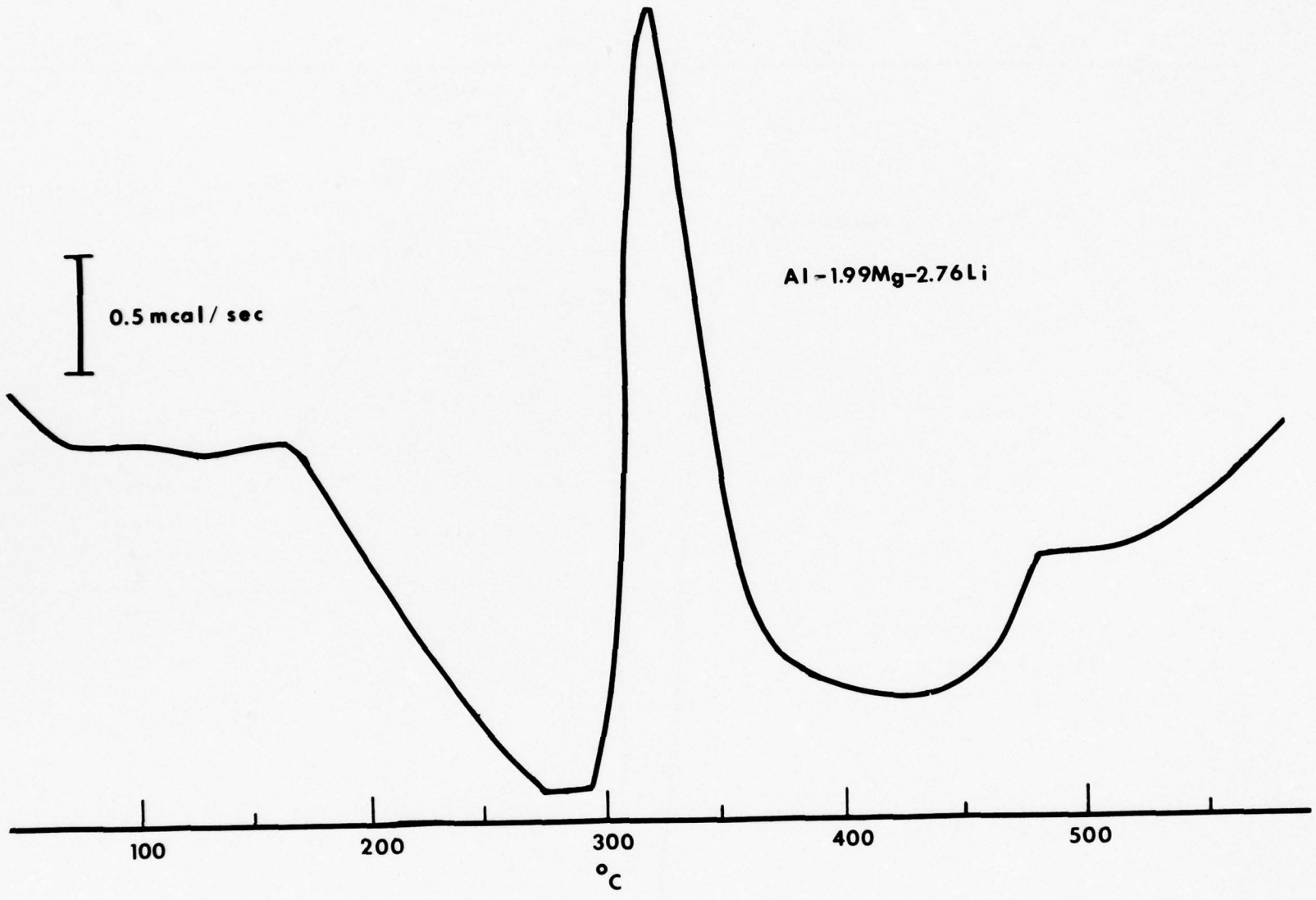

Figure B2 - DSC Thermogram of Al-Mg-Li Alloy

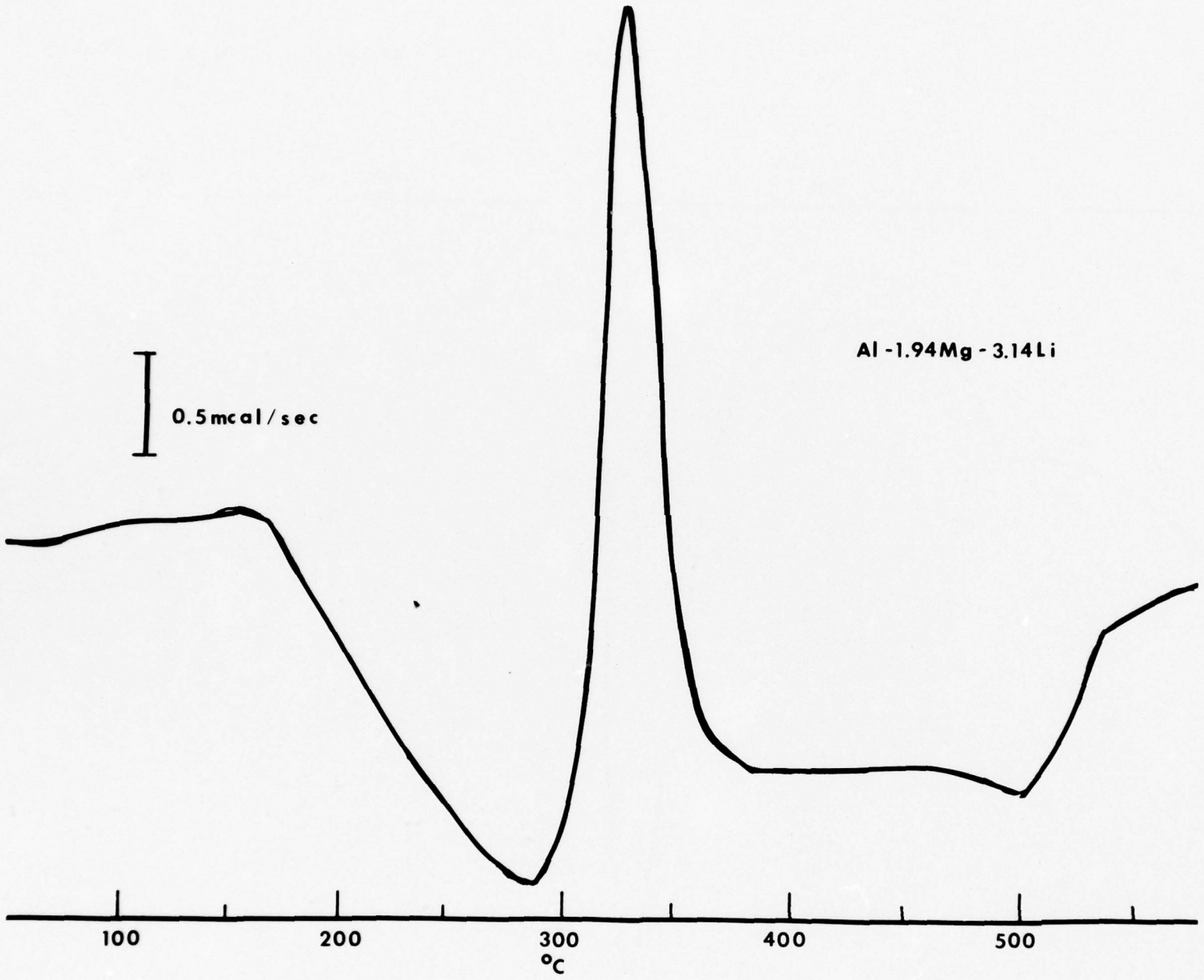

Figure B3 - DSC Thermogram of Al-Mg-Li Alloy

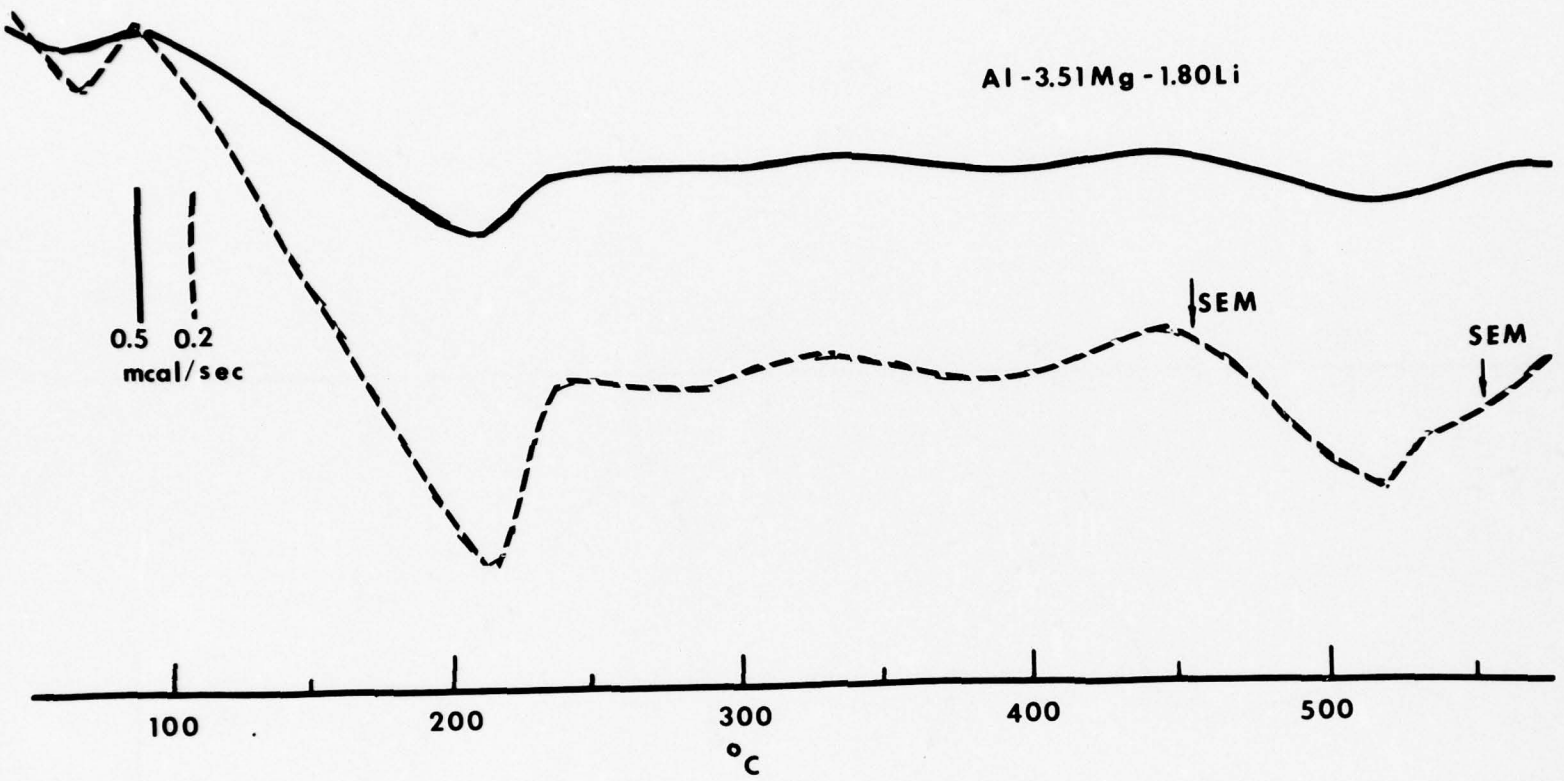

Figure B4 - DSC Thermogram of Al-Mg-Li Alloy

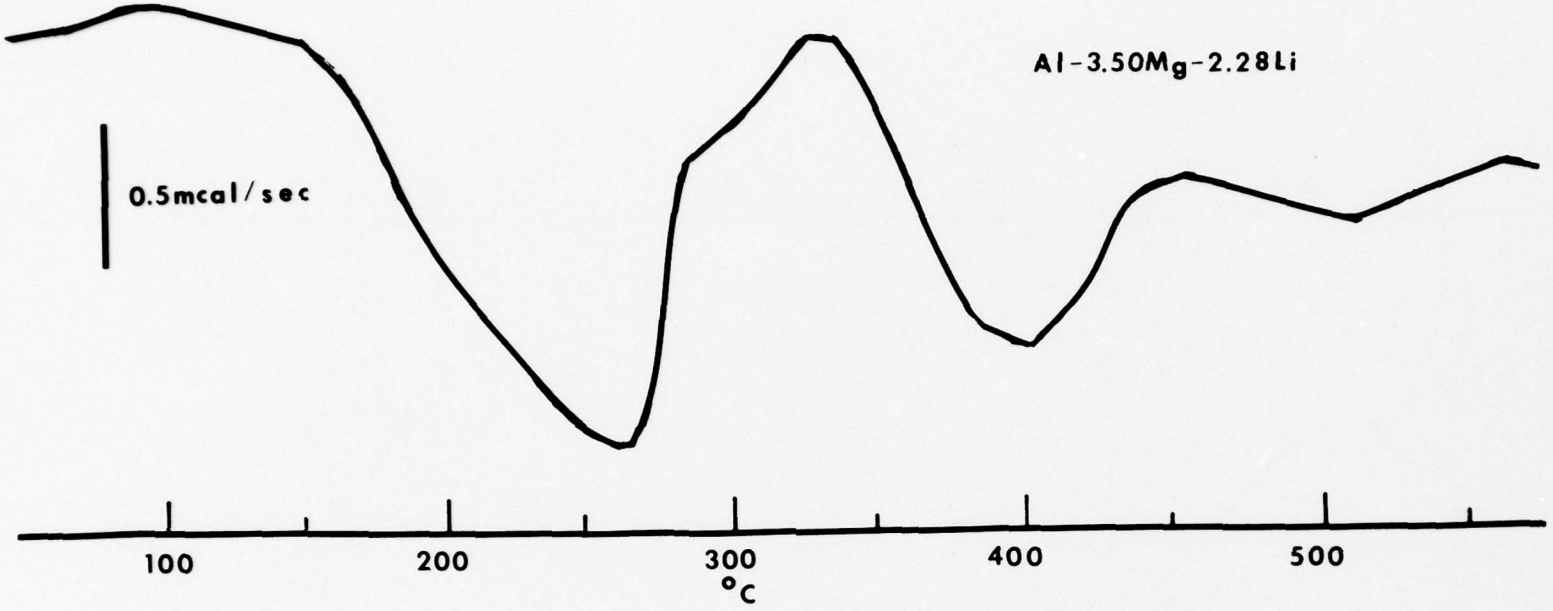

Figure B5 - DSC Thermogram of Al-Mg-Li Alloy

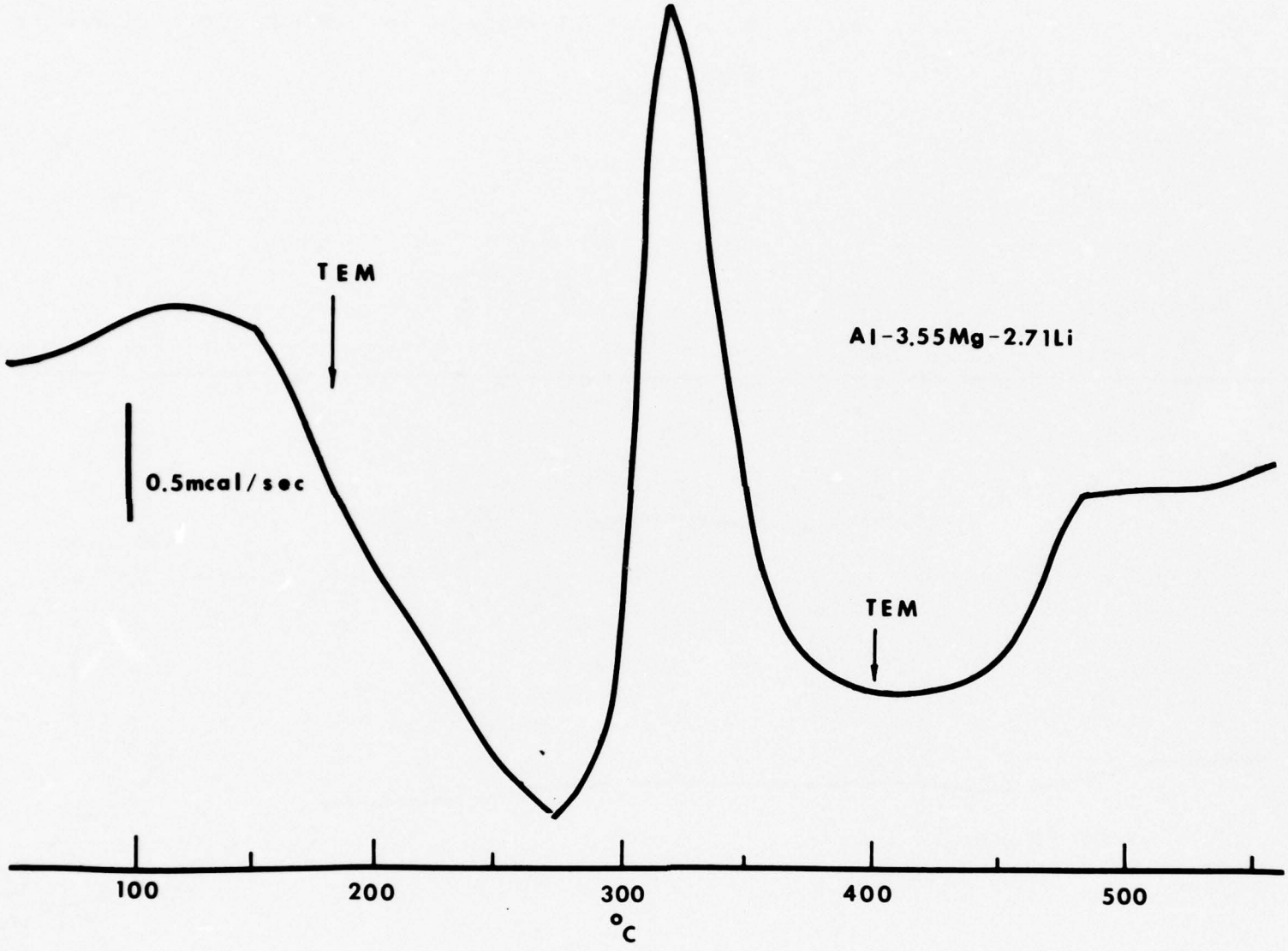

Figure B6 - DSC Thermogram of Al-Mg-Li Alloy

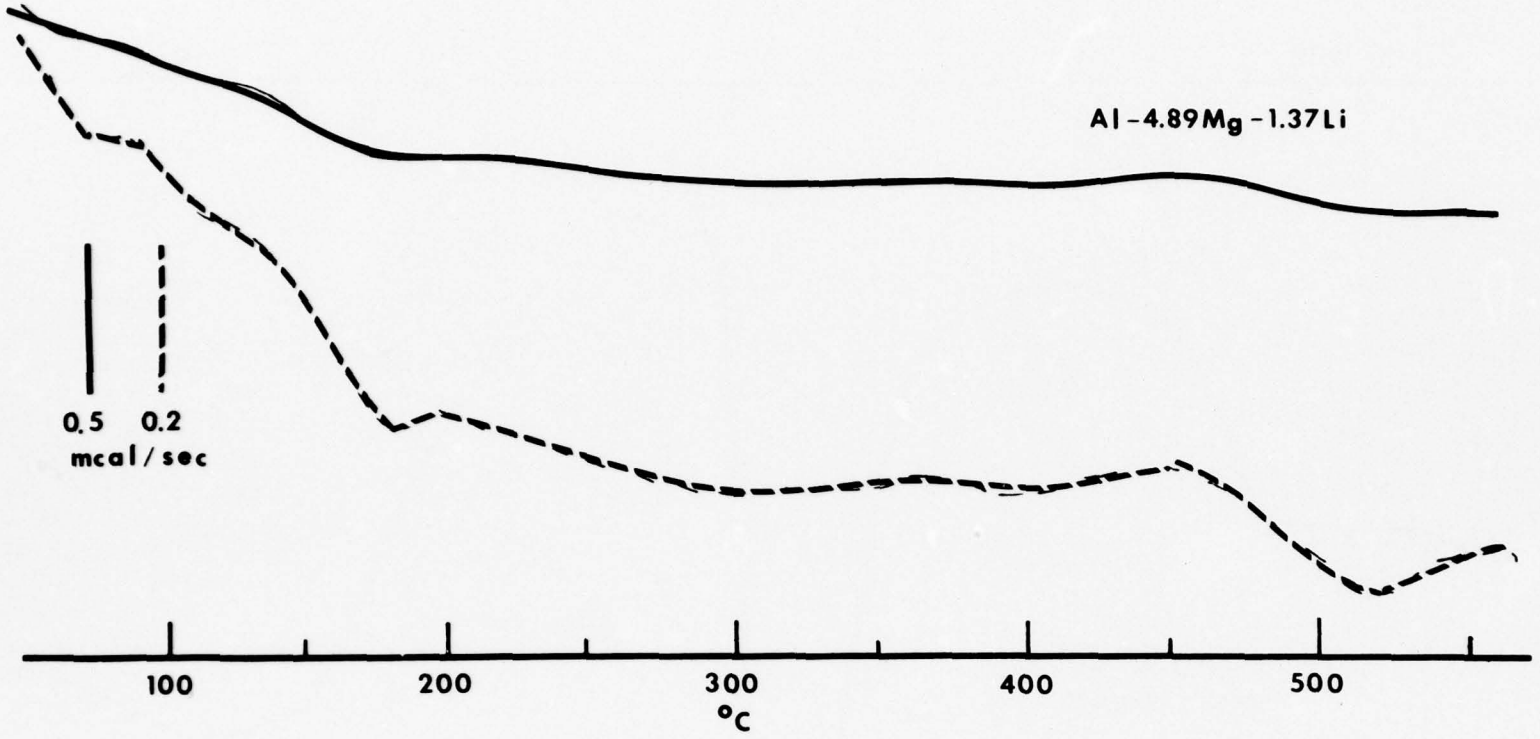

Figure B7 - DSC Thermogram of Al-Mg-Li Alloy

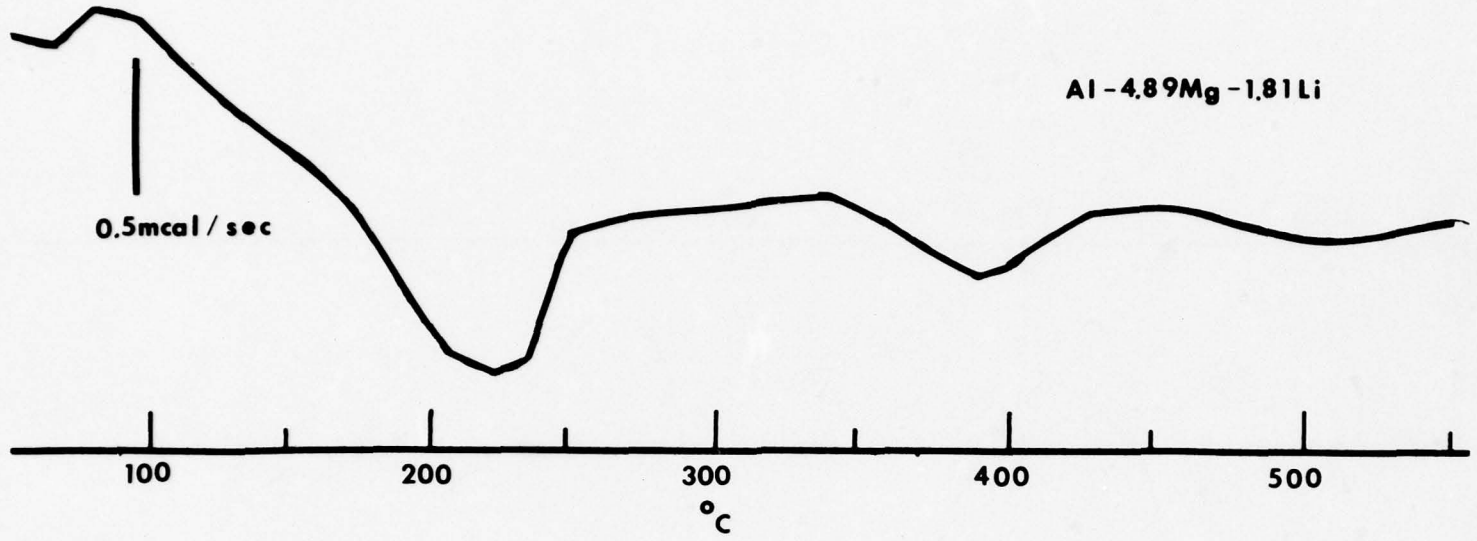

Figure B8 - DSC Thermogram of Al-Mg-Li Alloy

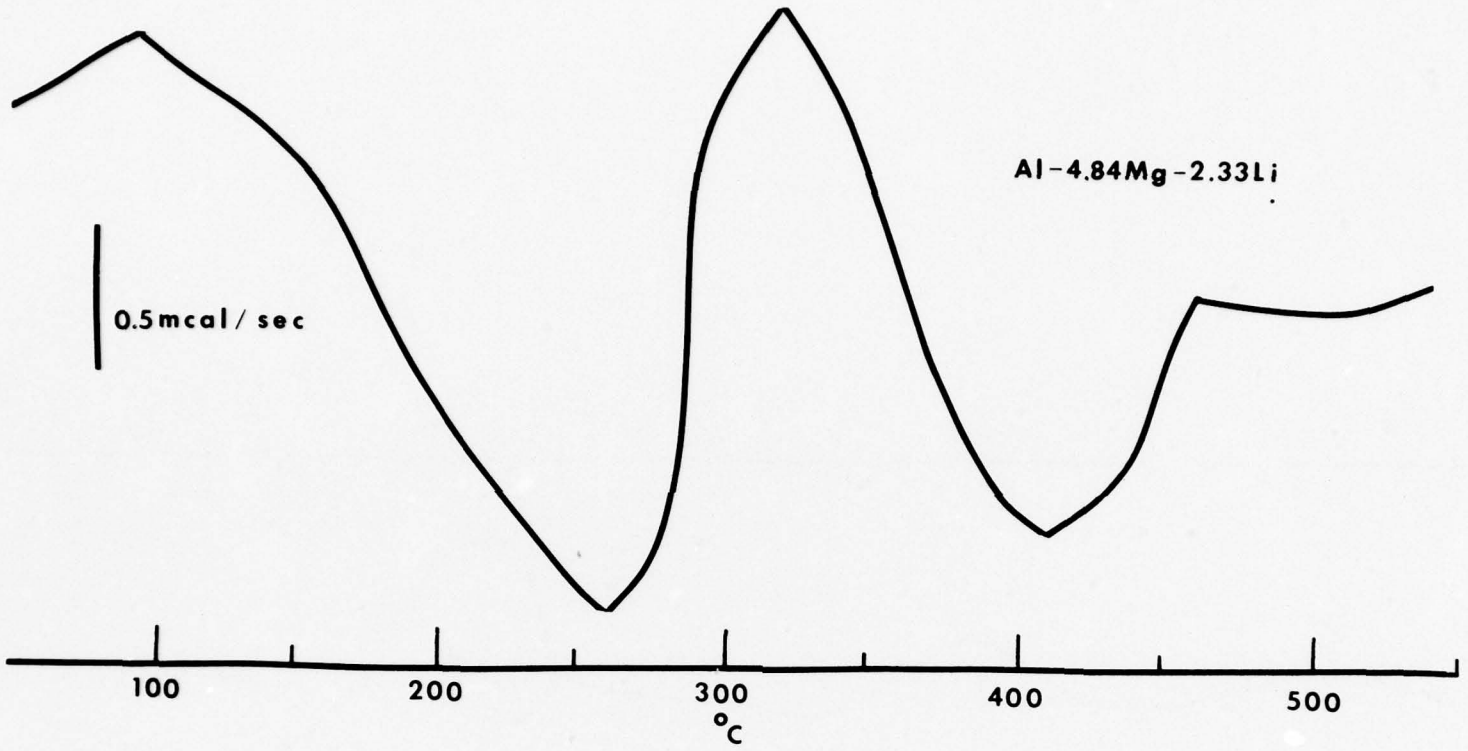

Figure B9 - DSC Thermogram of Al-Mg-Li Alloy

Figure B10 - Metastable Al_3Li Precipitates After Heatup to 200°C at 10°C/min.

Figure B11 - An Al-3.55 Mg-2.7 Li Alloy Heated Up to 400°C at 10°C/min in DSC and Quenched. Rod-like precipitates are Al_2MgLi.

2000X

(a)

(b) 2000X

Figure B12 - An Al-3.51 Mg-1.80 Li-0.28 Mn Alloy Heated Up in a DSC and Quenched from (a) 450°C and (b) 550°C. Fine white particles are Mn dispersoids (methanol-bromine etch).

APPENDIX C - DIFFRACTION EFFECTS AND TRANSMISSION ELECTRON MICROSCOPY

DIFFRACTION IN AN ORDERED LATTICE

The Cu_3Au-type superlattice (Ll_2 structure) can be derived from the close-packed, face centered cubic (FCC) lattice (Figure C1). The FCC structure permits the use of an orthogonal coordinate system. There are four crystallographically identical positions at which the origin of the orthogonal coordinates may be defined.

These lattice sites are related by 1/2<110> translational symmetry. Coincident with the origin, we can define a B lattice site. The B sites are located at the corner positions of the cube. Since each corner is surrounded by eight adjacent unit cells, a total of one B site per unit cell results. There are six face positions which are each shared by two adjacent unit cells, thus contributing three lattice points per unit cell. These sites will be identified as A sites.

In aluminum each A and B site can be occupied by an aluminum atom, or, in a random substitutional solid solution, each site would be occupied by a modified atom whose behavior could be expressed as a linear combination of atomic fractions.

The structure factor for a general lattice can be written as:

$$F_{hkl} = \sum_{n=1}^{N} f_n e^{2\pi i \left(hx_n + ky_n + lz_n \right)}.$$

The magnitude of the scattering thus depends on the spatial configuration $\left(x_n, y_n, z_n \right)$ of the N atoms in the unit cell and their respective scattering powers, f_n. A structure factor calculation for an FCC lattice leads to a zero structure factor for certain combinations of h, k, and l, and thus, during a diffraction event, these reflections would be systematically absent. It is the translational symmetry which gives rise to the systematic absences. Therefore, if the A and B sites are occupied by different atoms, these sites are no longer crystallographically equivalent. The translational symmetry of the lattice is eliminated. Consequently, reflections which were previously absent are now present. From a structure factor calculation, we would expect for a random substitution on A and B sites two different atoms,

h, k, l - all odd integers, or

h, k, l - all even,

to be present. However,

h, k, l - mixed,

would be systematically absent. As a result of order, all reflections would be present.

The presence of superlattice reflections have been shown by a number of investigators working in the Al-Li systems.[16,22] Figures C2 and C3 are two selected area diffraction (SAD) patterns of two different Al alloys. Figures C2a and C3a are 7075 as-quenched and are used for comparison. Figures C2b and C3b are SAD patterns for an Al-Li-Mg alloy aged in the vicinity of peak strength. Note the presence of the extra reflections which are systematically absent in the 7075. In Figure C4 is a dark field image of spherical Al_3Li precipitates in an Al-Mg-Li alloy.

ELECTRON MICROSCOPY AND SUPERLATTICE DISLOCATIONS

The image of a dislocation is uniquely dependent upon the triple scalar product $(\vec{g}\cdot\vec{b})\vec{s}$, where $\vec{g}_{hkl}$ is the operating reflection responsible for the image, $\vec{b}$ the Burgers vector of the dislocation, and s the deviation parameter. The deviation parameter is defined in Figure C5 as the position of the Ewald sphere with respect to the active reciprocal lattice vector, $\vec{g}_{hkl}$. The technique requires a strong two-beam condition. This is accomplished by bringing in a bend contour. The center of the contour defines s = o, either side defines $s>o$ or $s<o$. For any experiment, one can assign sign conventions to $\vec{g}$ and s. Figure C6 shows the effect of changing the sign of the scalar product on distance between the dislocation pairs.[29] When the triple scalar product changes sign, the distance between a pair of super dislocations is constant, but for a dipole, the separation distance changes. A tilting experiment in a deformed Al-Mg-Li alloy demonstrates the presence of super dislocations, Figure C7.

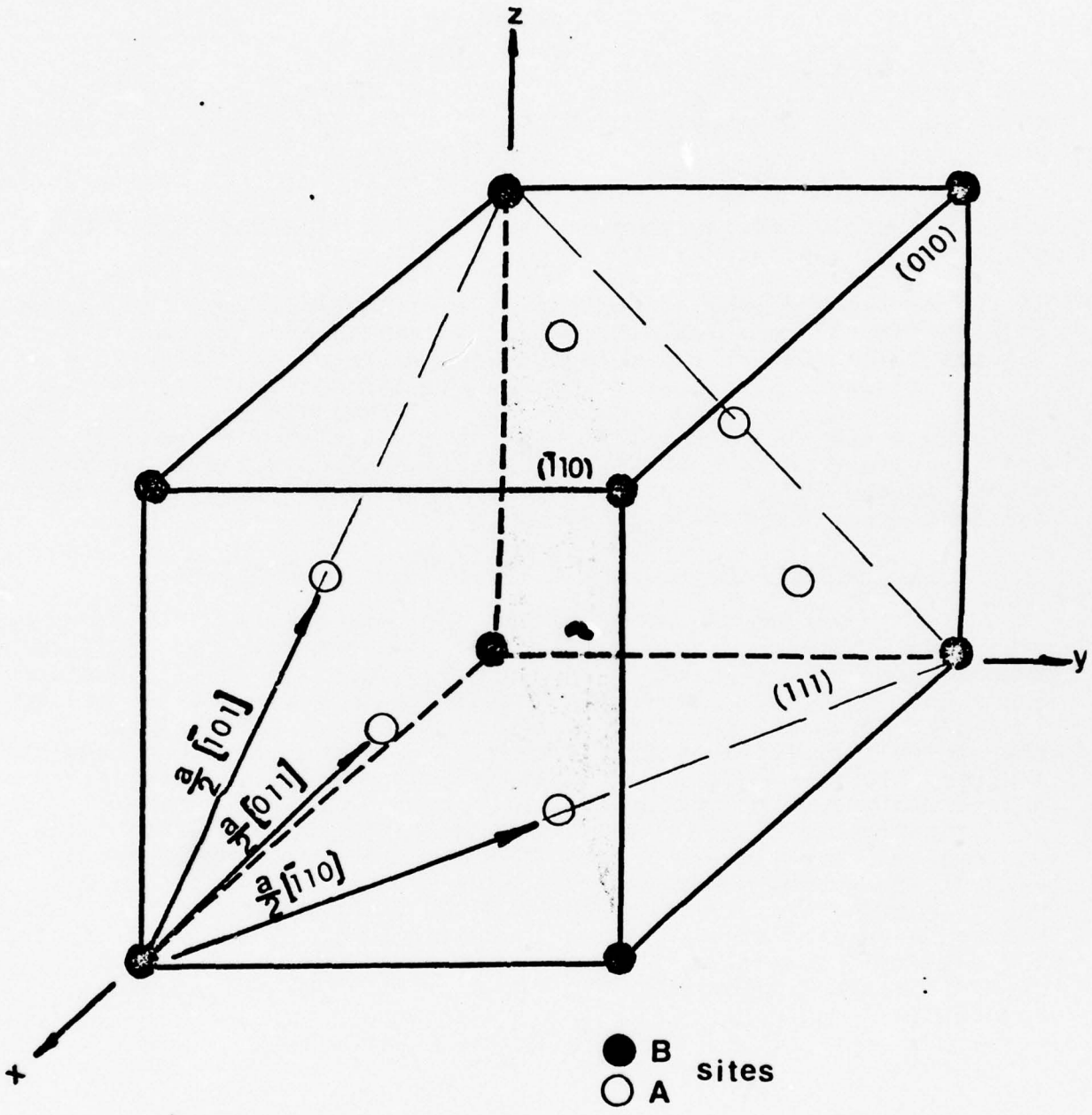

Figure C1 - Definition of Atomic Positions in the Face-Centered, Cubic (FCC) Lattice.

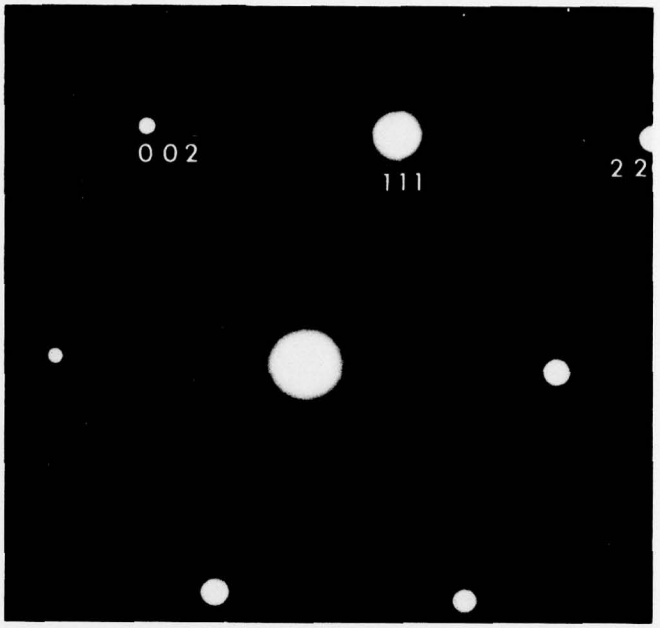

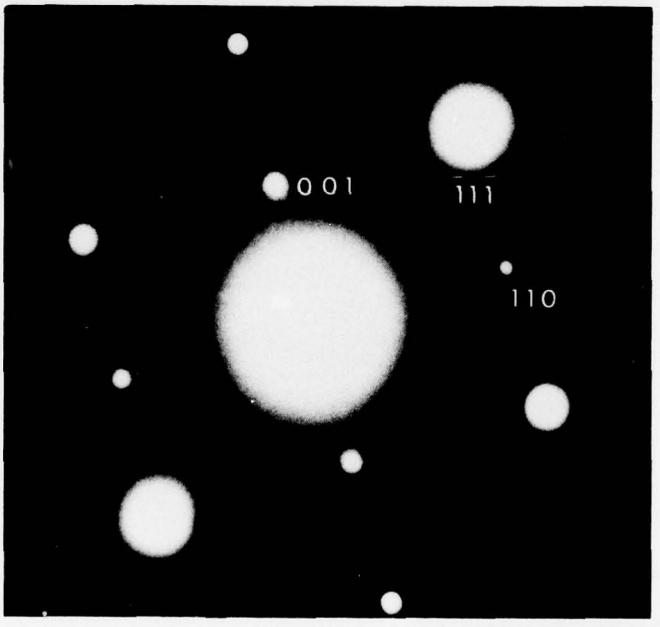

Figure C2 - a. SAD Pattern of As-quenched 7075, Foil Normal Parallel to $[\bar{1}\bar{1}0]$.
b. SAD Pattern of Al-Mg-Li Alloy Aged in the Vicinity of Peak Strength, Foil Normal Parallel to $[\bar{1}\bar{1}0]$.

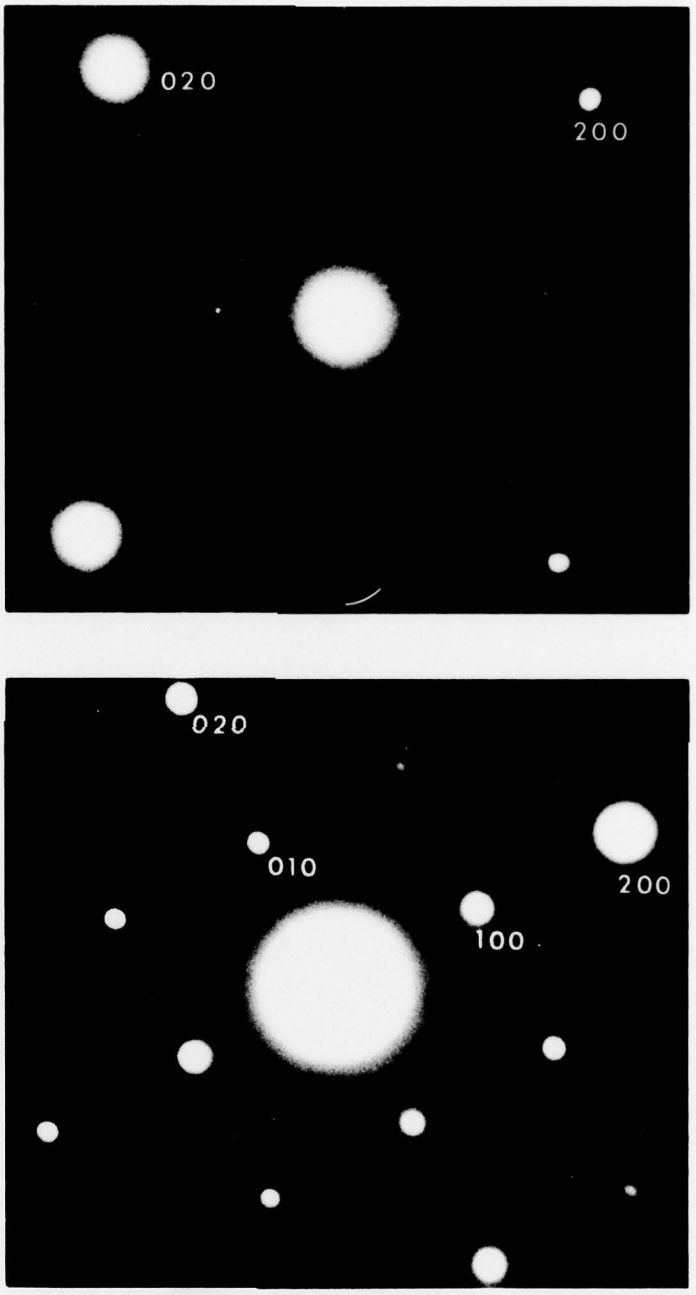

Figure C3 - a. SAD Pattern of As-quenched 7075, Foil Normal Parallel to [001].
b. SAD Pattern of Al-Mg-Li Alloy Aged in the Vicinity of Peak Strength, Foil Normal Parallel to [001].

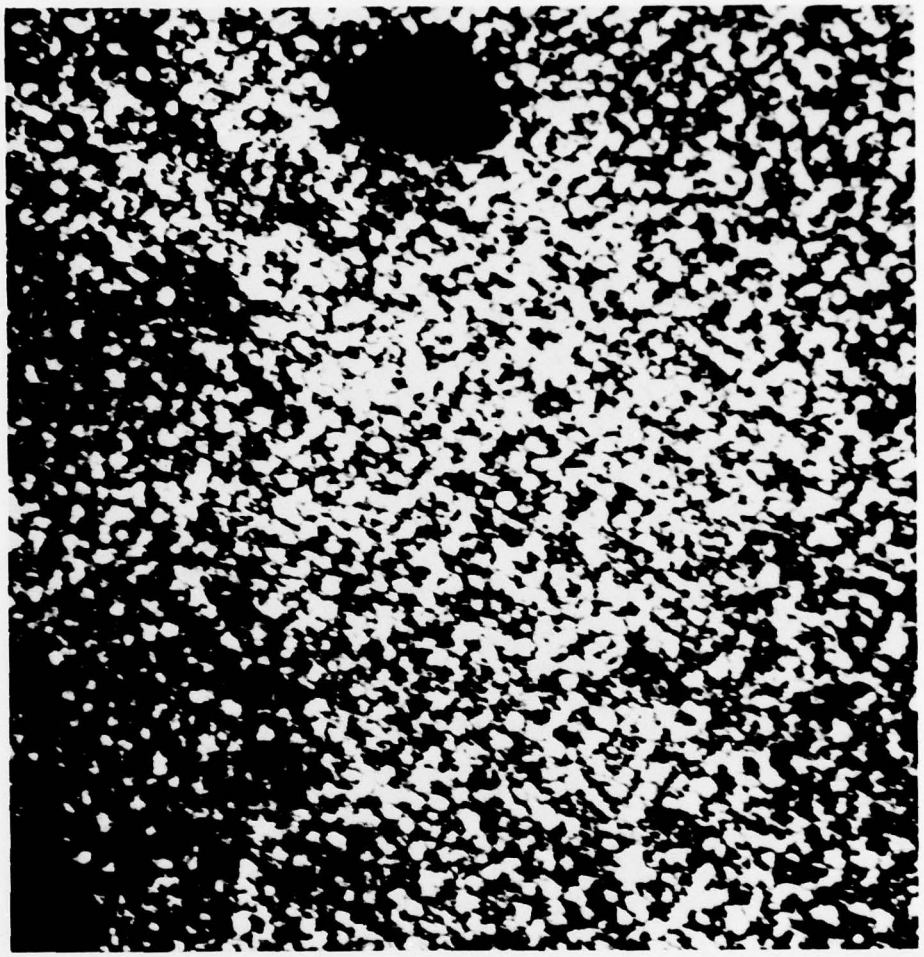

Figure C4 - Dark Field from Superlattic Reflection Showing the Fine, Spherical Al_3Li Precipitates in Al-Mg-Li Alloy Aged in the Vicinity of Peak Strength.

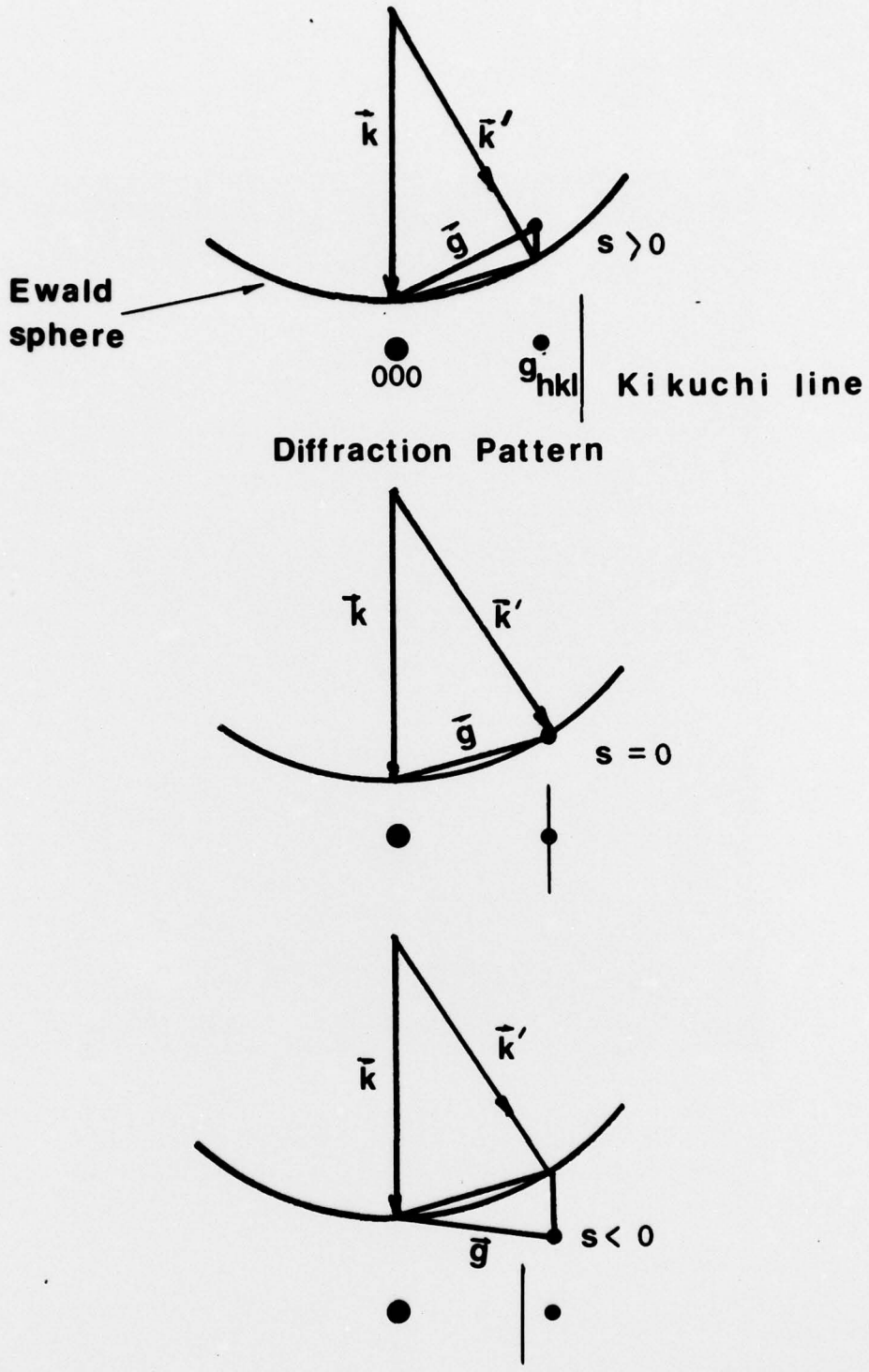

Figure C5 - Diagram Illustrating the Position of the Operating Reflection, $\vec{g}_{hkl}$, with Respect to the Ewald Sphere and the Sign of the Deviation Parameter. The position of an active reciprocal lattice point with respect to a KiKuchi Band can be used to define the sign of s.

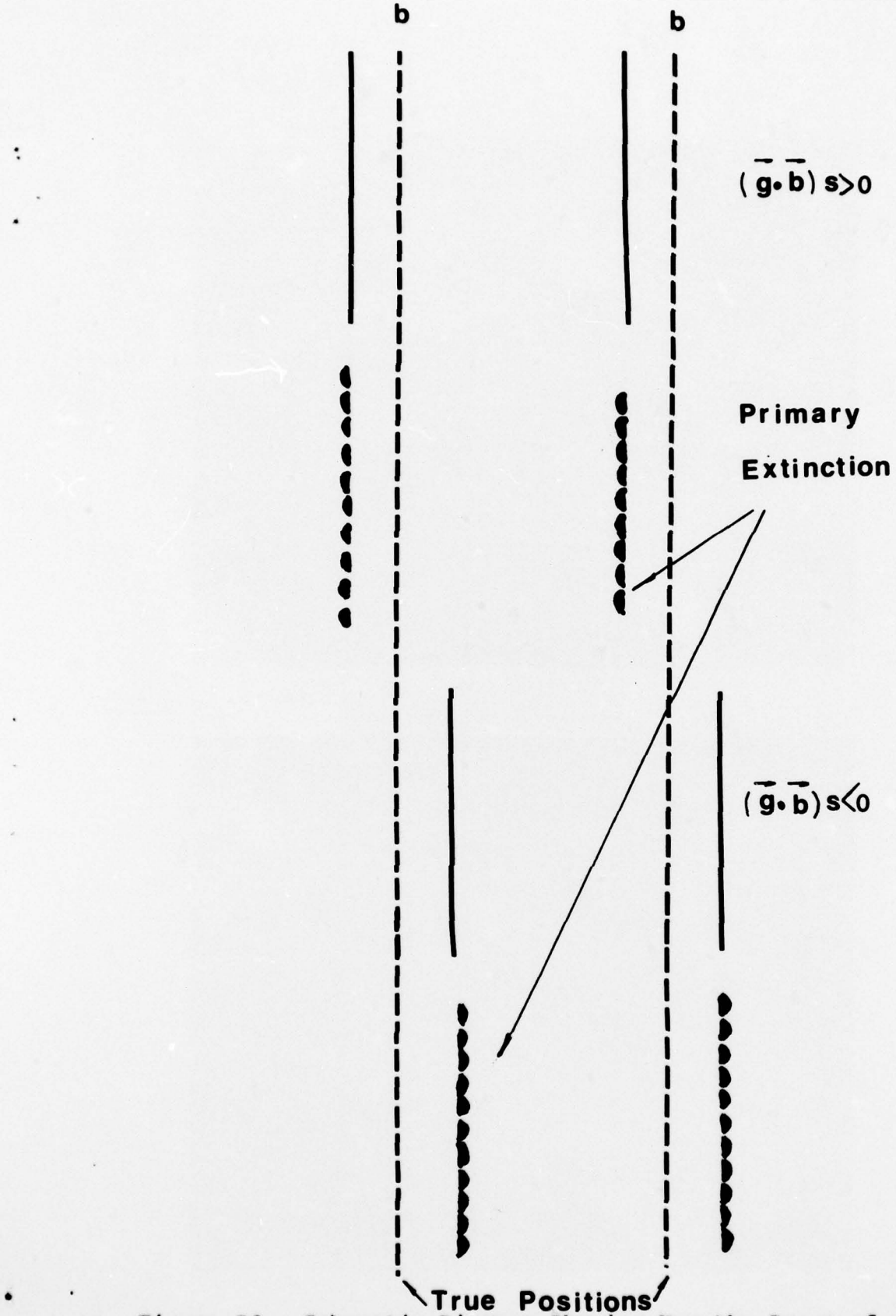

Figure C6 - Schematic Diagram Showing How the Image of a Dislocation Pair Depends on the Diffraction Conditions.

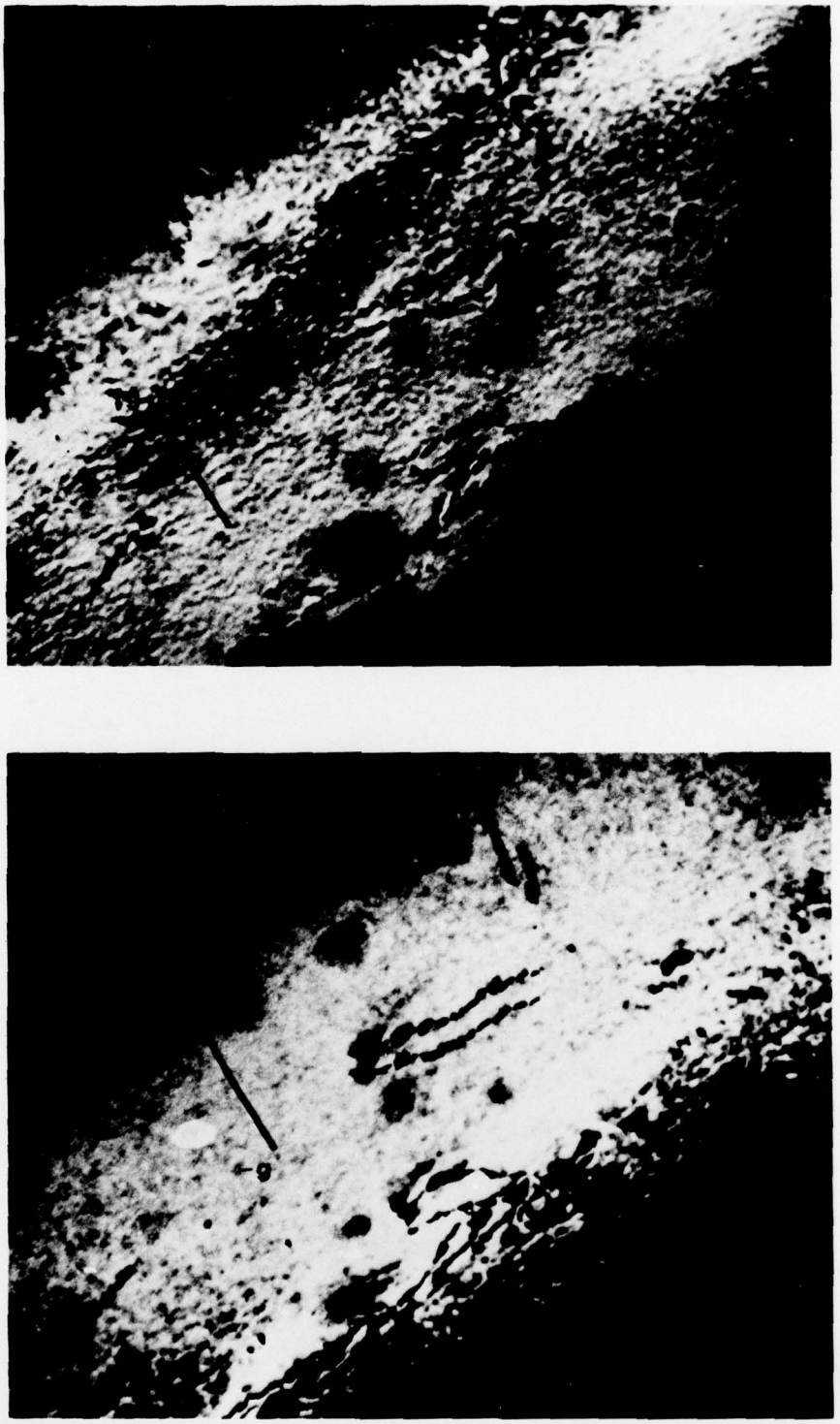

Figure C7 - Super Dislocations in Al-Mg-Li Alloy Aged in the Vicinity of Peak Strength.

0.1μm

Figure C7 - Continued

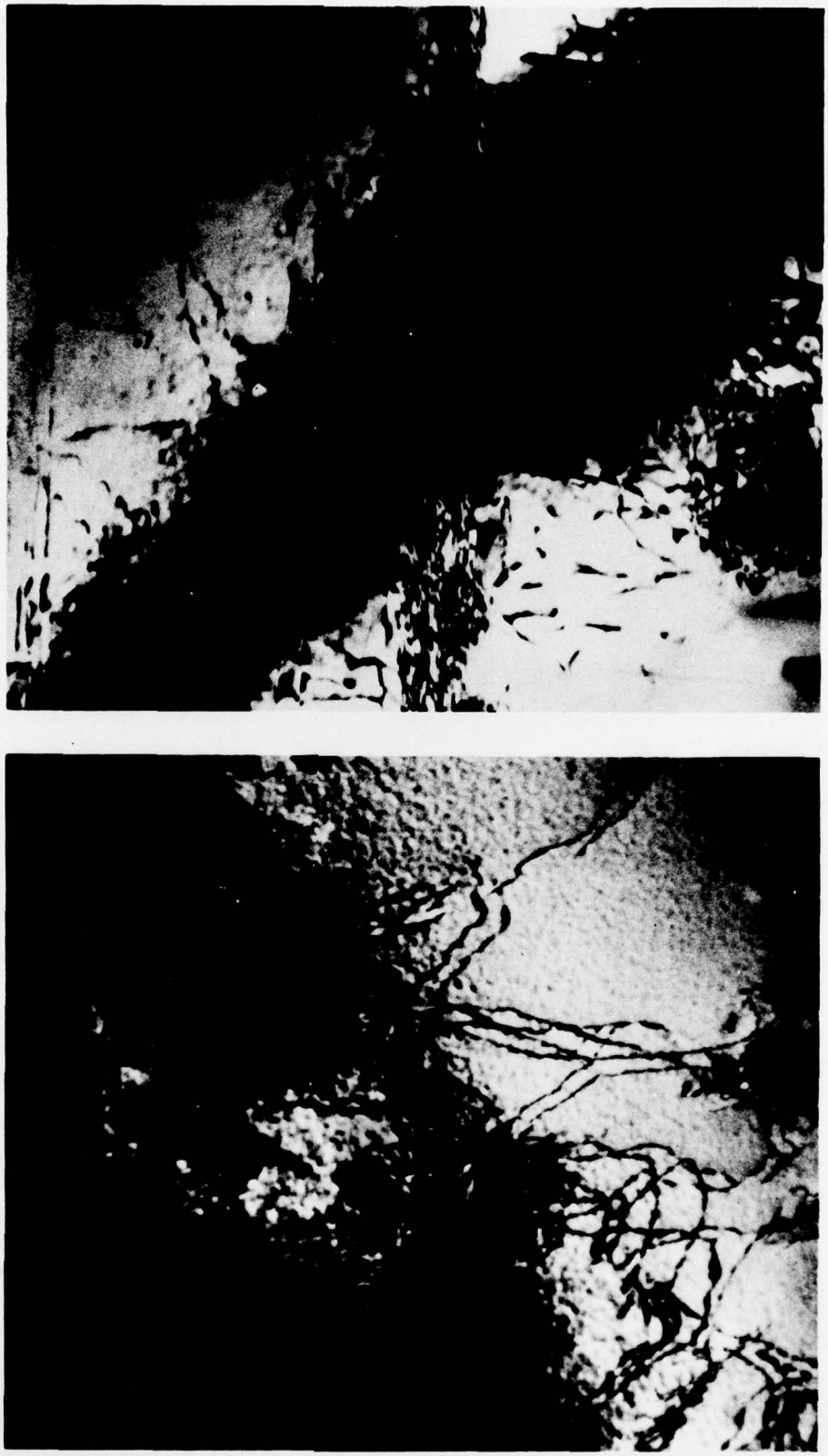

Figure C7 - Continued

0.1μm

REFERENCES

1. I. N. Fridlyander, V. F. Shamray, and N. V. Shiryaeva, Translated from Izvestiia Akademiia Nauk SSSR, Metally, (2), pp 153-158, 1965.

2. Undated Fulmer Research Institute advertising flyer.

3. I. N. Fridlyander, S. M. Ambartsumyan, N. V. Shiryaeva, and R. M. Gabidullin, Translated from Metallovedenie i Termicheskaya Obrabotka Metallov, No. 3, pp 50-52, March 1968.

4. V. G. Kovrizhnykh, V. A. Tikhomirov, N. I. Saitseva, and M. V. Ermanok, Translated from Metallovedenie i Termicheskaya Obrabotka Metallov, No. 2, pp 20-21, February 1969.

5. M. I. Paretskii, E. V. Giarsintov, and M. G. Veitsman, Translated from Metallovedenie i Termicheskaya Obrabotka Metallov, No. 3, pp 52-54, March 1968.

6. I. N. Fridlyander, V. S. Sandler, and T. I. Nikol'skaya, Translated from Metallovedenie i Termicheskaya Obrabotka Metallov, No. 5, pp 2-5, May 1971.

7. M. E. Drits, E. S. Kadaner, and N. I. Turkina, Izvestiia Akademiia Nauk SSSR, Metally, pp 231-235, July-August 1971.

8. British Patent No. 1,172,736.

9. F. S. Novik and N. I. Kolobnev, Translated from Metallovedenie i Termicheskaya Obrabotka Metallov, No. 4, pp 33-35, April 1969.

10. Dimitri Vvidenski, Foreign Science Bulletin, Vol 4, No. 12, pp 35-43, December 1968.

11. B. Noble and G. E. Thompson, Metal Science Journal, Vol 5, p 114, 1971.

12. J. W. Evancho, Final Report, Naval Air Development Center Contract No. N62269-73-C-0219, For Naval Air Systems Command.

13. Nucleation, A. C. Zettlemoyer, ed., Marcel Dekker, Inc., New York, 1969.

14. H. K. Hardy, Journal of the Institute of Metals, Vol 84, p 429, 1955-1956.

15. I. N. Fridlyander, V. S. Sandler, and T. I. Nikol'skaya, Translated from Fisika Metallov i Metallovedenie 32, No. 4, p 767, Cat. 1971.

16. I. N. Fridlyander, T. I. Nicol'skaya, V. S. Sandler, and B.V. Tyurin, Translated from Metallovedenie i Termicheskaya Obrabotka Metallov, No. 8, p 7, August 1972.

17. G. E. Thompson and B. Noble, Journal of the Institute of Metals, Vol 101, p 111, 1973.

18. A. Q. Khan, Transactions of the Japanese Institute of Metals, Vol 13, p 149, 1972.

19. M. E. Fine, Metallurgical Transactions, Vol 6A, p 625, 1975.

20. J. D. Boyd and R. B. Nicholson, Acta Metallurgica, Vol 19, p 1101, 1971.

21. P. B. Hirsch, A. Howie, R. B. Nicholson, D. W. Pasley, and M. J. Whelan, Electron Microscopy of Thin Crystals, William Clowes & Sons, Ltd, London and Beccles, 1969.

22. M. Tamura, T. Mori, and T. Nakamura, J. of Japan Inst. of Metals, Vol 34, p 919, 1970.

23. G. E. Thompson and B. Noble, J. Inst. Metals, Vol 101, p 111, 1973.

24. W. G. Fricke, Jr., Alcoa Internal Report, April 12, 1961.

25. N. S. Stoloff and R. G. Davies, "The Mechanical Properties of Ordered Alloys," Progress in Materials Science, Bruce Chalmers, ed., Vol 13, No. 1, 1966.

26. P. A. Flinn, Transactions of American Institute of Mining, Metallurgical and Petroleum Engineers, 218, 145, 1960.

27. G. I. Taylor, J. Inst. Metals, 62, 307, 1938.

28. L. V. Azaroff, Elements of X-Ray Crystallography, McGraw-Hill Book Company, New York, 1968.

29. W. Bell, W. R. Roser, and G. Thomas, Acta Met., 11, 124F, 1964.

30. D. B. Williams and J. W. Edington, Acta Met., 24, 323, 1976.

DISTRIBUTION LIST
(One copy unless otherwise noted)

(1 copy + balance after distribution)
Mr. E. S. Balmuth
AIR-52031C
Naval Air Systems Command
Washington, D.C. 20361

Commander
Naval Air Development Center
(Code 302)
Warminster, PA 18974

Naval Sea Systems Command
(Code 035)
Department of the Navy
Washington, D.C. 20360

Naval Ships Research & Development Center
(Code 2812)
Annapolis, MD 21402

Naval Ships Research & Development Center
Washington, D.D. 20007
Attn: Mr. Abner R. Willner
Chief of Metals Research

Commander
Naval Surface Weapons Center
(Metallurgy Division)
White Oak
Silver Spring, MD 20910

Director, Naval Research Laboratory
(Code 6320)
Washington, D.C. 20390

Office of Naval Research
The Metallurgy Program, Code 471
Arlington, VA 22217

Wright-Patterson Air Force Base
Ohio 45433
Attn: W. Griffith, AFML/LLS

Wright-Patterson Air Force Base
Ohio 45433
Attn: AFML/MXA

Wright-Patterson Air Force Base
Ohio 45433
Attn: H. Koenigsberg, FTD/PDIT

Pittsburgh DCAS District
1610-S Federal Building
1000 Liberty Avenue
Pittsburgh, PA 15222
Attn: Z. D. Mosko

Army Materials & Mechanics Research Center
Watertown, MA 02172
Attn: Dr. A. Gorum

Wright-Patterson Air Force Base
Ohio 45433
Attn: Dr. V. Russo, AFML/LLN

Commanding Officer
Office of Ordnance Research
Box CM, Duke Station
Durham, NC 27706

Commanding Officer
Frankford Arsenal
Philadelphia, PA 19137
Attn: Dr. J. Waldman
Bldg. 513 L30100

National Aeronautics & Space Administration (Code RWM)
600 Independence Ave., S.W.
Washington, D.C. 20546

National Aeronautics & Space Administration
Langley Research Center
Materials Division, Langley Station
Hampton, VA 23365
Attn: Mr. H. F. Hardrath
Stop 188M

Boeing-Vertol Company
Boeing Center
P.O. Box 16858
Philadelphia, PA 19142
Attn: Mr. J. M. Clark

The Boeing Company
Commercial Airplane
ORG. 6-8733, MS77-18
P.O. Box 3707
Seattle, WA 98124
Attn: Cecil E. Parsons

Northrop Corporation
Aircraft Division
Dept. 3771-62
3901 West Broadway
Hawthorne, CA 90250
Attn: Mr. Allen Freedman

Vought Corporation
P.O. Box 5907
Dallas, TX 75222
Attn: Mr. A. Hohman

McDonnell Aircraft Company
St. Louis, MO 63166
Attn: Mr. H. J. Siegel
Materials & Processes Dev.
General Engineering Division

Lycoming Division
AVCO Corporation
Stratford, CT 06497
Attn: Mr. Barry Goldblatt

Grumman Aerospace Corp.
Research Dept.
Bethpage, NY 11714
Attn: Dr. G. Geschwind

Detroit Diesel Allison Division
General Motors Corporation
Materials Laboratories
Indianapolis, Indiana 46206

AiResearch Manufacturing Co. of America
Sky Harbor Airport
402 S. 36th Street
Phoenix, AZ 85034
Attn: Mr. Jack D. Tree, Dept. 93-35-5M

General Electric Company
Aircraft Engine Group
Materials & Processes Technology
Laboratories
Evendale, Ohio 45215

Solar
2200 Pacific Highway
San Diego, CA 92112
Attn: Dr. A. Metcalfe

Dr. Charles Gilmore
Tompkins Hall
George Washington University
Washington, D.C. 20006

Mr. Michael Hyatt
The Boeing Company
P.O. Box 707
Seattle, Washington 98124

General Electric Co.
Corporate Research and Development
Building 36-441
Schenectady, NY 12345
Attn: Dr. J. H. Westbrook, Manager
Materials Information Services

General Electric Company
Corporate Research & Development
P.O. Box 8
Schenectady, NY 12301
Attn: Dr. D. Wood

Westinghouse Electric Company
Materials & Processing Laboratories
Beulah Road
Pittsburgh, PA 15235
Attn: Don E. Harrison

Dr. John D. Wood
Associate Professor
Lehigh University
Bethlehem, PA 18015

General Dynamics Corp.
Convair Aerospace Division
Forth Worth Operation
P.O. Box 748
Fort Worth, TX 76101
Attn: Tom Coyle

Hamilton Standard Division
United Technologies, Inc.
Windsor Locks, CN 06096
Attn: Mr. E. J. Delgrosso

TRW, Inc.
23555 Euclid Avenue
Cleveland, OH 44117
Attn: Elizabeth Barrett
T/M 3417

Bell Helicopter Co.
A Textron Division
P.O. Box 482
Fort Worth, TX 76101
Attn: M. A. Green

United Technology Center
P.O. Box 358
Sunnyvale, CA 94088
Attn: George Kreici

Hughes Helicoptors
Division Summa Corporation
Centinela & Teale Streets
Culver City, CA 90230
Attn: T. Matsuda

Norman A. Nielson
Engineering Technology Laboratories
E. I. Dupont de Nemours
Wilmington, DE 19898

Massachusetts Institute of Technology
Department of Metallurgy and Materials Science
Cambridge, MA 02139
Attn: Dr. N. J. Grant

Dr. J. Williams
Dept. of Metallurgy & Materials Science
Carnegie-Mellon University
Pittsburgh, PA 15213

The Franklin Institute Research Laboratories
Twentieth & Parkway
Philadelphia, PA 19103
Attn: Technical Director

Whittaker Corporation
Nuclear Metals Division
West Concord, MA 01718

Department of Metallurgical Engineering
Drexel University
32nd & Chestnut Streets
Philadelphia, PA 19104

Martin Marietta Aluminum
Attn: Mr. Paul E. Anderson
(M/C 5401)
19200 South Western Avenue
Torrance, CA 90509

Mr. W. Spurr
The Boeing Company
12842 72nd Ave., N.E.
Kirkland, WA 98033

Dr. John A. Sehey
Dept. of Materials Engineering
University of Illinois at Chicago Circle
Box 4348
Chicago, IL 60680

Rockwell International
P.O. Box 1082
1027 Camino Dos Rios
Thousand Oaks, CA 91320

Pratt & Whitney Aircraft
Division of United Technologies
Florida Research and Development Center
P.O. Box 2691
West Palm Beach, FL 33402

Martin Marietta Corporation
P.O. Box 5837
Orlando, FL 32805
Attn: Dr. Richard C. Hall
Mail Point 275

Southwest Research Institute
8500 Culebra Road
P.O. Drawer 28510
San Antonio, TX 78284
Attn: Dr. C. Gerald Gardner

National Aeronautics & Space Administration
George C. Marshall Space Flight Center
Huntsville, AL 35812
Attn: Mr. J. G. Williamson
S&E-ASTN-MMC

National Academy of Sciences
Materials Advisory Board
Washington, D.C. 20418
Attn: Dr. J. Lane

U.S. Energy Research and Development Administration
Savannah River Operations Office
P.O. Box A
Aiken, SC 29801
Attn: N. J. Donahue, Reactor Materials

Director
National Bureau of Standards
Washington, D.C. 20234
Attn: Dr. E. Passaglia

Battelle Memorial Institute
505 King Avenue
Columbus, OH 43201
Attn: Mr. Stephen A. Rubin, Mgr.
Information Operations

IIT Research Institute
Metals Research Department
10 West 35th Street
Chicago, Illinois 60616
Attn: Dr. N. Parikh

General Dynamics Convair Div.
P.O. Box 80847
San Diego, CA 92138
Attn: Mr. Jack Christian, Code 643-10

Kaman Aerospace Corporation
Old Windsor Road
Bloomfield, CT 06001
Attn: Mr. M. L. White

Rockwell International
Columbus Division
Columbis, OH 43216
Attn: Mr. P. Maynard, Dept. 75
Group 521

Rockwell International
Rocketdyne Division
Canoga Park, CA 91305
Attn: Dr. Al Jacobs
Group Scientist
Materials Branch

Rockwell International
Los Angeles Division
International Airport
Los Angeles, CA 90009
Attn: Gary Kelley
Materials Applicatiens

Lockheed Palo Alto Research Laboratories
Materials Science Laboratory
3251 Hanover Street
Palo Alto, CA 94303
Attn: Dr. D. Webster
Bldg. 201 Org. 52-31

Lockheed California Company
P.O. Box 551
Burbank, CA 91503
Attn: Mr. J. M. VanOrden
Dept. 74-71, Bldg. 221, Plt. 2

Lockheed-Georgia Company
Marietta, GA 30061
Attn: E. Bateh

Lockhedd Missile & Space Corp.
Box 504
Sunnyvale, California 94088
Attn: Mr. G. P. Pinkerton
Bldg. 154, Dept 8122

Douglas Aircraft Company
3855 Lakewood Blvd
Long Beach, CA 90808
Attn: Mr. Fred Mehe, C1-250

Sikorsky Aircraft
Division of United Technologies, Inc.
Stratford, CT 06497
Attn: Materials Dept.

Grumman Aerospace Corp.
Plant 12
Bethpage, NY 11714
Attn: R. Heitzmann

Avco Space Systems Division
Lowell Industrial Park
Lowell, MA 01851

Brush Wellman, Inc.
17876 St. Clair Avenue
Cleveland, OH 44110
Attn: Mr. Bryce King

Mr. H. S. Rubenstein
6803 Lemon Rd.
McLean, VA 22101

General Electric
Missile & Space Division
Materials Science Section
P.O. Box 8555
Philadelphia, PA 91901

Kawecki Berylco Industries
Attn: Mr. C. B. Criner
P.O. Box 1462
Reading PA 19603

Midwest Research Institute
425 Volker Boulevard
Kansas City, MO 64110

ERDA Division of Reactor
Development and Technology
Washington, D.C. 20545
Attn: Mr. J. M. Simmons, Chief
Metallurgy Section

Dr. F. N. Mandigo
Olin Metals Research Laboratories
91 Shelton Avenue
New Haven, CT 06515

Kaiser Aluminum & Chemical Corp.
Aluminum Division Research
Center for Technology
POB 870
Attn: T. R. Pritchett
Pleasonton, CA 94566

Reynolds Metals Company
Metallurgical Research Division
4th and Canal Streets
Richmond, VA 23219
Attn: Dr. J. H. Dedrick

The Dow Metal Products Company
Hopkins Building
Midland, MI 48640

United Technologies Research
Laboratories
East Hartford, CT 06108
Attn: Mr. Roy Fanti

Autonetics Division of Rockwell
International
P.O. Box 4173
Anaheim, CA 92803
Attn: Mr. A. G. Gross, Jr.
Dept. 522-92

(2 copies)
Commander, Naval Air Systems Command
AIR-954
Washington, D.C. 20361

(12 copies)
Defense Documentation Center
Cameron Station
Alexandria, VA 22314
VIA: Commander
Naval Air Development Center
Code 302
Warminster, PA 18974